Oncology and Translational Medicine

Volume 2 • Number 4 • August 2016

Oncology and Translational Medicine Volume 2 • Number 4 • August 2016 pp 143–193

邮发代号：38-121
ISSN 2095-9621

GENERAL INFORMATION
≫otm.tjh.com.cn

ISSN 2095-9621
CN 42-1865/R

Oncology and Translational Medicine

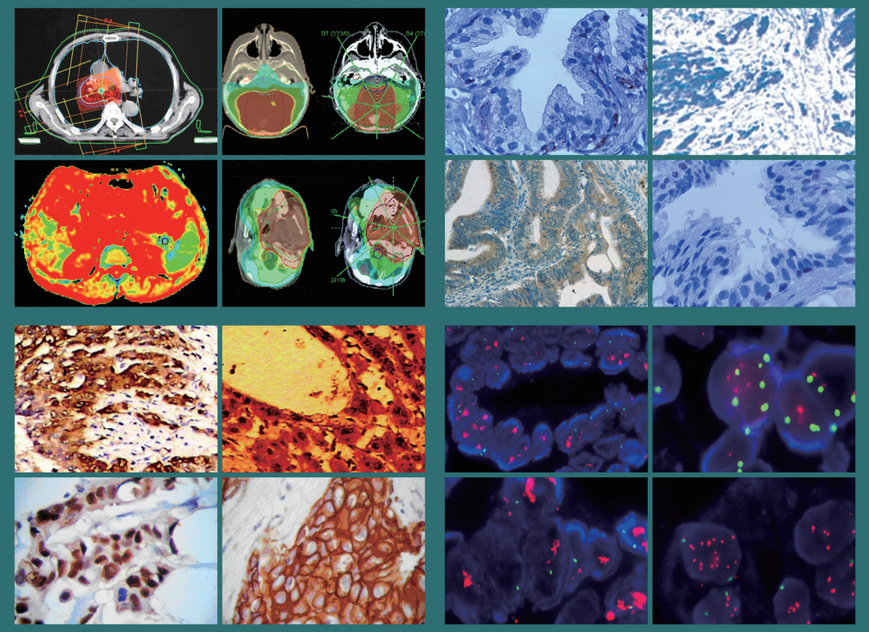

Volume 2
Number 4
August 2016

Oncology and Translational Medicine

Oncology and Translational Medicine
August 2016 Volume 2 Number 4

Contents

Oncology and Translational Medicine
DOI 10.1007/s10330-016-0176-2
August 2016, Vol. 2, No. 4, P143–P144

EDITORIAL

Progress of anti-checkpoint therapy in metastatic colorectal cancer*

Lizhen Zhu[1], Xuefeng Fang (Co-first author)[1, 2], Chenhan Zhong[1], Ying Yuan[1, 2] (✉)

[1] Department of Medical Oncology, The Second Affiliated Hospital, Zhejiang University School of Medicine, Hangzhou 310009, China
[2] Key Laboratory of Cancer Prevention and Intervention of Ministry of Education, The Second Affiliated Hospital, Zhejiang University School of Medicine, Hangzhou 310009, China

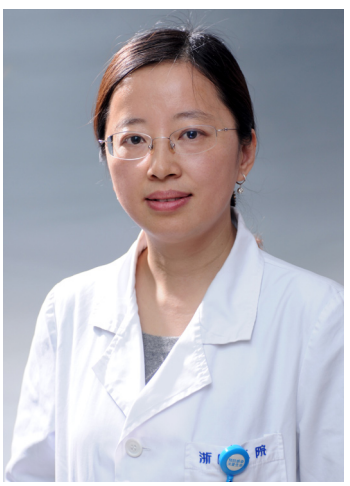

Ying Yuan, Professor, Department of Medical Oncology, The Second Affiliated Hospital of Zhejiang University School of Medicine, Hangzhou, Zhejiang Province, P. R. China. Prof. Yuan has focused on the clinical practice and research on personalized therapy of gastrointestinal cancer, especially of colorectal cancer. Prof. Yuan is also interested in the scientific research. She has acquired several grants and published 99 papers, including 42 SCI papers. Besides, she has achieved a few honors and awards, such as "The Southern California Society of Colorectal Surgeons Award", "Scientific Achievement Award of Zhejiang Province", "National Science and Technology Progress Award", and so on. Her current academic society memberships include: member and director of genetics group, colorectal cancer professional committee of Chinese Society of Clinical Oncology; member of clinical trial committee and molecular targeted drugs committee of Chinese Society of Clinical Oncology; core expert of gastrointestinal cancer rational drug use commission, National Health and Family Planning Commission; expert of colorectal cancer diagnostic and treatment practices group, National Health and Family Planning Commission; permanent member and secretary of colorectal cancer MDT management board, National Health and Family Planning Commission.

In the immune system, antigen-presenting cells, especially dendritic cells, process tumor antigens and present them to anti-tumor CD8+ cytotoxic T cells and CD4+ helper T cells, thereby promoting the proliferation and activity of these cells to kill tumor cells.

When binding to ligands, some receptors on the T cell surface, such as CD28, OX40, GITR, and CD27, can activate T cells and promote their anti-tumor effects. Conversely, some other receptors can suppress T cell activation when binding to their ligands. This results in inhibition of T cell proliferation and cytokine secretion to repress the tumor cell-killing function, and therefore maintain immune homeostasis. These receptors are collectively referred to as immune checkpoints, including cytotoxic T-lymphocyte-associated protein 4 (CTLA-4), programmed cell death protein 1 (PD-1), T-cell immunoglobulin and mucin-domain containing 3 (TIM-3) and lymphocyte-activation gene 3 (LAG-3) [1].

Tumor cells usually express ligands of the checkpoints at high levels to suppress the anti-tumor activity of T cells. Therefore, the discovery of drugs that can target these receptors or their ligands to attenuate their effect on T cells would reverse T cell inhibition and help to restore their anti-tumor activity. In recent years, certain anti-checkpoint receptors or ligands, such as anti-CTLA-4, anti-PD-1 and anti-programmed cell death protein ligand 1 (anti-PD-L1) have shown dramatic responses in some patients with different types of cancers.

In a phase II study conducted by Le DT *et al*, pembrolizumab (an anti-PD-1 drug) showed a great benefit to patients with mismatch repair-deficient (dMMR) metastatic colorectal cancer (mCRC). The immune-related ob-

✉ Correspondence to: Ying Yuan. Email: yuanying1999@zju.edu.cn
* Supported by a grant from the Key Projects of the National Science & Technology Pillar Program during the Twelfth Five-year Plan Period (No. 2014BAI09B07).

jective response rate (ORR) and immune-related progression-free survival (PFS) rate were 40% (4/10 patients) and 78% (7/9 patients), respectively, in patients with dMMR mCRC, whereas the ORR was 0% (0/18 patients) and the PFS was 11% (2/18 patients) in patients with mismatch repair-proficient (pMMR) mCRC [2]. The most recent data of this study were presented at the 2016 ASCO meeting, showing that after a median of 9.3 months of follow-up, the ORR was 57% (including 11% showing complete regression and 46% showing partial regression) for patients with dMMR mCRC, whereas the ORR remained at 0 for patients with pMMR mCRC after a median of 6 months follow-up. Interestingly, whole-exome sequencing suggested a mean of 1782 somatic mutations per tumor in dMMR tumors, but only 73 in pMMR tumors. A greater total mutation load would result in more tumor neoantigens, which would increase the activity of tumor-specific T cells to attack. Since anti-PD-1 therapy can promote T cell functions, these results suggest that dMMR mCRC patients would benefit more from anti-PD-1 therapy.

In addition, in a group of treatment-experienced patients with chemo-refractory mCRC, the combination of cobimetinib (an anti-MEK drug) and atezolizumab (an anti-PD-L1 drug) showed promising results, with an ORR of 17% and 6-month overall survival of 72%. Notably, 96% of the patients harbored *KRAS* mutations. The inhibition of MEK leads to upregulation of MHCI in tumor cells, causing intratumoral T cell infiltration, thereby enhancing anti-PD-L1 activity.

Although ipilimumab (an anti-CTLA-4 drug) has substantially improved the outcome of patients with melanoma, patients with mCRC cannot benefit from treatment with either ipilimumab or tremelimumab (another anti-CTLA-4 drug) alone [3–4]. At the 2016 ASCO meeting, Michael Overma demonstrated that the combination of nivolumab and ipilimumab had tolerable safety profiles and showed preliminary positive results, with an ORR of 33.3% for patients with microsatellite instability-high (MSI-H) CRC. Nivolumab monotherapy also demonstrated encouraging results in patients with MSI-H in this same study (ORR 25.5%). Notably, owing to the small sample, the results could not conclusively determine whether the combination of nivolumab and ipilimumab is superior to nivolumab monotherapy, and could also not indicate whether nivolumab is less effective than pembrolizumab.

In particular, in a phase II study of nivolumab in refractory metastatic squamous cell carcinoma of the anal canal (SCCA), among 37 patients who received at least one dose of nivolumab, 2 (5.4%) achieved complete regression and 7 (18.9%) achieved partial regression, and the median PFS was 3.9 months. Nivolumab was well-tolerated in these patients. Since there is currently no consensus treatment approach for SCCA, the results of these studies may offer some promise for these patients. SCCA is mainly driven by immune evasion of human papillomavirus (HPV)-specific CD8 and CD4 T cells; however, it remains unknown whether HPV infection is a predictor of the anti-PD-1 or anti-PD-L1 response, because pembrolizumab and durvalumab (an anti-PD-L1 drug) showed responses in cases of both HPV+ and HPV- squamous cell carcinoma of the head and neck.

In addition to nivolumab, pembrolizumab, atezolizumab, ipilimumab and tremelimumab, there are other drugs targeting PD-1, PD-L1 or CTLA-4 currently undergoing clinical trials. Moreover, clinical trials of drugs targeting other receptors or ligands related to the immune system are also actively recruiting patients, such as drugs targeting LAG-3.

In general, clinical trials of anti-PD-1 or anti-PD-L1 therapy have thus far revealed encouraging responses and safety profiles for patients with mCRC and SCCA, and the combination of anti-PD-1 and anti-CTLA-4 therapy may be tolerable, with promising preliminary responses. In addition, the combination of anti-MEK and anti-PD-L1 may be a potential therapy for *KRAS* mutation-positive mCRC. Moreover, some studies are focusing on the value of anti-checkpoint treatment in combination or in comparison with chemotherapy. Nevertheless, close attention must be paid to the data emerging from more studies.

Conflicts of interest

The authors indicated no potential conflicts of interest.

References

1. Drake CG, Lipson EJ, Brahmer JR. Breathing new life into immunotherapy: review of melanoma，lung and kidney cancer. Nat Rev Clin Oncol, 2014, 11: 24–37.
2. Le DT, Uram JN, Wang H, *et al*. PD-1 Blockade in Tumors with Mismatch-Repair Deficiency. N Engl J Med, 2015, 372: 2509–2520.
3. Chung KY, Gore I, Fong L, *et al*. Phase Ⅱ study of the anti-cytotoxic T-lymphocyte-associated antigen 4 monoclonal antibody, tremelimumab, in patients with refractory metastatic colorectal cancer. J Clin Oncol, 2010, 28: 3485–3490.
4. O'Mahony D, Morris JC, Quinn C, *et al*. A pilot study of CTLA-4 blockade after cancer vaccine failure in patients with advanced malignancy. Clin Cancer Res, 2007, 13: 958–964.

DOI 10.1007/s10330-016-0176-9
Cite this article as: Zhu LZ, Fang XF, Zhong CH, *et al*. Progress of anti-checkpoint therapy in metastatic colorectal cancer. Oncol Transl Med, 2016, 2: 143–144.

Oncology and Translational Medicine
DOI 10.1007/s10330-016-0164-6

August 2016, Vol. 2, No. 4, P145–P149

REVIEW ARTICLE

Molecular subtypes of colorectal cancer: Evaluation of outcomes and treatment

Weijing Sun (✉)

University of Pittsburgh School of Medicine, University of Pittsburgh Medical Center (UPMC), University of Pittsburgh Cancer Institute (UPCI), Pittsburgh, USA

Abstract

Colorectal cancer (CRC) is a biologically heterogeneous disease with diverse clinical outcomes and responses to treatment. In the past two to three decades, a major effort has focused on classifying colorectal cancer subtypes based on causation, etiology, gene expression profiles, different pathways, and translational data from clinical trials. The goal is to uncover prognostic and predictive factors for outcomes in patients with colorectal cancer and to guide therapeutic approaches and management for the improvement of overall survival. Significant advances have been achieved in this area. However, tremendous work is still needed to accomplish the goal of better understanding intratumoral heterogeneity and the influence of the colonic environment, among other facets of colorectal cancer.

Received: 8 June 2016
Revised: 9 July 2016
Accepted: 25 July 2016

Key words: colorectal cancer (CRC); molecular subtype; evaluation

Colorectal cancer (CRC) is the third most common cancer in the United States and the world (95 300 new cases in the United States and 1.4 million worldwide in 2016) [1, 2]. Patient survival and treatment options are still largely dependent on TNM stage at the time of diagnosis, even though we know colorectal cancer is a biologically heterogeneous disease that develops via distinct pathways involving alternative combinations of genetic and epigenetic factors [3]. Subtypes of colorectal cancer based on molecular and pathway profiles with defined prognostic markers would predict individual patient outcomes more precisely and therefore better inform on appropriate therapeutic intervention, especially targeted therapy. Various methods have been attempted and different directions taken to achieve this goal. Some approaches are as simple as focusing on the implication of defects in a single oncogene or tumor suppressor gene or assessing the consequences of a limited combination of gene mutations [4]. Other approaches are based on morphological characteristics, clinical and molecular features [5], or gene expression-based data classification [6].

To date, the microsatellite instability (MSI)-H phenotype has demonstrated the most robust prognostic role in terms of improved survival in stages II and III CRC patients [7]. Most single gene mutation markers have modest prognostic or predictive value, except Braf and Kras mutations. The Braf mutation ($BRAF^{V600E}$) has been associated with poorer survival in CRC. Kras and Nras mutations are associated with resistance to epidermal growth factor receptor (EGFR) targeted therapy [4].

'Pathway' based CRC subtype classification has been proposed because of the distinctive association of 'serrated polyps/adenocarcinoma' with MSI-H, CpG island methylation phenotype (CIMP) with Braf mutation; as well as the predictive and potential prognostic value of Kras [5]. At the same time, it has been also been learned that as a somatic genetic disease that is generally sporadic in nature, pathogenesis is influenced by the local colonic environment as well as the genetic background of the individual patient.

There have been many attempts to find consensus in classification of subtypes of CRC based on causation, etiology, gene expression profiles, different pathways, and translational data from clinical trials. Such efforts are geared towards revealing prognostic and predictive factors for patient outcomes and to guide therapeutic approaches and management to eventually improve overall survival. However, no universal subclassification has been agreed upon because of the various views and opinions of different groups of investigators and experts [6, 8–11]. Overall,

✉ Correspondence to: Weijing Sun. Email: sunw@upmc.edu

the proposed models are similar and based on the types and frequency of genetic alterations, epigenetic modifications, and molecular pathways.

Genetic alterations and epigenetic modifications

Whole genome sequencing has confirmed research findings from the past three decades on the genetic and epigenetic abnormalities underlying CRCs. CRCs are formed through the accumulation of genetic and epigenetic events, which include gain-of-function defects as well as loss-of-function defects of selected tumor suppressor genes. It is suggested that approximately 25 different genes are commonly affected by somatic mutations in CRCs, with tumor suppressor genes outnumbering oncogenes by about four to one [9, 12]. Events conferring growth advantage are considered 'driver' mutations and the remaining mutations are called 'passenger' mutations that are the result of genomic chaos and random events with no clear effects on the disease process. Only two to eight driver gene alterations are found in a typical sporadic CRC. It is important to know that driver mutations in one CRC patient may differ from those in another patient [9, 13]. Additional genetic and epigenetic events are acquired in progeny cells beyond those inherited from parental cells.

Based on the commonalities among CRCs, the disease has been grouped into hypermutated (approximately 16% of sporadic CRCs) with mutation rates of > 12 per 10^6 bases and nonhypermutated (approximately 84% of sporadic CRCs) with mutation rates of < 8.24 per 10^6 bases based on TCGA data [9]. The median number of non-silent mutations is 728 in tumors of the hypermutated group compared to 58 in tumors of the nonhypermutated group. The etiology for hypermutated tumors is driven largely by the presence of MSI-H and CIMP resulting from defects in the MMR (DNA mismatch repair, MMR-D) genes hMSH6, hMSH2, hMSH3, and, hMLH3, as well as POLE (DNA polymerase ε). Hypermethylation of the hMLH1 promoter should also be noted. Most hypermutated CRCs have mutations in genes that contain intrinsic coding microsatellites. Nonhypermutated CRCs are more frequently associated with somatic copy-number alterations with more chromosomal or subchromosomal changes including either gains (1q, 7p and q, 8p and q, 12q, 13q, 19q, and 20p and q) or deletions (18p and q: 66% with SMD4; 17p and q: 56% with TP53; 1p, 4q, 5q, 8p, 14q, 15q, 20p, and 22q). Chromosomal region 10p25.2 is commonly involved (*FHIT, RBFOX1, WWOX, SMAD4, APC, PTEn, SMAD3,* and *TCF7L2*) as well as segment amplifications (*USP12, CDK8, KLF5, HNF4A, WHSC1L1, MYC, ERBB2,* and *IGF2*) [9].

Although hypermutated and nonhypermutated CRCs progress through different sequences of genetic events, there is some overlap of affected pathways. For example, APC is mutated in both groups, consistent with its role as a gatekeeper mutation. Alterations of MYC transcriptional targets are also noticed in both groups. Consistent activation of Wnt, RAS, PI3K signaling, inactivation of TGFβ signaling, and inactivation of TP53 function are demonstrated in both groups [9, 13].

Besides the direct genetic and epigenetic analysis of CRC tissue, single nucleotide polymorphisms (SNPs) from blood of CRC patients have also been examined as potential biomarkers. However, these genome-wide association studies are unable to determine the cause or mechanism of tumor initiation, progression, and/or metastasis. MicroRNA (miR) mutations and polymorphisms may also have profound effects on tumor behavior and offers potential therapeutic options [14].

Molecular pathways

The simplified model of normal-adenoma-carcinoma-metastasis sequence has been established and accepted by investigators for many years in understanding and evaluating CRC initiation and processing. With recent molecular biology analysis, various molecular subtypes have been established and discussed [6, 8–11]. Although there is some disagreement among them, they are all based on three identified molecular pathways: CIN (chromosomal instability), MSI-H (microsatellite instability-high), and CIMP (CpG Island Methylator Phenotype). These molecular pathways may dictate the timing and process of tumor initiation, progression, and metastasis with distinguishes in epidemiology, mutational events, and immune response, therefore, treatment approaches could be vary as well.

The CIN pathway is affected in approximately 85% of CRC cases and is the most common and the first described molecular pathway in CRC. However, the mechanisms leading to CRC are still unclear but are thought to include extensive copy number of somatic mutations throughout the genome, which results in aneuploidy tumors with nonhypermutated adenomas [13, 15, 16]. Loss of APC and TP53 appears sufficient for generation of significant aneuploidy, particularly when additive with SMAD4 and mutant KRAS [17]. APC is a part of the Wnt signaling pathway, which regulates cytoplasmic levels of β-lactenin and is related to cellular proliferation as a tumor suppressor gene. Wnt signaling is deregulated in 93% of all nonhypermutated CRCs with APC being the most commonly mutated component (81%). KRAS mutation as the oncogenic activator is the next most common event. KRAS is a part of the ERBB/KRAS/BRAF/MAPK signaling axis. Mutant KRAS protein causes acceleration of tumor proliferation. In nonhypermutated CRCs, the prevalence

of KRAS mutation is 41% and overall active mutations of KRAS, NRAS, or BRAF is approximately 55% [9]. Clinical evidence demonstrated that patients with mutations in KRAS, NRAS, or BRAF have poorer outcomes compared to those with wild type genes. PIK3CA, the catalytic subunit of the mitogenic PI3K complex, controls levels of phosphatidylinositol triphosphate and is antagonized by PTEN. Mutations of PIK3CA are found in 18% of nonhypermutated CRCs. Alteration of these two pathways is found in about 33% of CRCs. Therefore, inhibiting both pathways simultaneously may be beneficial in clinic management of CRC [9].

MSI-H is defined as > 30% of microsatellite markers demonstrating a frameshift mutation and is a biomarker for defective DNA MMR function in CRC [9]. DNA MMR recognizes and repairs nucleotide mismatches and mispairing during DNA replication. MSI-H is observed in approximately 15% of sporadic CRCs, consistent with the frequency of hypermutated CRCs. The defect in DNA MMR is caused by aberrant bi-allelic hypermethylation of the DNA MMR gene hMLH1 (for the most part), thereby preventing its transcription [18–20]. MSI-H CRCs accumulate mutations in driver genes with frameshift mutations and subsequently cause stop codons, which creates a truncated transcript and proteins that are neo-antigenic to the patients' immune system [21]. The other common feature of the MSI-H CRC pathway is an activating oncogenic mutation of BRAF (most commonly $BRAF^{V600E}$) in about 40% of cases via this pathway [9]. CRC via the MSI-H pathway seems to have low copy number variation and tends to be diploid with fewer TP53 (20%) and ACP (51%) mutations compared to CIN-derived CRC. Both types have a similar frequency of Wnt deregulation. Histologically, MSI-H CRCs are more likely to be poorly differentiated, contain mucin, and possess subepithelial lymphoid aggregates and intraepithelial lymphocytes due to the immune response to truncated neo-antigens produced from the epithelium. MSI-H CRCs are more commonly (approximately 70%) located proximal to the splenic flexure [22, 23]. Recent analysis showed that CRCs with MSI-H pathway involvement are less frequent among African-American populations than in Caucasians or Asians, which may partially explain the poor outcomes of CRCs in African-Americans compared with in Caucasians stage-by-stage [24].

CIMP is defined by increased or excessive epigenetic methylation of genetic loci, which contains CpG islands typically located in the promoter and upstream regulatory regions of genes. The etiology of CIMP development is less definitive with several possible mechanisms or combinations of abnormalities including DNA methyltransferase overexpression, mutations in chromatin remodeling genes (e.g., *CHD8*), mutations in *IDH1* and *TET*, or environmental exposure (e.g., tobacco use) [22, 25–28]. Based on the number of markers (*RUNX3, SoCS1, NEUROG1, CACNA1G,* and *IGF2*) positive for methylation, CIMP can be further classified as 'high' (≥ 3 markers of methylation) or 'low' (≤ 2 markers of methylation) [29]. CIMP CRCs overlap with MSI-H and CIN pathways. CIMP-H occurs as hypermutated tumors in approximately 20% of CRCs with BRAF mutation and hypermethylation of hMLH1 (for the most part). CIMP-H CRCs are most likely to manifest a serrated morphology, including sessile serrated adenomas and traditional serrated adenomas. CIMP-L occurs as nonhypermutated tumors in 20% of CRCs with some of them derived from traditional serrated adenomas with MSS and containing KRAS mutations. The CIMP pathway can be helpful for understanding pathogenesis of CRC. However, it does not appear to be a useful tool or biomarker clinically.

Clinical evaluation

CRC subtypes/subclassifications based on distinct histopathologic and molecular alterations, as well as involved pathways, may better predict patient outcomes and will likely advance effective drug development strategies.

Recently, two large studies with more than 2000 stage III CRC patients in each revealed new and important associations between molecular alterations and patient survival [30, 31]. One study prospectively collected samples from 2720 stage III patients participating in an adjuvant chemotherapy trial (NCCTG N0147). Mutations in BRAF ($BRAF^{V600E}$) and in KRAS were tested and tumor DNA MMR status (proficiency or deficiency) was identified based on detection of MLH1, MSH2, and MSH6 proteins and methylation of the *MLH1* promoter. Findings were validated using tumor samples from a separate set of patients with stage III cancer (n = 783). Based on MMR status and detection of $BRAF^{V600E}$ or mutations in KRAS (which were mutually exclusive), tumors were categorized into five subtypes: MMR-P (also as MSS or MSS-L) with $BRAF^{V600E}$ in 6.9%; MMR-P with KRAS mutations in 35%; MMR-P with no BRAF or KRAS mutations in 49%; MMR-D with $BRAF^{V600E}$ or hypermethylation of MLH1 (as the sporadic type) in 6.8%; and MMR-D with no BRAF mutation or hypermethylation of MLH1 (familial type) in 2.6%. Their findings were consistent with the molecular subtype model prediction described above. A higher percentage of MMR-P tumors with $BRAF^{V600E}$ were proximal (76%), high grade (44%), N2 stage (59%), and detected in women (59%), compared to MMR-P tumors without BRAF or KRAS mutations (33%, 19%, 41%, and 42%, respectively; all $P < 0.0001$). A significantly lower 5-year disease free survival (DFS) in patients with MMR-P and $BRAF^{V600E}$ mutations was found compared to patients who were MMR-P with no mutations in either gene. DFS in patients with MMR-D sporadic or familial

subtypes was similar to that in patients with MMR-P with no *BRAF*^{V600E} or KRAS mutations.

The other study is based on the Seattle Colon Cancer Family Registry. A total of 2706 patients were diagnosed with invasive CRC from 1998 through 2007 in western Washington State and followed for survival through 2012. Tumor samples were collected from 2050 participants and classified into five subtypes based on combinations of tumor markers: type 1 as MSI-H, CIMP-positive with BRAF mutation; type 2 as MSS or MSI-L, CIMP-positive with BRAF mutation; type 3 as MSS or MSI-L, non-CIMP, positive for KRAS mutation; type 4 as MSS or MSI-L, non-CIMP, with no mutations in BRAF and KRAS; and type 5 as MSI-H, non-CIMP, and negative for mutations in BRAF and KRAS. Hazard ratios (HR) and 95% confidence intervals (CI) were assessed for associations of subtypes with disease-specific and overall mortality after adjusting for age, sex, body mass, diagnosis year, and smoking history. The results showed that compared with patients with type 4 tumors (MSS or MSI-L, non-CIMP, without BRAF or KRAS mutations, the most predominant), the patients with type 2 tumors (MSS or MSI-L, CIMP-positive, with BRAF mutation) had the highest disease-specific mortality (HR = 2.20, 95% CI: 1.47–3.31). Patients with type 3 tumors (MSS or MSI-L, non-CIMP, with KRAS mutation) also had higher disease-specific mortality (HR = 1.32, 95% CI: 1.07–1.63). Patients with type 5 tumors (MSI-H, non-CIMP, and without BRAF or KRAS mutations) had the lowest disease-specific mortality (HR = 0.30, 95% CI: 0.14–0.66). Associations with overall mortality in each type were similar to those with disease-specific mortality. These two studies confirmed that CRC subtypes, defined by proposed molecular pathways, are associated with marked differences in survival.

As mentioned above, MSI-H CRCs accumulate mutations with frameshift mutations and subsequently create truncated transcripts and proteins that are neo-antigenic to the patients' immune system. A recent study confirmed that MSI status is predictive of immune checkpoint blockage in advanced CRC [32].

In summary, integration of molecular pathways and subtypes with the TNM staging system is important for us to guide treatment for patients with active disease, and for surveillance/monitoring their status post potential curative procedure and adjuvant therapy. However, CRC heterogeneity has been observed at the intratumoral, intermetastatic, and intrametastatic levels. Rare variant cell populations may have important roles in clinical outcome. New strategies such as deep sequencing of primary CRC cell populations, comprehensive single-cell analyses, and analyses of circulating tumor-derived DNA are future molecular approaches that are needed to better define prognosis and predict likely responses to existing and new targeted therapies.

Conflicts of interest

The author indicated no potential conflicts of interest.

References

1. Siegel RL, Miller KD, Jemal A. Cancer statistics, 2016. CA Cancer J Clin, 2016, 66: 7–30.
2. Jorgensen ML, Young JM, Solomon MJ. Optimal delivery of colorectal cancer follow-up care: improving patient outcomes. Patient Relat Outcome Meas, 2015, 6: 127–138.
3. Grady WM, Carethers JM. Genomic and epigenetic instability in colorectal cancer pathogenesis. Gastroenterology, 2008, 135: 1079–1099.
4. Herzig DO, Tsikitis VL, Molecular markers for colon diagnosis, prognosis and targeted therapy. J Surg Oncol, 2015, 111: 96–102.
5. Jass JR. Classification of colorectal cancer based on correlation of clinical, morphological and molecular features. Histopathology, 2007, 50: 113–130.
6. Guinney J, Dienstmann R, Wang X, *et al*. The consensus molecular subtypes of colorectal cancer. Nat Med, 2015, 21: 1350–1356.
7. Popat S, Hubner R, Houlston RS. Systemic review of microsatellite instability and colorectal cancer prognosis. J Clin Oncol, 2005, 23: 609–618.
8. Hoadley KA, Yau C, Wolf DM, *et al*. Multiplatform analysis of 12 cancer types reveals molecular classification within and across tissues of origin. Cell, 2014, 158: 929–944.
9. Cancer Genome Atlas Network. Comprehensive molecular characterization of human colon and rectal cancer. Nature, 2012, 487: 330–337.
10. Roepman P, Schlicker A, Tabernero J, *et al*. Colorectal cancer intrinsic subtypes predict chemotherapy benefit, deficient mismatch repair and epithelial-to-mesenchymal transition. Int J Cancer, 2014, 134: 552–562.
11. Sadanandam A, Lyssiotis CA, Homicsko K, *et al*. A colorectal cancer classification system that associates cellular phenotype and responses to therapy. Nat Med, 2013, 19: 619–625.
12. Seshagiri S, Stawiski EW, Durinck S, *et al*. Recurrent R-spondin fusion in colon cancer. Nature, 2012, 488: 660–664.
13. Vogelstein B. Papadopoulos N, Velculescu VE, *et al*. Cancer genome landscapes. Science, 2013, 339: 1546–1558.
14. Hutchison J, Cohen Z, Onyeagucha BC, *et al.* How microRNAs influence both hereditary and inflammatory-mediated colon cancers. Cancer Genet, 2013, 206: 309–316.
15. Fearon ER, Vogelstein B. A genetic model for colorectal tumorigenesis. Cell, 1990, 61: 759–767.
16. Pino MS, Chung DC. The chromosomal instability pathway in colon cancer. Gastroenterology, 2010, 138: 2059–2072.
17. Drost J, van Jaarsveld RH, Ponsioen B, *et al*. Sequential cancer mutations in cultured human intestinal stem cells. Nature, 2015, 521: 43–47.
18. Kane MF, Loda M, Gaida GM, *et al*. Methylation of the hMLH1 promoter correlates with lack of expression of hMLH1 in sporadic colon tumors and mismatch repair-defective human tumor cell lines. Cancer Res, 1997, 57: 808–811.
19. Herman JG, Umar A, Polyak K, *et al.* Incidence and functional consequences of hMLH1 promoter hypermethylation in colorectal carcinoma. Proc Natl Acad Sci USA, 1998, 95: 6870–6875.
20. Veigl ML, Kasturi L, Olechnowicz J, *et al*. Biallelic inactivation of hMLH1 by epigenetic gene silencing, a novel mechanism causing

human MSI cancers. Proc Natl Acad Sci USA, 1998; 95: 8698–8702.
21. Schwitalle Y, Kloor M, Eiermann S, *et al*. Immune response against frameshift-induced neopeptides in HNPCC patients and healthy HNPCC mutation carriers. Gastroenterology, 2008, 134: 988–997.
22. Grady WM, Carethers JM. Genomic and epigenetic instability in colorectal cancer pathogenesis. Gastroenterology, 2008, 135: 1079–1099.
23. Boland CR, Goel A. Microsatellite instability in colorectal cancer. Gastroenterology, 2010, 138: 2073–2087.
24. Carethers JM, Murali B, Yang B, *et al.* Influence of race on microsatellite instability and CD8+ T cell infiltration in colon cancer. PLoS One, 2014, 9: e100461.
25. Tahara T, Yanamoto E, Madireddi P, *et al.* Colorectal carcinomas with CpG island methylator phenotype 1 frequently contain mutations in chromatin regulators. Gastroenterology, 2014, 146: 530–538.
26. Hinshelwood RA, Melki JR, Huschtscha LI, *et al.* Aberrant de novo methylation of the p16INK4A CpG island is initiated post gene silencing in association with chromatin remodelling and mimics nucleosome positioning. Hum Mol Genet, 2009, 18: 3098–3109.
27. Limsui D, Vierkant RA, Tillmans LS, *et al*. Cigarette smoking and colorectal cancer risk by molecularly defined subtypes. J Natl Cancer Inst, 2010, 102: 1012–1022.
28. Ichimura K. Molecular pathogenesis of IDH mutations in gliomas. Brain Tumor Pathol, 2012, 29: 131–139.
29. Hinoue T, Weisenberger DJ, Lange CP, *et al*. Genome-scale analysis of aberrant DNA methylation in colorectal cancer. Genome Res, 2012, 22: 271–282.
30. Sinicrope FA, Shi Q, Smyrk TC, *et al*. Molecular markers identify subtypes of stage III colon cancer associated with patient outcomes. Gastroenterology, 2015, 148: 88–99.
31. Phipps AI, Limburg PJ, Baron JA, *et al.* Association between molecular subtypes of colorectal cancer and patient survival. Gastroenterology, 2015, 148: 77–87.
32. Le DT, Uram JN, Wang H, *et al.* PD-1 blockade in tumors with mismatch-repair deficiency. N Engl J Med, 2015, 372: 2509–2520.

DOI 10.1007/s10330-016-0164-6
Cite this article as: Sun WJ. Molecular subtypes of colorectal cancer: Evaluation of outcomes and treatment. Oncol Transl Med, 2016, 2: 145–149.

Oncology and Translational Medicine
DOI 10.1007/s10330-016-0158-4

August 2016, Vol. 2, No. 4, P150–P155

REVIEW ARTICLE

Precision medicine in the treatment of pancreatic ductal adenocarcinoma

Jianlin Chen[1], Yunmian Chu[2], Jin He[3], Lei Zheng[4] (✉), Xu Che[2] (✉)

[1] Department of Hepatobiliary Oncology, Sun Yat-sen University Cancer Center, State Key Laboratory of Southern China, Collaborative Innovation Center for Cancer Medicine, Guangzhou 510060, China
[2] Department of Abdominal Surgery, Cancer Hospital, Chinese Academy of Medical Sciences and Perking Union Medical College, Beijing 100021, China
[3] Department of Surgery, Johns Hopkins University School of Medicine, Baltimore, MD 21287, United States
[4] Department of Oncology, The Sidney Kimmel Cancer Center, Department of Surgery, The Skip Viragh Center for Pancreatic Cancer Research and Clinical Care, Johns Hopkins University School of Medicine, Baltimore, MD 21287, United States

Abstract

Pancreatic cancer has a poor prognosis. Current therapies for pancreatic cancer have limited effects. In the past decade, precision medicine has shown great potential for clinical applications. In this review, different strategies for applying precision medicine to the treatment of pancreatic cancer are described.

Key words: pancreatic ductal adenocarcinoma (PDAC); precision medicine; chemotherapy; immunotherapy; cancer genomics

Received: 5 May 2016
Revised: 25 May 2016
Accepted: 10 June 2016

Pancreatic ductal adenocarcinoma (PDAC) is the fourth leading cause of cancer-related death in the United States, with 5-year survival of less than 5% despite advances in treatment [1]. 1 Without treatment, the overall median survival is only 6–9 months, and surgical resection offers the only chance of a cure. However, of the estimated 44,030 new cases diagnosed in the United States in 2011, only 15% of patients present with resectable disease, whereas 40% present with locally advanced unresectable disease, and 45% present with metastatic disease [2]. Even with adjuvant therapies, the prognosis remains dismal because PDAC is highly resistant to chemotherapy and radiation therapy. Human cancer genome studies have unveiled the mutational landscape of PDAC, which is quite heterogeneous in the mutational profiles of individual PDACs [3]. Conventional clinical trial designs have mostly failed to demonstrate a high efficacy in lowering recurrent risk following surgical resection in unselected patients, thus there is an increasing demand for selection of therapies for individual patients according to their individual mutation profiles.

Contemporary therapies

Patients with PDAC might be offered one or more of the following treatments: surgery, chemotherapy, or radiation therapy. Surgery offers the only chance of a cure, even when PDAC is diagnosed at an early stage. However, at the time of diagnosis, only 20% of patients have resectable PDAC. The phase III CONKO-1 study has established a role for adjuvant chemotherapy following curative resection, with 6 monthly cycles of gemcitabine [4]. Nevertheless, as many as 80% of patients in the CONKO-1 study did not survive beyond 5 years, even though they received gemcitabine adjuvant therapy following curative surgery. Moreover, when adjuvant therapy with gemcitabine was compared with 5-FU, in an ESPAC-3 study using mainly European patients, no difference in efficacy was found [5]. However S1, an oral prodrug of 5-FU, was shown to double survival time compared to gemcitabine in a phase III JASPAC 01 and GEST study for resected pancreatic cancer in Japan and unresectable advanced pancreatic cancer in Japan and Taiwan, respectively [6–7]. For advanced, unresectable PDAC or metastatic PDAC, chemotherapy

✉ Correspondence to: Xu Che. Email: xu.che@cicams.ac.cn; Lei Zheng. Email: lzheng6@jhmi.edu

is palliative. Combination chemotherapy regimens such as FOLFIRINOX and nab-paclitaxel/gemcitabine were found to be superior to gemcitabine alone in improving the survival time of patients with metastatic PDAC in recently completed phase III clinical trials [8]. Although it is intriguing to examine the efficacy of these combination therapies in the adjuvant setting, the severe toxicities associated with these combinations would be of concern if administered to an unselected patient population. Whether addition of radiation therapy to adjuvant therapy provides an added benefit remains to be seen, but a phase III study is underway. Given the known resistance of PDAC to radiation, we would favor a more selective approach, administering radiation therapy only to patients who are likely to benefit. Moreover, concerning the high incidence of recurrence following surgical resection of PDACs, appropriate selection of patients who would benefit from neoadjuvant therapy may further increase the benefits of surgery for resectable or borderline resectable PDAC patients [9]. Therefore, the limitations of contemporary therapies for PDAC have increased the demand to apply precision medicine to the management of PDAC.

Basis for precision medicine

Precision medicine is defined as administration of the right treatment at the right dose at the right time. With the rapid progress in the fields of biotechnology, genetics, and molecular biology, it has become possible for clinicians to utilize precision medicine techniques to tailor the management of many medical conditions.

New PDAC classification based on genomics and transcriptomics

The mutational landscape of pancreatic neoplasms has begun to be integrated with patient's clinical outcomes. The Vogelstein group conducted the first whole-genome sequencing of PDACs [10]. In this study, 69 gene sets were found to be genetically altered in the majority of the 24 PDACs examined. Thirty-one of these sets could be further grouped into 12 core signaling pathways that were each altered in 67–100% of the 24 PDACs. The core pathways included those involving KRAS signaling and regulation of the G1/S cell cycle transition, in which a single, frequently altered gene was predominant; those involving TGF-β signaling, in which a few altered genes were predominant; and those involving integrin signaling, regulation of invasion, hemophilic cell adhesion, and small guanine triphosphatase–dependent signaling, in which many different genes were altered. On average, each PDAC contains 63 genetic alterations, the majority of which are point mutations, and the pathway components altered in each individual tumor vary widely. Which core pathways and regulatory processes are altered becomes evident only when the coding regions of the genome are analyzed in depth.

Waddell *et al* [3] performed whole-genome sequencing and copy number variation analysis, including analysis for widespread and complex patterns of chromosomal rearrangement, in 100 PDACs. Chromosomal rearrangements leading to gene disruption were prevalent, affecting genes known to be important in pancreatic cancer (*TP53*, *SMAD4*, *CDKN2A*, *ARID1A*, and *ROBO2*) and new candidate drivers of pancreatic carcinogenesis (*KDM6A* and *PREX2*). A significant proportion harbored focal amplifications, many of which contained druggable oncogenes (*ERBB2*, *MET*, *FGFR1*, *CDK6*, *PIK3R3*, and *PIK3CA*), but at low prevalence in individual patients. Genomic instability co-segregated with inactivation of DNA maintenance genes (*BRCA1*, *BRCA2*, or *PALB2*) and a mutational signature of DNA damage repair deficiency. Based on structural variation profiles, PDACs were classified into four subtypes based on predominant genetic alterations with different clinical outcomes, including stable, locally rearranged, scattered, and unstable. The 'stable' subtype contains ≤ 50 structural variation events and often exhibits widespread aneuploidy, suggesting the presence of defects in cell cycle regulation. The 'locally rearranged' subtype contains a copy number gain that harbors known oncogenes. Known oncogenes include common focal amplifications in *KRAS*, *SOX9*, and *GATA6* and potential therapeutic targets such as *ERBB2*, *MET*, *CDK6*, *PIK3CA*, and *PIK3R3*. The remaining genetic alterations in the 'locally rearranged' subtype involve complex genomic events such as breakage–fusion–bridges or chromothripsis, which is linked to *TP53* mutations in medullobastoma and acute myeloid leukemia. The scattered class exhibit a moderate level of non-random chromosomal damage and 50–200 structural variation events. The 'unstable' subtype has defects in maintaining DNA integrity and could be sensitive to DNA-damaging agents. A platinum-containing combination therapy is emerging as a treatment option for advanced PDAC. Defining biomarkers of platinum responsiveness would significantly alter current treatment approaches to PDAC and improve overall outcomes. The researchers defined biomarkers, based on a combination of changes in gene structure, genetic mutations, and mutation features, that characterize the effectiveness of this treatment method. In a series of 8 patients who received platinum-based chemotherapy, of the 5 patients with unstable genomes and/or a high *BRCA* mutational signature burden, 2 had exceptional responses (defined as complete radiological resolution of disease and normalization of CA19.9 levels), and 2 had robust partial responses based on RECIST 1.1 criteria. None of the 3 patients without an 'unstable' genome showed a response. These results support the efficacy of individual tumor therapy.

Bailey *et al* [11] performed an integrated genomic and RNA sequencing analysis of 456 PDACs and classified PDACs into four subtypes: squamous, pancreatic progenitor, aberrantly differentiated endocrine exocrine, and immunogenic PDACs. The 'squamous' subtype is characterized by four core gene signatures, including inflammation, hypoxia response, metabolic reprogramming, TGF-β signaling. These gene signatures are independent poor prognostic factors. They are also highly expressed in tumors of breast, bladder, lung, and head and neck cancers, suggesting that treatments for these other types of cancer could be applied to PDAC. The 'progenitor' subtype is primarily defined by the expression of transcriptional networks containing the transcription factors *PDX1, MNX1, HNF4G, HNF4A, HNF1B, HNF1A, FOXA2, FOXA3*, and *HES1*. These transcription factors are pivotal for determination of the cell fate of pancreatic endoderm towards a pancreatic lineage. The 'aberrantly differentiated endocrine exocrine' (ADEX) subtype is characterized by the upregulation of transcription factors such as *NR5A2, MIST1*, and *RBPJL*, whose downstream targets are important for acinar cell differentiation and regeneration following the occurrence of pancreatitis, and genes associated with endocrine differentiation and MODY (including *INS, NEUROD1, NKX2-2*, and *MAFA*). Importantly, several patient-derived pancreatic cancer cell lines were enriched with gene programs associated with the ADEX subtype. Moreover, these cell lines expressed multiple genes associated with terminally differentiated pancreatic tissues, including *AMY2B, PRSS1, PRSS3, CEL*, and *INS*. In addition, the methylation pattern of the ADEX-type tumors was distinct from that of healthy pancreas tissue, and clustered with that of other pancreatic cancers. The 'immunogenic' subtype shares many of the characteristics of the pancreatic progenitor subtype, but is associated with evidence of abundant immune infiltrates. The 'immunogenic' subtype is also associated with immune gene signatures including B cell signaling, antigen presentation, and CD4+ T cell, CD8+ T cell, and Toll-like receptor signaling pathways. Enrichment analysis identified upregulated expression of genes associated with nine different immune cell types and/or phenotypes. It is intriguing to consider that the 'immunogenic' subtype may be more sensitive to immunotherapy. These four different subtypes of PDACs have different prognoses. The 'squamous' subtype has a median survival time of 13.3 months; the 'progenitor' subtype, 23.7 months, the 'aberrantly differentiated endocrine exocrine' subtype, 25.6 months; and the 'immunogenic' subtype, 30.0 months [11].

Tumor assessment for precision medicine

To guide the practice of precision medicine, it is essential to obtain tumor specimens; however, tumor biopsy often requires invasive procedures and may not be feasible. Recently, circulating tumor cells (CTCs), circulating cell-free DNA (cfDNA), and exosomes, which can be detected in blood obtained through a minimally invasive 'liquid biopsy,' have been shown to potentially represent the molecular landscape of a patient's overall tumor burden and to permit monitoring of the clonal evolution of individual PDACs during the course of treatment and disease progression.

CTCs

CTCs can be found in most patients with PDAC of any stage [12]. Study of CTCs may also help in understanding the biology of metastases, characterizing tumor genetic alterations, and predicting the prognosis for PDAC. Yu *et al* [13] identified Wnt2 as a candidate gene enriched in CTCs through single molecular RNA sequencing in a genetically engineered mouse PDAC model. Non-canonical Wnt signaling pathways have been suggested to contribute to the metastatic potential of human PDAC. The effectiveness of Tak1 inhibition in suppressing this pathway has identified a novel, potential drug target for metastasis suppression. Kulemann *et al* [14] reported that patients with KRAS-mutated CTCs had better survival than patients with KRAS wild-type CTCs following surgical treatment of PDACs (19.4 vs 7.4 months). Poruk *et al* [15] assessed CTCs with epithelial and mesenchymal phenotypes and found that CTCs expressing vimentin, a mesenchymal marker, were associated with a high risk of recurrence following surgical resection of PDACs.

cfDNA

cfDNA is a cancer-derived material that is enriched in tumors and that likely originates from CTCs; it holds promise for directly detecting and monitoring the molecular characteristics of tumors. The presence of cfDNA has been reported to be associated with distant organ metastasis, and mutations in potential therapeutic target genes have been detected in 29.2% of cfDNA samples collected from a retrospective cohort of patients [16].

Exosomes

Exosomes, lipid bilayer–enclosed extracellular vesicles that contain tumor cell materials, can avoid degradation in blood. Kahlert *et al* [17] found that exosomes from PDAC patients contain genomic DNA, RNA, and proteins, as well as mutations in KRAS and p53 in the genomic DNA. It has been reported that the level of glypican-1(+) circulating exosomes is correlated with the tumor burden and the survival of pre- and post-surgical patients with PDAC [18].

Strategies for precision medicine

Precision medicine shows excellent potential for treatment of PDACs, and various strategies are being tested in clinical trials (Fig. 1).

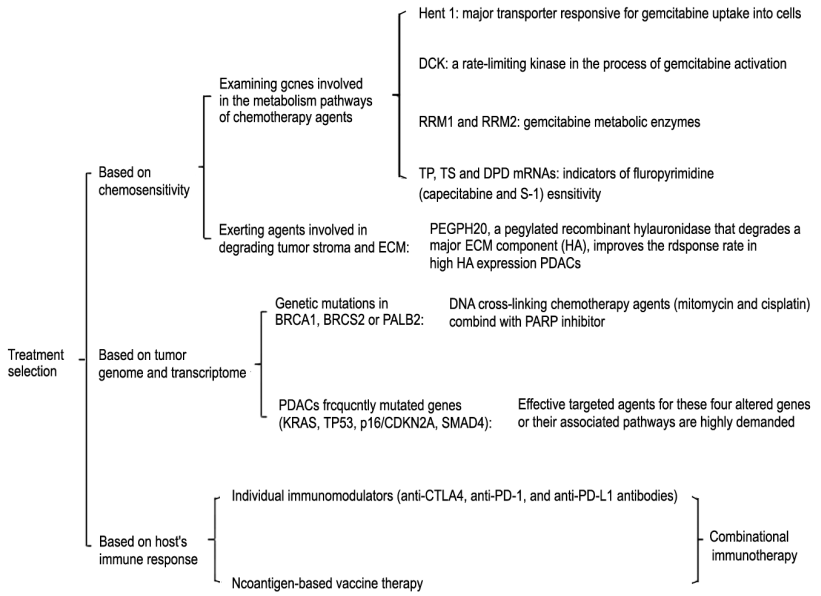

Fig. 1 Strategies for precision medicine in the treatment of PDACs. Different strategies for applying precision medicine to the treatment of PDACs. Hent 1, human equilibrative nucleoside transporter-1; DCK, Deoxycytidine kinase; RRM1 and RRM2, ribonucleoside reductases M1 and M2; TP, thymidine phosphorylase; TS, thymidylate synthase; DPD, dihydropyrimidine dehydrogenase; HA, hylauronic acid; PARP, poly ADP-ribose polymerase; CTLA-4, cytotoxic T lymphocyte antigen-4; PD-1, programmed cell death protein-1; PD-L1, the ligand of PD-1

Treatment selection based on chemosensitivity

The first strategy for selection of chemotherapy for individual patients involves examining genes that are involved in the metabolism of chemotherapeutic agents. Human equilibrative nucleoside transporter-1 (hENT1) is the major transporter responsible for uptake of gemcitabine into cells. A retrospective study including 27 patients with PDAC who underwent resection and treatment with adjuvant gemcitabine therapy revealed that high expression of hENT1 in PDAC is associated with longer survival in patients who received adjuvant gemcitabine monotherapy [19]. Similar results were also reported in other studies [20–21]. Deoxycytidine kinase (DCK) plays an important role in the process of gemcitabine activation and is a rate-limiting kinase in gemcitabine metabolism [22]. Expression of DCK at the gene and protein levels is closely associated with gemcitabine sensitivity in patients with PDAC, and high levels are associated with increased survival [23–25]. The ribonucleotide reductases M1 and M2 are also gemcitabine metabolic enzymes, and decreased levels are associated with gemcitabine resistance and a worse prognosis [26–28]. Recently, the orally administered fluoropyrimidine prodrugs, capecitabine and S-1, have been used for treatment of PDAC. One study showed that expression levels of thymidine phosphorylase, thymidylate synthase, and dihydropyrimidine dehydrogenase mRNA are indicators of fluropyrimidine sensitivity [29].

Tumor stroma and extracellular matrix (ECM) are associated with PDAC aggressiveness and chemotherapy resistance. Members of the lysyl oxidase protein family, which mediate collagen cross-linking and promote ECM stiffening, have been proposed as novel targets for improving chemosensitivity [30]. PEGPH20, a pegylated recombinant hylauronidase that degrades a major ECM component, hylauronic acid (HA), is already on the horizon of clinical development. ECM with high HA expression has been shown to have high hydrostatic pressure that compresses intratumoral blood vessels. By degrading HA, PEGPH20 reopens blood vessels and thus facilitates delivery of chemotherapeutic drugs [31]. A randomized phase 2 study of gemcitabine and Nab-paclitaxel, with or without PEGPH20, showed that the subgroup of patients whose PDACs have high HA expression had a significantly higher response rate to gemcitabine and Nab-paclitaxel combined with PEGPH20 than to gemcitabine and Nab-paclitaxel without PEGPH20 [32]. A phase 3 study of gemcitabine and Nab-paclitaxel, with or without PEGPH20, for treatment of patients with high HA expression has recently been initiated [33].

Treatment selection based on tumor genome and transcriptome

The *BRCA1, BRCA2*, and *PALB2* genes are inactivated in approximately 10% of familiar pancreatic cancers. Their protein products contribute to repair of DNA cross-linking damage and double-strand breaks. Studies have suggested that PDACs with genetically inactivated *BRCA1, BRCA2*, or *PALB2* are significantly more susceptible to DNA cross-linking agents, such as mitomycin and cisplatin. However, tumor cells harboring DNA repair defects due to mutations in *BRCA1, BRCA2*, or *PALB2* can survive with damaged DNA. Inhibition of poly ADP-ribose polymerase (PARP) would inhibit repair of the damaged DNA by the alternative DNA repair machinery,

preventing survival of the tumor cells. Therefore, genetic mutations in *BRCA1, BRCA2*, or *PALB2* have been used to select patients with PDAC for treatment with PARP inhibitors in clinical trials [34–35]. DNA repair defects also commonly occur in sporadic PDACs. Tumor genome- and transcriptome-based subtyping of PDACs may show promise to select patients for DNA cross-linking chemotherapy agents and PARP inhibitor treatments.

The landscape of the PDAC genome is notable for containing four frequently mutated genes (*KRAS, TP53, p16/CDKN2A*, and *SMAD4*). Ideally, driver mutations in these four genes would be used to select the best treatment options for patients. However, effective targeted agents are not available for any of these four altered genes. Therefore, therapeutic agents that target these four altered genes or their associated pathways are in high demand and may be key to the success of precision medicine in PDACs.

Treatment selection based on host immune response

Advances in immunotherapy have facilitated breakthroughs in the treatment of many cancer diseases. Cytotoxic T lymphocyte antigen-4 (CTLA-4) provides an inhibitory signal in the early phase of T-cell activation. The first immune checkpoint inhibitor to be approved is ipilimumab, a fully humanized IgG1 monoclonal antibody that inhibits CTLA-4. Programmed cell death protein-1 (PD-1) and its ligand, the ligand of PD-1 (PD-L1), function in the exhaustion of activated T cells, which can be blocked by therapeutic antibodies such as nivolumab and pembrolizumab, which are now United States Food and Drug Administration-approved. Although T-cell checkpoint inhibitors, including anti-CTLA4, anti-PD-1, and anti-PD-L1 antibodies, have shown substantial clinical benefits for treatment of other cancers, such as melanoma, non-small cell lung cancers, and renal cell carcinoma, their application in PDAC as single agents has shown limited efficacy [36]. Nevertheless, Lutz *et al* [37] showed that vaccine therapy can induce PD-1 and PD-L1 signaling and thus prime PDACs for anti-PD-1/PD-L1 antibody therapies. Soares *et al* [38–39] demonstrated that vaccine therapy can enhance the antitumor activity of anti-PD-1 or PD-L1 antibodies in a preclinical model of PDAC. Based on the rationale established by this preclinical study, multiple clinical trials have been initiated to test the combination of vaccines and anti-PD-1 antibodies in all four stages of PDACs. However, Lutz *et al* [37] highlighted the significant heterogeneity of the intratumoral immune response to vaccine therapy in different patients with PDAC. Thus, assessment of the intratumoral response to vaccine therapy has helped to reveal the immune regulatory signals that should be targeted by different immune modulating agents in individual patients. Moreover, a neoantigen-based vaccine therapy, designed based on whole-exome sequencing of mutated genes, will facilitate further tailoring of vaccine therapies for individual patients [36].

Summary

In the last decade, precision medicine has shown considerable potential for clinical applications, largely owing to advancements in cancer genome research and in our understanding of the tumor microenvironment and the host immune response. However, before we are able to apply precision medicine to our routine practice for managing PDACs, more large-scale prospective clinical studies are warranted, to provide support for precision medicine approaches and to establish guidelines for application of precision medicine.

Conflicts of interest

The authors indicated no potential conflicts of interest.

References

1. Siegel RL, Miller KD, Jemal A. Cancer statistics, 2015. CA: a cancer journal for clinician,. 2015, 65: 5–29.
2. Konstantinidis IT, Warshaw AL, Allen JN, *et al*. Pancreatic ductal adenocarcinoma: is there a survival difference for R1 resections versus locally advanced unresectable tumors? What is a "true" R0 resection? Ann Surg, 2013, 257: 731–736.
3. Waddell N, Pajic M, Patch AM, *et al*. Whole genomes redefine the mutational landscape of pancreatic cancer. Nature, 2015, 518: 495–501.
4. Oettle H, Neuhaus P, Hochhaus A, *et al*. Adjuvant chemotherapy with gemcitabine and long-term outcomes among patients with resected pancreatic cancer: the CONKO-001 randomized trial. Jama, 2013, 310: 1473–1481.
5. Valle JW, Palmer D, Jackson R, *et al*. Optimal duration and timing of adjuvant chemotherapy after definitive surgery for ductal adenocarcinoma of the pancreas: ongoing lessons from the ESPAC-3 study. J Clin Oncol, 2014, 32: 504–512.
6. Akira Fukutomi KU, Narikazu Boku, Hideyuki Kanemoto, *et al*. JASPAC 01: Randomized phase III trial of adjuvant chemotherapy with gemcitabine versus S-1 for patients with resected pancreatic cancer. Oral Abstract Session, Gastrointestinal (Noncolorectal) Cancer presented at 2013 ASCO Annual Meeting, 2013.
7. Ueno H, Ioka T, Ikeda M, *et al*. Randomized phase III study of gemcitabine plus S-1, S-1 alone, or gemcitabine alone in patients with locally advanced and metastatic pancreatic cancer in Japan and Taiwan: GEST study. J Clin Oncol, 2013, 31: 1640–1648.
8. Schober M, Javed MA, Beyer G, *et al*. New advances in the treatment of metastatic pancreatic cancer. Digestion, 2015, 92: 175–184.
9. Zheng L, Wolfgang CL. Which patients with resectable pancreatic cancer truly benefit from oncological resection: is it destiny or biology? Cancer Bio Ther, 2015, 16: 360–362.
10. Jones S, Hruban RH, Kamiyama M, *et al*. Exomic sequencing identifies PALB2 as a pancreatic cancer susceptibility gene. Science, 2009, 324: 217.
11. Bailey P, Chang DK, Nones K, *et al*. Genomic analyses identify molecular subtypes of pancreatic cancer. Nature, 2016, 531: 47–52.
12. Kulemann B, Pitman MB, Liss AS, *et al*. Circulating tumor cells found

in patients with localized and advanced pancreatic cancer. Pancreas, 2015, 44: 547–550.
13. Yu M, Ting DT, Stott SL, *et al.* RNA sequencing of pancreatic circulating tumour cells implicates WNT signalling in metastasis. Nature, 2012, 487: 510–513.
14. Kulemann B, Liss AS, Warshaw AL, *et al*. KRAS mutations in pancreatic circulating tumor cells: a pilot study. Tumour biology, 2016, 37: 7547–7554.
15. Poruk KE, Valero V, 3rd, Saunders T, *et al*. Circulating tumor cell phenotype predicts recurrence and survival in pancreatic adenocarcinoma. Anna Surg, 2016 Jan 7.
16. Takai E, Totoki Y, Nakamura H, *et al.* Clinical utility of circulating tumor DNA for molecular assessment in pancreatic cancer. Sci Rep, 2015, 5: 18425.
17. Kahlert C, Melo SA, Protopopov A, *et al*. Identification of double-stranded genomic DNA spanning all chromosomes with mutated KRAS and p53 DNA in the serum exosomes of patients with pancreatic cancer. J Bio Chem, 2014, 289: 3869–3875.
18. Melo SA, Luecke LB, Kahlert C, *et al*. Glypican-1 identifies cancer exosomes and detects early pancreatic cancer. Nature, 2015, 523: 177–182.
19. Morinaga S, Nakamura Y, Watanabe T, *et al*. Immunohistochemical analysis of human equilibrative nucleoside transporter-1 (hENT1) predicts survival in resected pancreatic cancer patients treated with adjuvant gemcitabine monotherapy. Ann Surg Oncol, 2012, 3: 558–564.
20. Greenhalf W, Ghaneh P, Neoptolemos JP, *et al.* Pancreatic cancer hENT1 expression and survival from gemcitabine in patients from the ESPAC-3 trial. J Nat Cancer Inst, 2014, 106: 347.
21. Nakagawa N, Murakami Y, Uemura K, *et al*. Combined analysis of intratumoral human equilibrative nucleoside transporter 1 (hENT1) and ribonucleotide reductase regulatory subunit M1 (RRM1) expression is a powerful predictor of survival in patients with pancreatic carcinoma treated with adjuvant gemcitabine-based chemotherapy after operative resection. Surgery, 2013, 153: 565–575.
22. Wong A, Soo RA, Yong WP, *et al*. Clinical pharmacology and pharmacogenetics of gemcitabine. Drug Metab Rev, 2009, 41: 77–88.
23. Marechal R, Bachet JB, Mackey JR, *et al*. Levels of gemcitabine transport and metabolism proteins predict survival times of patients treated with gemcitabine for pancreatic adenocarcinoma. Gastroenterology, 2012, 143: 664–674.
24. Ohmine K, Kawaguchi K, Ohtsuki S, *et al*. Quantitative targeted proteomics of pancreatic cancer: deoxycytidine kinase protein level correlates to progression-free survival of patients receiving gemcitabine treatment. Mol Pharm, 2015, 12: 3282–3291.
25. Xiong J, Altaf K, Ke N, *et al*. dCK Expression and gene polymorphism With gemcitabine chemosensitivity in patients with pancreatic ductal adenocarcinoma: a strobe-compliant observational study. Medicine, 2016, 95: e2936.
26. Fisher SB, Patel SH, Bagci P, *et al*. An analysis of human equilibrative nucleoside transporter-1, ribonucleoside reductase subunit M1, ribonucleoside reductase subunit M2, and excision repair cross-complementing gene-1 expression in patients with resected pancreas adenocarcinoma: implications for adjuvant treatment. Cancer, 2013, 119: 445–453.
27. Ulker M, Duman BB, Sahin B, *et al*. ERCC1 and RRM1 as a predictive parameter for non-small cell lung, ovarian or pancreas cancer treated with cisplatin and/or gemcitabine. Contemp Oncol, 2015, 19: 207–213.
28. Wang C, Zhang W, Fu M, *et al.* Establishment of human pancreatic cancer gemcitabineresistant cell line with ribonucleotide reductase overexpression. Oncol Rep, 2015, 33: 383–390.
29. Kurata N, Fujita H, Ohuchida K, *et al.* Predicting the chemosensitivity of pancreatic cancer cells by quantifying the expression levels of genes associated with the metabolism of gemcitabine and 5-fluorouracil. Int J Oncol, 2011, 39: 473–482.
30. Le Calve B, Griveau A, Vindrieux D, *et al*. Lysyl oxidase family activity promotes resistance of pancreatic ductal adenocarcinoma to chemotherapy by limiting the intratumoral anticancer drug distribution. Oncotarget, 2016 April 1.
31. Provenzano PP, Cuevas C, Chang AE, *et al*. Enzymatic targeting of the stroma ablates physical barriers to treatment of pancreatic ductal adenocarcinoma. Cancer Cell, 2012, 21: 418–429.
32. Sunil R. Hingorani WPH, Joseph Thaddeus Beck, Boris A. Berdov, et al. Final results of a phase Ib study of gemcitabine plus PEGPH20 in patients with stage IV previously untreated pancreatic cancer. 2015 Gastrointestinal Cancers Symposium Abstract presented at ASCO Gastrointestinal Cancers Symposium Abstract; January, 15, 2015, 2015.
33. Sunil R. Hingorani WPH, Tara Elisabeth Seery, Lei Zheng, *et al*. Interim results of a randomized phase II study of PEGPH20 added to nab-paclitaxel/gemcitabine in patients with stage IV previously untreated pancreatic cancer. 2016 Gastrointestinal Cancers Symposium Abstract; 2016.
34. Kaufman B, Shapira-Frommer R, Schmutzler RK, *et al.* Olaparib monotherapy in patients with advanced cancer and a germline BRCA1/2 mutation. J Clin Oncol, 2015, 33: 244–250.
35. Lowery MA, Kelsen DP, Stadler ZK, *et al.* An emerging entity: pancreatic adenocarcinoma associated with a known BRCA mutation: clinical descriptors, treatment implications, and future directions. Oncol, 2011, 16: 1397–1402.
36. Foley K, Kim V, Jaffee E, Zheng L. Current progress in immunotherapy for pancreatic cancer. Cancer letters, 2015 Dec 23.
37. Lutz ER, Wu AA, Bigelow E, *et al.* Immunotherapy converts nonimmunogenic pancreatic tumors into immunogenic foci of immune regulation. Cancer Immunology Res, 2014, 2: 616–631.
38. Soares KC, Rucki AA, Wu AA, *et al*. PD-1/PD-L1 blockade together with vaccine therapy facilitates effector T-cell infiltration into pancreatic tumors. J Immunother, 2015, 3: 1–11.
39. Soares KC, Rucki AA, Kim V, *et al*. TGF-beta blockade depletes T regulatory cells from metastatic pancreatic tumors in a vaccine dependent manner. Oncotarget, 2015, 6: 43005–43015.

DOI 10.1007/s10330-016-0158-4
Cite this article as: Chen JL, Chu YM, He J, *et al*. Precision medicine in the treatment of pancreatic ductal adenocarcinoma. Oncol Transl Med, 2016, 2: 150–155.

Oncology and Translational Medicine
DOI 10.1007/s10330-016-0163-7

August 2016, Vol. 2, No. 4, P156–P164

ORIGINAL ARTICLE

Anticancer effect and enhanced chemotherapy potential of resveratrol in human pancreatic cancer cell lines*

Sumei Chen[1], Ke Zhang[1] (Co-first author), Yuanyuan Chen[1], Ruzhen Zheng[1], Penjun Zhao[1], Jianwei Zhu[2], Shuming Wu[3], Qinghua Deng[1, 4] (✉), Shenglin Ma[1, 4] (✉), Guangsu Xiong[3] (✉)

[1] Department of Radiation Oncology, Hangzhou Cancer Hospital, Hangzhou 310002, China
[2] Department of Oncology, Hangzhou Cancer Hospital, Hangzhou 310002, China
[3] Division of Gastroenterology and Hepatology, Renji Hospital, Shanghai Jiao Tong University, Shanghai Institute of Digestive Disease, Shanghai 200001, China
[4] Affiliated Hangzhou First People's Hospital of Zhejiang Chinese Medical University, Hangzhou 310006, China

Abstract

Objective Gemcitabine, the only approved drug for the treatment of pancreatic cancer, is not very effective. Novel and effective cancer chemopreventive agents are urgently needed. Recently, emerging studies determined resveratrol possessed anticancer effects on various cancer cells. We explored the anticancer effect of resveratrol in pancreatic cancer cells and investigated the involved moleculars of action. We also examined whether resveratrol enhanced antitumor activity of gemcitabine *in vitro*.

Methods Proliferation inhibition was assessed by cell count kit-8 assay. Cell cycle phase distribution and apoptotic cells were measured by flow cytometric analysis. We determined the expression of bcl-2, cyclinD1, and activation of caspases-3 and poly (ADP-ribose) polymerase1 proteins used Western blot analysis.

Results Resveratrol inhibited the proliferation of three pancreatic cancer cell lines in a dose dependent fashion, and induced accumulation of cells at the G1 phase as well as apoptosis. Our data also demonstrated that resveratrol enhanced gemcitabine-induced apoptosis in pancreatic cancer cells. In addition, resveratrol inhibited the expression of cyclinD1, bcl-2, and induced activation of caspase-3 and poly (ADP-ribose) polymerase1.

Conclusion Our results suggested that resveratrol might be not only a potential regimen, but also an effective chemosensitizer for the chemotherapy of pancreatic cancer.

Key words: resveratrol; gemcitabine; pancreatic cancer; apoptosis; proliferation

Received: 28 May 2016
Revised: 26 July 2016
Accepted: 5 August 2016

In the United States, it was estimated that 45,220 men and women would be diagnosed with pancreatic cancer (PaCa) and 38,460 would die from this disease in 2013. [1]. PaCa is ranked as the fourth leading cause of cancer-related deaths after lung, prostate (breast in women), and colorectal cancer in the United States since the 1970s, with a relative 5-year survival rate of only 5%–6% [2]. Metastatic disease present at the time of first diagnosis, aggressive progression, and limited effective therapies account for the high mortality. Surgical resection may provide the only chance for a cure or long-term survival in PaCa patients. However, most PaCa patients with locally advanced or incurable metastatic disease are diagnosed for the first time, and only 15%–20% of patients with potentially resectable disease have the chance for surgery at presentation. Furthermore, over 80% of patients experience recurrence within 2 years of surgery [3–4]. Median survival after recurrence is 7 months for local and 3 months for metastatic recurrence cases [5]. Thus, palliative treatment may be a good choice for patients with ad-

✉ Correspondence to: Guangsu Xiong, Email: wusm2002@hotmail.com; Shenglin Ma, Email: mashenglin@medmail.com.cn; Qinghua Deng, Email: dengqinghua69@163.com

* Supported by grants from the Eight Natural Science Foundation (No. 81272611) and Major Science and Technology Innovation Project of Hangzhou (No. 20112312A01), China.

vanced-stage PaCa. Gemcitabine, the only approved drug for the treatment of PaCa, offers a poor partial response (< 6%) in patients [6]. This disappointing outcome strongly suggests that novel, effective, and less toxic chemopreventive agents or chemosensitizers are urgently needed.

Resveratrol (trans-3, 4′,5-trihydroxy-trans-stilbene) is found in more than 70 plant species, including grapes, peanuts, berries, and pines, and is particularly abundant in the skin of red grapes (50 to 100 μg of resveratrol per gram wet weight) [7–8]. It is produced by plants in response to infection by the pathogen Botrytis cinerea [9]. This compound might account for the reduced risk of coronary heart disease in individuals with moderate red wine consumption [10–11].

Since 1997 when Jang *et al* [12] demonstrated that resveratrol had cancer-chemopreventive activity in three major phases of carcinogenesis, namely initiation, promotion, and progression, numerous studies about the anticancer effect of this compound have emerged. Extensive experimental data have shown that resveratrol induced growth inhibition, cell cycle arrest, apoptosis, blockade of angiogenesis, and inhibited metastasis of numerous cancers, such as gastric carcinoma [13], colorectal cancer [14], skin cancer [15], glioma [16], and lung carcinoma [17]. Despite the potential interest, very little data are available regarding the precise mechanism underlying the anticancer effect of this compound. It is also not known whether resveratrol can potentiate the effect of gemcitabine in PaCa cells.

Therefore, we investigated whether resveratrol induces an anticancer effect on human PaCa cells, and if it can potentiate the effect of gemcitabine in these cells. In addition, we further explored the macromolecules involved in the anticancer effect of this compound.

Materials and methods

Cell culture and experimental reagents

Three human PaCa cell lines (SW1990, PANC-1, and BxPC-3) were used. SW1990 and PANC-1 were stored by our laboratory (Shanghai Institute of Digestive Disease, Shanghai, China). BxPC-3 was a gift from Ruijin Hospital, Shanghai Jiaotong University School of Medicine (Shanghai, China). All cell lines were cultured in Dulbecco's Modified Eagle's Medium (DMEM) supplemented with 10% fetal bovine serum, 100 units/mL penicillin, and 100 mg/mL streptomycin (Gibco BRL, Waltham, MA, USA) in a 5% CO_2 incubator at 37 ℃. All experiments were performed during the exponential growth phase of the cells. Each treatment condition was a single dose of resveratrol at the indicated concentration or 0.1% dimethyl sulfoxide (DMSO; vehicle) as control.

Resveratrol (trans-3,4′,5-trihydroxystilbene) and propidium iodide (PI) were purchased from Sigma-Aldrich Corp. (St. Louis, MO, USA). A stock solution of resveratrol was prepared in DMSO at a concentration of 250 mmol/L and stored in the dark at –20 ℃. The DMSO concentration in all drug-treated cells was always less than 0.1% (v/v). Gemcitabine was purchased from Jiangsu Hansen Pharmaceutical Co., Ltd (Jiangsu Province, China). The annexin V/fluorescein isothiocyanate (FITC)-PI staining kit was obtained from BD Biosciences Inc. (Heidelberg, Germany). Cell Counting Kit-8 (CCK-8) was obtained from Dōjindo Laboratories (Kumamoto, Japan). The probes used were rabbit anti- BCL2, apoptosis regulator (Bcl-2), anti-procaspase-3, and anti-activated caspase-3 polyclonal antibodies; rabbit anti-α-tubulin monoclonal antibody (Cell Signaling Technology, Danvers, MA, USA); and mouse anti-cyclin D1 antibody (Santa Cruz Biotechnology, Inc., Dallas, TX, USA). Goat anti-rabbit/mouse horseradish peroxidase (HRP)-conjugated secondary antibody was from Cell Signaling Technology (Danvers, MA, USA).

Proliferation assay

Antiproliferative effect of resveratrol in human pancreatic cancer cells was analyzed by CCK-8 assay. Briefly, SW1990, PANC-1, and BXPC-3 cells (5000 per well) were incubated in 96-well plates overnight and treated with various doses of resveratrol, or the combination of resveratrol and gemcitabine for 24, 48, and 72 h. Treatment with each concentration was repeated three times in three replicates. After various treatments, the cells were incubated with 100 μL of DMEM supplemented with 10 μL of CCK-8 reagent for 0 to 4 h at 37 °C. Cell viability was determined by scanning the absorbance with a microplate reader at 450 nm. The results were expressed as the percentage of viable cells as follows:

Relative viability (%) = $(A_{450[\text{treated}]} - A_{450[\text{blank}]}) / (A_{450[\text{control}]} - A_{450[\text{blank}]}) \times 100\%$.

Apoptosis and cell cycle analysis by flow cytometry

To quantify the percentage of apoptosis, we performed a flow cytometry analysis. In the resveratrol-alone treatment, cells were seeded in 6-well culture plates overnight and subsequently treated with 50, 100, and 150 μM resveratrol, or were untreated (0.1% DMSO) for 24 h. In the combination treatment, pancreatic cancer cells were treated with resveratrol (50 μM), gemcitabine (2 μM), or a combination of the two compounds. Then, both floating and trypsinized adherent cells were collected and incubated in 500 μL of binding buffer containing 5 μL of annexin-V/FITC for 30 min at 37 °C, and were then treated with 5 μL of PI for 5 min in the dark at room temperature. Analysis was immediately performed using a flow cytometer (BD Biosciences, San Jose, CA, USA). Cells for the cell cycle analysis were washed in cold phosphate-

buffered saline (PBS) twice and incubated in 300 μL of PBS containing 0.5% saponin, 50 μg/mL PI, and RNase 0.1 mg/mL for 30 min at 4 °C. The cells were analyzed by a flow cytometer, and cell-cycle phase distribution was analyzed using the Cell-Fit program. Data acquisition was gated to exclude cell doublets.

Western blot analysis

Western blot analysis was performed using standard techniques, as described previously [18]. Briefly, equal protein aliquots in each sample were resolved in 12% sodium dodecyl sulfate polyacrylamide gel electrophoresis and the proteins were transferred onto nitrocellulose membranes. After blocking with 5% skimmed dried milk, the membranes were incubated with a 1:2000 dilution of primary antibodies. The membranes were then incubated with a horseradish peroxidase-conjugated secondary antibody (1:2000; Pierce, Thermo Fisher Scientific Inc., Waltham, MA, USA). The proteins were detected by an enhanced chemiluminescence detection system (SuperSignal™ West Femto Substrate; Pierce, Thermo Fisher Scientific Inc., Waltham, MA, USA), and light emission was captured on Kodak X-ray films.

Statistical analysis

Unless otherwise indicated, all results were representative of three separate experiments. Values represented the mean ± standard deviation (SD) of these experiments. The statistical significance of differential findings between experimental groups and the control was determined by one-way analysis of variance (ANOVA) using SPSS 13.0 and significance was set at $P < 0.05$.

Results

Cell growth inhibition by resveratrol in pancreatic cancer cells

The cytotoxicity of resveratrol on pancreatic cancer cells was first determined using CCK-8 assay to investigate the effect of resveratrol on cell proliferation in three PaCa cell lines. The decrease in absorbance in this assay could either be a consequence of cell death or cell proliferation inhibition. Resveratrol inhibited growth in all the cell lines (SW1990, PANC-1, and BxPC-3) in a dose-dependent manner (Fig. 1). In addition, we calculated the IC50 in each cell line and found that the sensitivity of the three PaCa cell lines to resveratrol differed. The IC_{50} values of PANC-1, BxPC-3, and SW1990 cells were 118.21 ± 2.91, 117.09 ± 9.94, and 99.97 ± 2.03 μM, respectively.

Cell apoptosis induced by resveratrol

To investigate whether resveratrol induced apoptosis of PaCa cells, three cell lines were treated for 24 h with 50, 100, or 150 μM resveratrol, or 0.1% DMSO. In general, we found that resveratrol induced apoptosis in a dose-dependent fashion in the three cell lines (Fig. 2a). For example, 50 μM resveratrol did not significantly induce apoptosis compared with that in the control group, whereas the 100 μM and 150 μM groups showed a marked increase in apoptosis in PANC-1 cells (Fig. 2b). In the case of SW1990 cells, a similar result was obtained. Nevertheless, in BxPC-3 cells, only 150 μM resveratrol induced marked apoptosis.

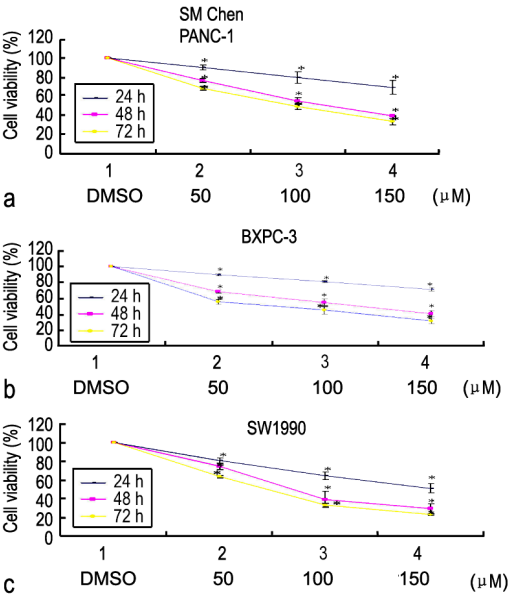

Fig. 1 Effect of resveratrol on PANC-1, BxPC-3, and SW1990 cell proliferation. Dose and time-dependent inhibition of cell proliferation by resveratrol in three pancreatic cancer cell lines. Each value represents the mean ± SD ($n = 4$) of three independent experiments. * $P < 0.05$, compared with the DMSO group

Effect of resveratrol on cell-cycle phase distribution

To investigate resveratrol induced cell proliferation inhibition further, cell-cycle phase distribution was examined using flow cytometry. Compared with control cells, the cell cycle profiles of PANC-1 (Fig. 3a), BxPC-3 (Fig. 3b), and SW1990 (Fig. 3c) changed significantly after incubation with 100 μM of resveratrol for 24 h. In general, resveratrol led to an arrest in the G1 phase, correspondingly, causing a decrease of cells in the S and G2 phases of the cell cycle. As shown in Table 1, the number of cells in the G1 phase significantly increased from 45.70% to 66.79% in PANC-1, from 47.23% to 72.35% in BxPC-3, and from 48.97% to 73.29% in SW1990. The number of cells in the S and G2 phases was decreased in the three PaCa cell lines; although in the PANC-1 cells, the reduction was not significant (Table 1).

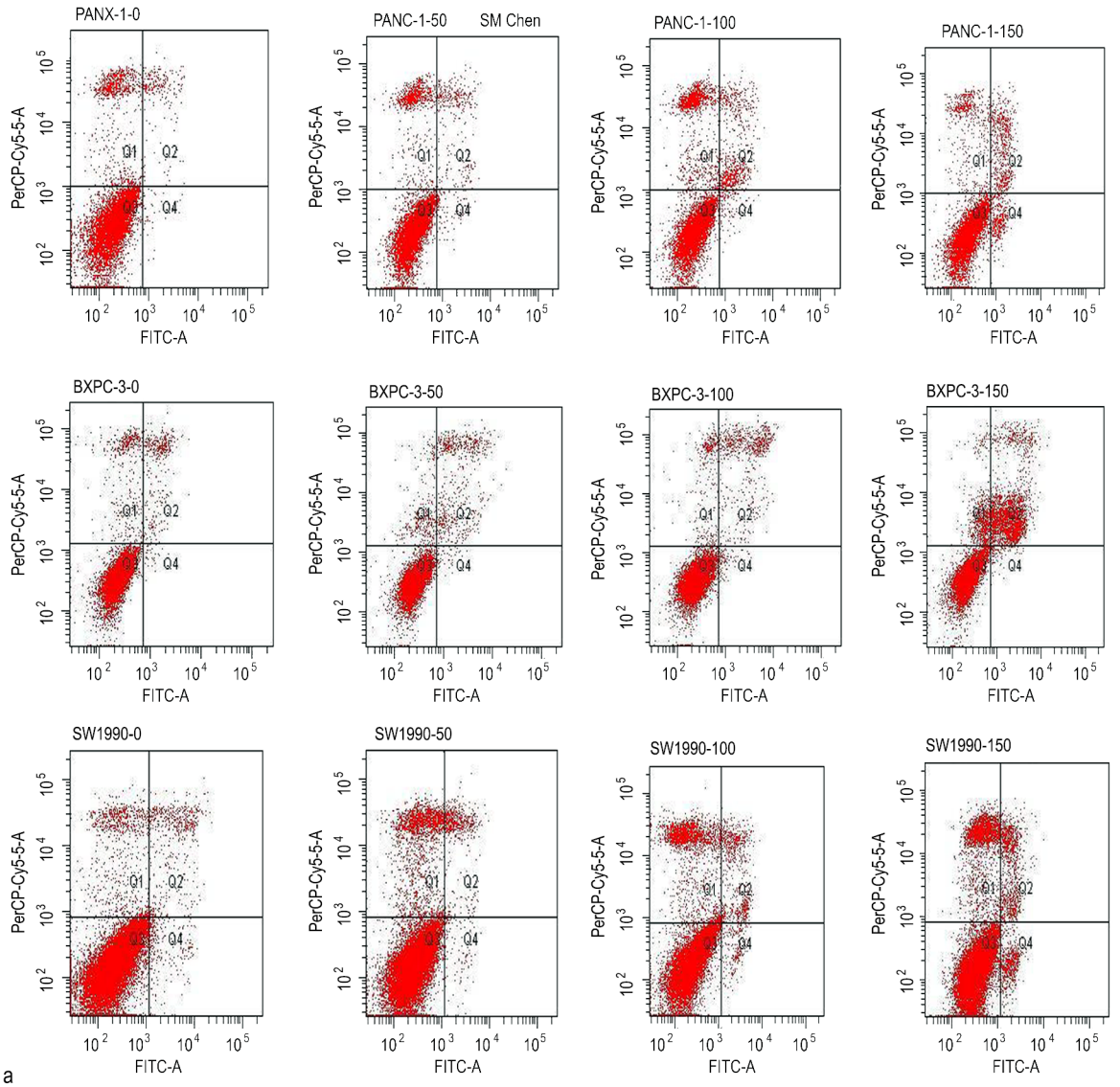

Fig. 2 Effect of resveratrol on PANC-1, BxPC-3, and SW1990 cell apoptosis. PANC-1, BxPC-3, and SW1990 cells were stained and analyzed by flow cytometry to detect Annexin V-FITC positive and/or PI positive cells. The unaffected, early apoptotic, late apoptotic, and necrotic cells are present in the lower left, lower right, upper right, and upper left quadrant, respectively. Representative data from one experiment are shown, and two additional experiments yielded similar results. * $P < 0.05$ and ** $P < 0.01$ compared with the control

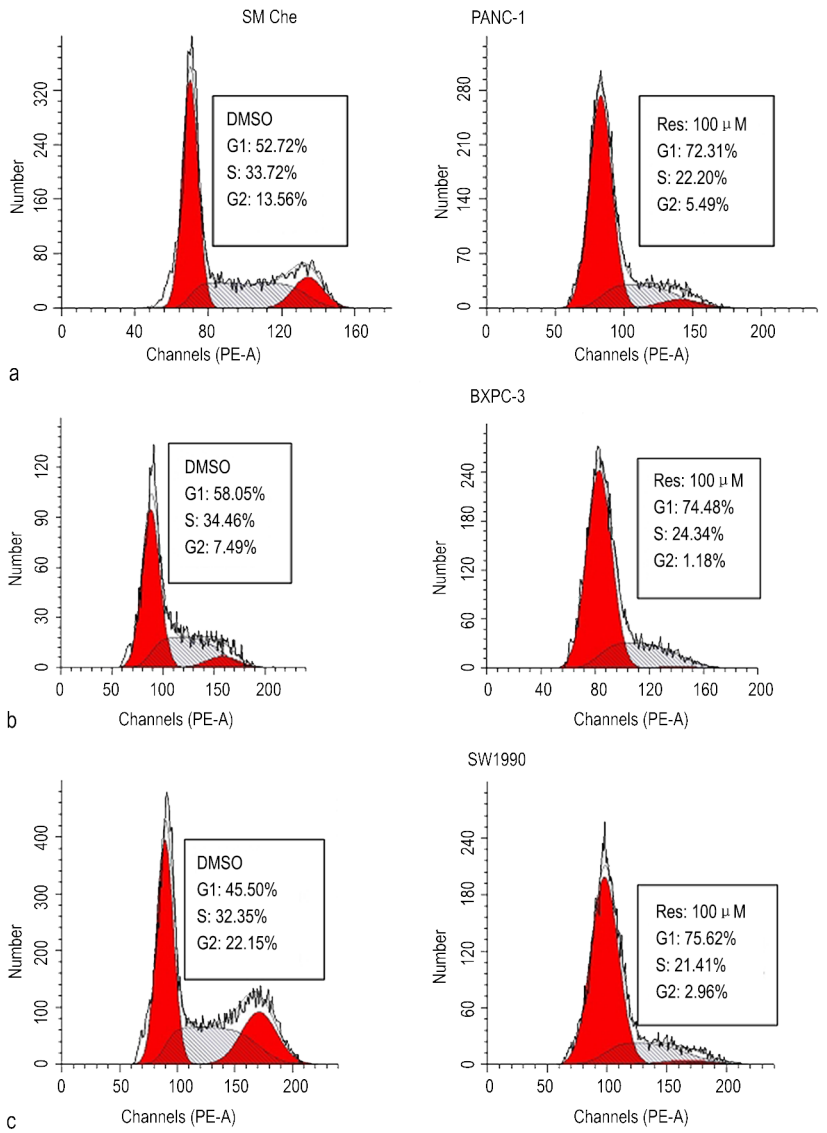

Fig. 3 Analysis of cell-cycle phase distribution by flow cytometry. PANC-1, BxPC-3, and SW1990 cells were treated with 0.1% DMSO, or 100 μM resveratrol for 24 h and incubated in 300 μL PBS containing 0.5% saponin, 50 μg/mL PI, and RNase 0.1 mg/mL for 30 min at 4 ℃ for flow cytometric analysis of DNA content. Representative data from one experiment are shown, and two additional experiments yielded similar results

Resveratrol blocks cyclin D1 and Bcl-2 expression and induces activation of procaspase-3 and poly (ADP-ribose) polymerase 1 in pancreatic cancer cells

To further understand the mechanism of resveratrol-induced cell proliferation inhibition and apoptosis, we examined the expression of cyclin D1, Bcl-2, caspase-3, and poly (ADP-ribose) polymerase 1 (PARP1) after resveratrol treatment. The PaCa cell lines were exposed to 50, 100, 150 μM resveratrol, or 0.1% DMSO for 48 h. Consistent with the results of the cell-cycle phase distribution, the level of cyclin D1 was reduced in a dose-dependent fashion in the PaCa cell lines. A major decrease was seen in the 150 μM group among all cell lines, but in the SW1990 cells 50 μM resveratrol did not significantly reduce protein expression (P = 0.055) (Fig. 4). We also observed that resveratrol repressed Bcl-2 expression, and induced the proteolytic cleavage of procaspase-3 into its 17-kD active form as well as the activation of its substrate PARP1, resulting in effector caspase and activated PARP1 up-regulation (Fig. 4). In conclusion, these data suggested that cell growth inhibition and apoptosis were at least in part related to the expression levels of cyclin D1 and Bcl-2 as well as activated caspase-3 and PARP1, although the sensitivity to resveratrol was dependent on the individual cell type.

Cell growth inhibition with a combination of resveratrol and gemcitabine

We also investigated whether resveratrol enhanced antitumor activity of gemcitabine in PANC-1 and BxPC-3 cells. As detected by the CCK-8 assay, data showed that

Table 1 Effects of resveratrol on PANC-1, BxPC-3, and SW1990 cell-cycle phase distribution

Cell	Treatments	G1 (%)	S (%)	G2 (%)
PANC-1	DMSO	45.70 ± 6.72	37.65 ± 7.83	16.65 ± 4.98
	100 μM	66.79 ± 6.93*	29.86 ± 8.93	3.35 ± 2.94*
BXPC-3	DMSO	48.97 ± 9.56	37.14 ± 3.42	13.89 ± 6.26
	100 μM	73.29 ± 1.1*	24.22 ± 1.97**	2.49 ± 2.61*
SW1990	DMSO	47.23 ± 2.46	37.25 ± 6.22	15.52 ± 6.3
	100 μM	72.35 ± 3.21**	20.85 ± 1.09*	3.46 ± 2.55*

* $P < 0.05$ and ** $P < 0.01$ versus the DMSO group. Values are the mean and SD of three independent assays

the resveratrol (50 μM), gemcitabine (2 μM), and combination (50 μM resveratrol and 2 μM gemcitabine) treatment decreased the growth of PaCa cells in a time-dependent manner (Fig. 5). However, the combination treated cells showed a more significant decrease ($P < 0.05$). After treatment for 24 h, 48 h, and 72 h, the inhibition in rate of cell growth in the combination group was 31.36 ± 7.34%, 61.03 ± 0.52%, and 67.26 ± 3.27%, respectively.

Cell apoptosis induced by resveratrol and gemcitabine

Cell apoptosis induced by resveratrol and gemcitabine was detected in PANC-1 and BxPC-3 cells. As shown in Fig. 6, 48 h after various treatments the apoptosis rates in the DMSO (0.1%), resveratrol (50 μM), gemcitabine (2 μM), and combination (50 μM and 2 μM) group were 4.34 ± 1.53%, 12.80 ± 1.71%, 16.07 ± 1.34%, and 23.3 ± 3.01% in PANC-1 cells, respectively; and in BxPC-3 cells were 7.87 ± 0.8%, 13.33 ± 1.21%, 16.50 ± 5.30%, and 29.07 ± 3.59%, respectively. This meant that resveratrol could significantly increase cell apoptosis induced by gemcitabine ($P < 0.05$). Taken together, our data demonstrate that resveratrol not only inhibited cell growth but also enhanced gemcitabine-induced apoptosis in PaCa cells, and that resveratrol markedly enhanced the chemosensitivity of these cells.

Discussion

Pancreatic cancer is a highly aggressive malignant disease, which is currently treated using available chemotherapy regimens but with limited success and dismal outcomes. Gemcitabine, the only approved drug, has not resulted in radically improved outcomes for the treatment of PaCa. Over several decades, numerous agents have been tested in combination with gemcitabine including erlotinib, platinum analogs, bevacizumab, and celecoxib, but all have afforded disappointing results [19]. Emerging evidence suggests that many dietary compounds exhibit beneficial effects for the prevention of cancer [20–22]. Resveratrol is derived from a Chinese traditional medicinal plant (Polygonum cuspidatum) as well as grapes, peanuts, berries, and pines, and is regarded as safe to consume [8]. Extensive data show that resveratrol affects tumor initiation, promotion, and progression, and suppresses angiogenesis and metastasis by involving multiple pathways [8]. Consistent with previous reports, this study demonstrated that resveratrol induced cell growth inhibition and apoptosis in a dose-dependent manner in SW1990, PANC-1, and BxPC-3 PaCa cell lines. The mechanism of resveratrol's anticancer effect is not fully understood. Yang Shu found that resveratrol elicits anti-colorectal cancer effect by activating miR-34c that targets KIT ligand *in vitro* and *in vivo* [23]. In this study, we found that resveratrol blocked cell cycle progression in three PaCa cell lines with cells remaining in the G1 phase, which resulted in cell proliferation inhibition. To explore which proteins may be involved in resveratrol-induced cell proliferation inhibition and apoptosis, we investigated the cell cycle regulator, cyclin D1, and apoptotic proteins Bcl-2, caspase-3, and PARP1. Western blot analysis showed that resveratrol repressed cyclin D1 and Bcl-2 expression in a dose-dependent fashion and upregulated activation of caspase-3. We also observed that the proteolytic cleavage of procaspase-3 was followed by proteolytic degradation of PARP1, a specific substrate of both effector caspases-

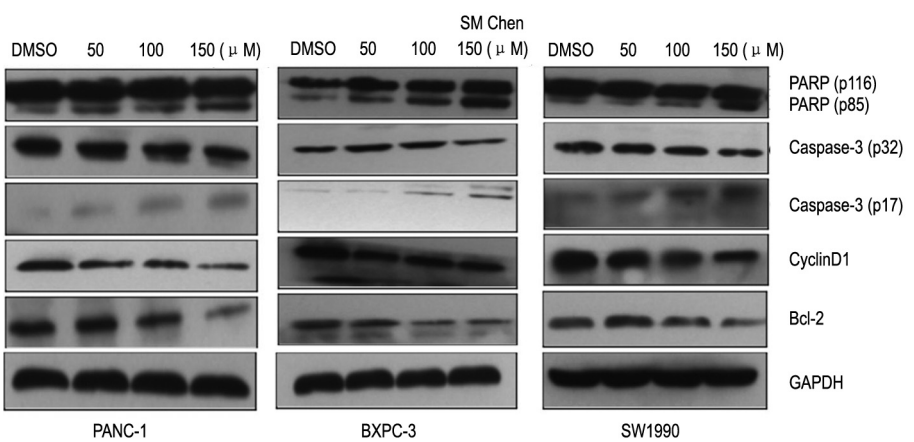

Fig. 4 Effect of resveratrol on expression of cell cycle- and apoptosis-related proteins. Pancreatic cancer cells were incubated with increasing concentrations of resveratrol for 48 h. Levels of Bcl-2, cyclin D1, caspase-3, and PARP1 proteins were detected by western blotting. GAPDH was inserted as a control. Results are representative of three independent experiments

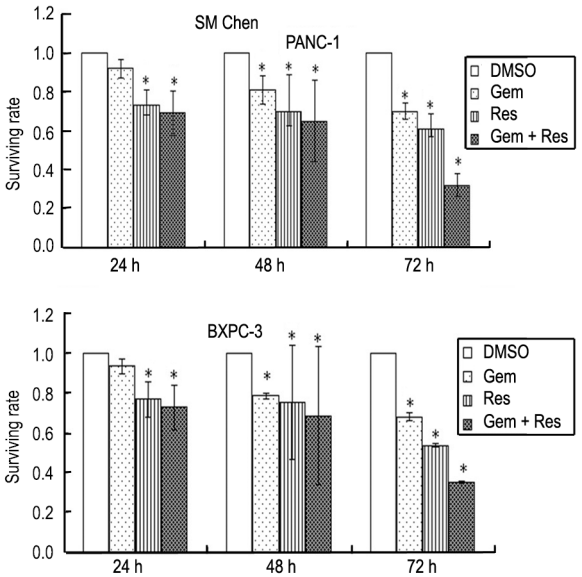

Fig. 5 Synergistic effect of resveratrol and gemcitabine on PANC-1 and BxPC-3 cells. Dose and time-dependent inhibition of cell proliferation were observed. Each value represents the mean ± SD (n = 4) of three independent experiments. * P < 0.05, compared with the DMSO group

3 and -7, suggesting that resveratrol-induced cleavage of procaspase-3 leads to activation of the protease. This down-regulation of cyclin D1 may be related with the G1 arrest observed. Cyclin D1 appears in the G1 phase and interacts with cyclin-dependent kinase (CKD) regulating the progression of cells from late G1 phase into the S phase. Cells accumulated in the G1 phase, and correspondingly, the percentage of cells in the S and G2/M phase decreased. The results suggest that resveratrol could reduce DNA synthesis and induce DNA fragmentation in all three examined cell lines.

In chemotherapeutic drug-induced apoptosis of tumor cells, three different death signaling pathways lead to apoptosis [22], namely the extrinsic death receptor-dependent pathway [23], the intrinsic mitochondria-dependent pathway [24], and the intrinsic endoplasmic reticulum (ER) stress-mediated pathway [25]. The mitochondria-dependent death signaling begins with the release of mitochondrial cytochrome c into the cytoplasm, which together with the apoptotic protease activating factor-1 (APAF-1) activates caspase-9 in the presence of dATP, and then activates caspase-3, leading to cell death [26–27]. In the ER stress-mediated apoptotic pathway, activation of caspase-12 can directly activate caspase-9 [28–29] .ER stress also triggers activation of caspase-8 and c-jun N-terminal kinase (JNK), both of which are known to cause mitochondrial cytochrome c release [30–31]. Thus, the caspases, a family of cysteine-dependent aspartate-directed proteases, appear to be involved in three different death signaling pathways, and caspase-3 is at the intersection of these pathways. We also found that the proteolytic cleavage of procaspase-3 was followed by proteolytic degradation of PARP1, a substrate of caspase-3, suggesting that resveratrol induced activation of procaspase-3 leads to activation of the protease. Proteolytic degradation of PARP1 results in DNA fragmentation in the process of apoptosis, which is known to play an important role in protecting chromosomal DNA [32].

The Bcl-2 family is another critical component involved in apoptosis. The family includes a number of

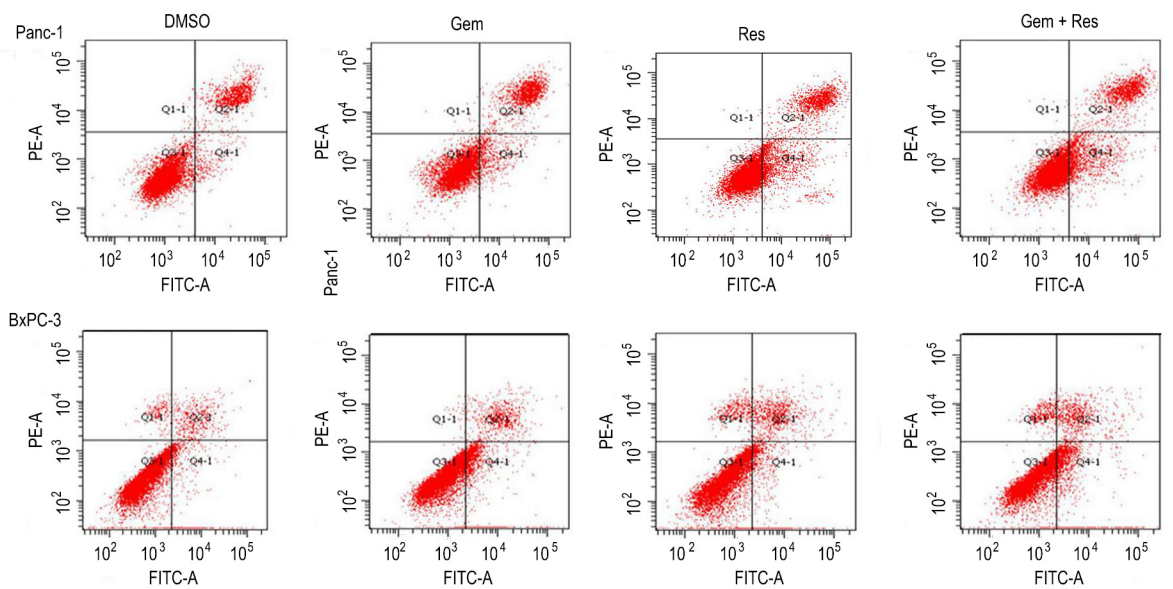

Fig. 6 Synergistic apoptotic effect of resveratrol and gemcitabine on PANC-1 and BxPC-3 cells. Representative data from one experiment are shown, and two additional experiments yielded similar results. * P < 0.05 and ** P < 0.01 compared with the control

proteins, which have homologous amino acid sequences, including antiapoptotic members such as Bcl-2, BCL2 like 1 (bcl-xL), and X-linked inhibitor of apoptosis (XIAP), as well as proapoptotic members including BCL2 associated X, apoptosis regulator (BAX). Interestingly, Kirsch [33] found that the Bcl-2 protein was cleaved at Asp-34 by caspases during apoptosis and by recombinant caspase-3 in vitro. Arnoult [34] also observed that antiapoptotic proteins, Bcl-2, bcl-xL, and XIAP, are cleaved by caspase-3 and are converted to proapoptotic proteins similar to BAX. The proapoptotic Bcl-2 cleavage product localizes on the mitochondrial membrane and causes a release of cytochrome c [35–36], and then triggers mitochondria-dependent death signaling and results in apoptosis. In this study, we examined the expression of Bcl-2 protein, to confirm the participation of caspases in cell death. The results showed that resveratrol induced activation of caspase-3 and repressed Bcl-2 expression. Therefore, it seems that the apoptotic effects of resveratrol are accomplished by a caspases signaling-dependent mechanism through the downregulation of Bcl-2.

We next tried to determine whether resveratrol has potential in combination with gemcitabine in the treatment of PaCa, one of the most lethal cancers. We found that resveratrol not only inhibited cell growth but also enhanced gemcitabine-induced apoptosis in the cells. Our results were in agreement with a previous report that resveratrol when used in combination with gemcitabine, was highly effective in inducing apoptosis in PaCa cells [37]. It has been speculated that downregulation of NF-κB, which was constitutively activated in PaCa, could be one of the mechanisms to explain this observation. However, the mechanism of the observed synergistic effects of the combinatorial treatment was not fully investigated. As far as we know NF-κB, which mediates inflammatory signaling pathway closely linked to drug resistance, also regulates Bcl-xL, Bcl-2, prostaglandin-endoperoxide synthase 2 (PTGS2 or COX2), cyclin D1, vascular endothelial growth factor A (VEGFA), and matrix metallopeptidase 9 (MMP-9). In the present study, we also observed that resveratrol inhibited protein expression of cyclin D1 and Bcl-2, and induced activation of caspase-3 and PARP1, which may explain why resveratrol enhanced anticancer activity of gemcitabine in pancreatic cancer.

Conclusions

Our results showed that resveratrol played an important role in cell proliferation inhibition, cell cycle arrest, and apoptosis in pancreatic cancer cells. In addition, resveratrol markedly increased the chemosensitivity of pancreatic cancer cells to gemcitabine. Nevertheless, we did not explore the anticancer effect of this compound *in vivo*. In the present study, we only investigated the expression level of Bcl-2, caspase-3, and PARP1, but did not explore the precise interaction of these proteins in the apoptosis progression. Therefore, to obtain a better understanding of its chemopreventive activity, the cell death signaling pathways of resveratrol-induced apoptosis in the PaCa cell should be fully explored. Furthermore, the potential biological activities of resveratrol *in vivo* should be investigated in future studies. Based on these results, further studies are required to explore the potential of resveratrol as an anticancer agent for pancreatic cancer treatment.

Conflicts of interest

The authors indicated no potential conflicts of interest.

References

1. Siegel R, Naishadham D, Jemal A. Cancer Statistics, 2013. CA Cancer J Clin, 2013, 63: 11–30.
2. Jemal A, Siegel R, Xu J, *et al.* Cancer statistics, 2010. CA Cancer J Clin, 2010, 60: 277–300.
3. Hattangadi JA, Hong TS, Yeap BY, *et al*. Results and patterns of failure in patients treated with adjuvant combined chemoradiation therapy for resected pancreatic adenocarcinoma. Cancer, 2009, 115: 3640–3650.
4. Hernandez JM, Morton CA, Al-Saadi S, *et al.* The natural history of resected pancreatic cancer without adjuvant chemotherapy. Am Surg, 2010,76: 480–485.
5. Sperti C, Pasquali C, Piccoli A, *et al*. Recurrence after resection for ductal adenocarcinoma of the pancreas. World J Surg, 1997, 21: 195–200.
6. Chua YJ, and Cunningham D. Chemotherapy for advanced pancreatic cancer. Best Pract Res Clin Gastroenterol, 2006, 20: 327–348.
7. Baliga MS, Meleth S, Katiyar SK. Growth inhibitory and antimetastatic effect of green tea polyphenols on metastasis-specific mouse mammary carcinoma 4T1 cells in vitro and in vivo systems. Clin Cancer Res, 2005, 11: 1918–1927.
8. Athar M, Back JH, Tang X, *et al*. Resveratrol: a review of preclinical studies for human cancer prevention. Toxicol Appl Pharmacol, 2007, 224: 274–283.
9. Delmas D, Lancon A, Colin D, *et al.* Resveratrol as a chemopreventive agent: a promising molecule for fighting cancer. Curr Drug Targets, 2006, 7: 423–442.
10. Goldberg DM, Hahn SE, Parkes JG. Beyond alcohol: beverage consumption and cardiovascular mortality. Clin Chim Acta, 1995, 237: 155–187.
11. Rimm EB. Alcohol consumption and coronary heart disease: good habits may be more important than just good wine. Am J Epidemiol, 1996, 143: 1094–1098.
12. Jang M, Cai L, Udeani GO, *et al.* Cancer chemopreventive activity of resveratrol, a natural product derived from grapes. Science, 1997, 275: 218–220.
13. Holian O, Wahid S, Atten MJ, *et al*. Inhibition of gastric cancer cell proliferation by resveratrol: role of nitric oxide. Am J Physiol Gastrointest Liver Physiol, 2002, 282: G809–816.
14. Delmas D, Rebe C, Lacour S, *et al.* Resveratrol-induced apoptosis is associated with Fas redistribution in the rafts and the formation of a death-inducing signaling complex in colon cancer cells. J Biol Chem, 2003, 278: 41482–41490.
15. Reagan-Shaw S, Afaq F, Aziz MH, *et al*. Modulations of critical cell

cycle regulatory events during chemoprevention of ultraviolet B-mediated responses by resveratrol in SKH-1 hairless mouse skin. Oncogene, 2004, 23: 5151–5160.
16. Chen JC, Chen Y, Lin JH, *et al*. Resveratrol suppresses angiogenesis in gliomas: evaluation by color Doppler ultrasound. Anticancer Res, 2006, 26: 1237–1245.
17. Busquets S, Ametller E, Fuster G, *et al*. Resveratrol, a natural diphenol, reduces metastatic growth in an experimental cancer model. Cancer Lett, 2007, 245: 144–148.
18. Xiong GS, Sun HL, Wu SM, *et al.* Small interfering RNA against the apurinic or apyrimidinic endonuclease enhances the sensitivity of human pancreatic cancer cells to gemcitabine *in vitro*. J Dig Dis, 2010, 11: 224–230.
19. Rocha-Lima, CM. New directions in the management of advanced pancreatic cancer: a review. Anticancer Drugs, 2008, 19: 435–446.
20. Sarkar FH, Li Y. Soy isoflavones and cancer prevention. Cancer Invest, 2003, 21: 744–757.
21. Sarkar FH, Li Y. Indole-3-carbinol and prostate cancer. J Nutr, 2004, 134: 3493S–3498S.
22. Siddiqui IA, Sanna V, Ahmad N, *et al.* Resveratrol nanoformulation for cancer prevention and therapy. ANN N Y Acad Sci, 2015, 1348: 20–31.
23. Yang S, Li W, Sun H, *et al*. Resveratrol elicits anti-colorectal cancereffect by activating miR-34c-KITLG *in vitro* and *in vivo*. BMC Cancer, 2015, 15: 969.
24. Woo HJ, Jun do Y, Lee JY, *et al*. Apoptogenic activity of 2alpha, 3alpha-dihydroxyurs-12-ene-28-oic acid from Prunella vulgaris var. lilacina is mediated via mitochondria-dependent activation of caspase cascade regulated by Bcl-2 in human acute leukemia Jurkat T cells. J Ethnopharmacol, 2011, 135: 626–635.
25. Wallach D, Boldin M, Varfolomeev E, *et al.* Cell death induction by receptors of the TNF family: towards a molecular understanding. FEBS Lett, 1997, 410: 96–106.
26. Desagher S, Martinou JC. Mitochondria as the central control point of apoptosis. Trends Cell Biol, 2000, 10: 369–377.
27. Nakagawa T, Yuan J. Cross-talk between two cysteine protease families. Activation of caspase-12 by calpain in apoptosis. J Cell Biol, 2000, 150: 887–894.
28. Kaufmann SH, Earnshaw WC. Induction of apoptosis by cancer chemotherapy. Exp Cell Res, 2000, 256: 42–49.
29. Herr I, Debatin KM. Cellular stress response and apoptosis in cancer therapy. Blood, 2001, 98: 2603–2614.
30. Morishima N, Nakanishi K, Takenouchi H, *et al.* An endoplasmic reticulum stress-specific caspase cascade in apoptosis. Cytochrome c-independent activation of caspase-9 by caspase-12. J Biol Chem, 2002, 277: 34287–34294.
31. Rao RV, Castro-Obregon S, Frankowski H, *et al*. Coupling endoplasmic reticulum stress to the cell death program. An Apaf-1-independent intrinsic pathway. J Biol Chem, 2002, 277: 21836–21842.
32. Jimbo A, Fujita E, Kouroku Y, Ohnishi J, *et al.* ER stress induces caspase-8 activation, stimulating cytochrome c release and caspase-9 activation. Exp Cell Res, 2003, 283: 156–166.
33. Urano F, Wang X, Bertolotti A, *et al.* Coupling of stress in the ER to activation of JNK protein kinases by transmembrane protein kinase IRE1. Science, 2000, 287: 664–666.
34. Park JA, Lee KY, Oh YJ, *et al*. Activation of caspase-3 protease via a Bcl-2-insensitive pathway during the process of ginsenoside Rh2-induced apoptosis. Cancer Lett, 1997, 121: 73–81.
35. Kirsch DG, Doseff A, Chau BN, *et al.* Caspase-3-dependent cleavage of Bcl-2 promotes release of cytochrome c. J Biol Chem, 1999, 274: 21155–21161.
36. Arnoult D. Apoptosis-associated mitochondrial outer membrane permeabilization assays. Methods, 2008, 44: 229–234.
37. Kluck RM, Bossy-Wetzel E, Green DR, *et al.* The release of cytochrome c from mitochondria: a primary site for Bcl-2 regulation of apoptosis. Science, 1997, 275: 1132–1136.
38. Yang J, Liu X, Bhalla K, *et al*. Prevention of apoptosis by Bcl-2: release of cytochrome c from mitochondria blocked. Science, 1997, 275: 1129–1132.
39. Harikumar KB, Kunnumakkara AB, Sethi G, *et al.* Resveratrol, a multitargeted agent, can enhance antitumor activity of gemcitabine in vitro and in orthotopic mouse model of human pancreatic cancer. Int J Cancer, 2010, 127: 257–268.

DOI 10.1007/s10330-016-0163-7
Cite this article as: Chen SM, Zhang K, Chen YY, *et al*. Anticancer effect and enhanced chemotherapy potential of resveratrol in human pancreatic cancer cell lines. Oncol Transl Med, 2016, 2: 156–164.

Oncology and Translational Medicine
DOI 10.1007/s10330-016-0155-7

August 2016, Vol. 2, No. 4, P165–P168

ORIGINAL ARTICLE

Mammography combined with breast dynamic contrast-enhanced-magnetic resonance imaging for the diagnosis of early breast cancer

Yakun He, Guohui Xu (✉), Jin Ren, Bin Feng, Xiaolei Dong, Hao Lu, Changjiu He

Department of Radiology, Sichuan Cancer Hospital, Chengdu 610041, China

Abstract

Objective The aim of this study was to investigate the application of mammography combined with breast dynamic contrast-enhanced magnetic resonance imaging (DCE-MRI) for the diagnosis of early breast cancer.

Methods Mammography and DCE-MRI were performed for 120 patients with breast cancer (malignant, 102; benign; 18).

Results The sensitivity of mammography for early diagnosis of breast cancer was 66.67%, specificity was 77.78%, and accuracy was 68.33%. The sensitivity of MRI for early diagnosis of breast cancer was 94.12%, specificity was 88.89%, and accuracy was 93.33%. However, the sensitivity of mammography combined with DCE-MRI volume imaging with enhanced water signal (VIEWS) scanning for early diagnosis of breast cancer was 97.06%, specificity was 94.44%, and accuracy was 96.67%.

Conclusion Mammography combined with DCE-MRI increased the sensitivity, specificity, and accuracy of diagnosing early breast cancer.

Received: 26 March 2016
Revised: 28 April 2016
Accepted: 25 May 2016

Key words breast carcinoma; mammography; nuclear magnetic resonance; dynamic enhancement; time signal curve

In recent years, there has been an upward trend in the incidence of breast cancer in our country, and it tends to occur at a younger age. Further, breast cancer has become one of the most common malignant tumors in women, and is therefore one of the most significant threats to a woman's health. Based on the statistics, breast cancer mortality in China has increased by 96% over the last thirty years [1]. Early detection, diagnosis, and treatment plays an important role in the prognosis of breast cancer, and imaging examination is important for the detection and diagnosis of breast cancer. Mammography is widely used for the diagnosis of breast cancer and breast screening, and with the technological advancements in recent years, magnetic resonance imaging (MRI) for breast examination plays an important role in breast cancer detection, diagnosis, and operation method selection. In this study, we aimed to investigate the application of mammography combined with breast dynamic contrast-enhanced (DCE) MRI for the early diagnosis of breast cancer.

Patients and methods

Patients

A retrospective analysis was conducted of 120 patients, who underwent MRI examination at our hospital (Sichuan Cancer Hospital, Chengdu, China) from November 2008 to December 2012. The patients were women, aged 28–72 years (mean age, 47 years), who were definitely diagnosed after pathological examination. Out of the 120 patients, 102 patients had malignant cancers (50 with invasive ductal carcinomas, 23 with invasive lobular carcinomas, 12 with ductal carcinomas, 12 with papillary carcinomas, and 8 with mixed carcinomas), while 18 patients had benign cancers.

Methods

Mammography

Mammography was performed using a PHILIP MammoDiagnostDR machine with automatic exposure conditions. The patients underwent mammography with

✉ Correspondence to: Guohui Xu. Email: xgh0913@hotmail.com

standard craniocaudal, mediolateral oblique, and mediolateral when needed. Additionally, patients with dense or multiple glands, or those who had undergone mammary gland transplantations were examined in the spot compression view. Galactography was performed when a nipple discharge was observed.

MRI

MRI was performed using a Siemens Avanto 1.5T MRI machine, and the patients were positioned in the prone position on the dedicated phase array breast surface coil, with both the breasts suspended in the coil tank. The patients were fitted with a high-pressure syringe injection channel, and then the inversion recovery fat-suppressed T2WI axial scan was performed along with breast DCE-MRI VIEWS scanning (3D volumetric interpolated spoiled gradient echo fat-suppressed T1WI axial scan). The sequence parameters were as follows: TR, 4.4 ms; TE, 1.5 ms; FA, 12; matrix 512 × 338; FOV, 320 mm × 320 mm; and thickness, 1 mm (continuous uninterrupted scanning). The first scanning was performed for Mask, with a scanning time of 1 min, and the intravenous bolus injected was Gd-DTPA (0.2 mmol/kg; rate 1.5 mL/s). Five DCE scans were performed, and the parameters of the scans were automatically copied for Mask's, with a 1-min scanning period for each scan. Subtraction images were generated automatically in sequence, which were five breast angiographies obtained after injection of the contrast medium. Five plain and enhanced images were processed using the mean curve software. The central area of the lesion was selected as the region of interest (ROI), and a time-signal intensity curve of the ROI was generated.

Statistical analysis

All data were statistically analyzed using the SPSS11.5 software. The results of the mammography and DCE-MRI were analyzed with χ^2 test. The sensitivity and specificity of the differential diagnosis for benign and malignant lesions and the accuracy of the diagnosis when using mammography, DCE-MRI, and mammography combined with DCE-MRI were calculated separately.

Results

Mammography for the early diagnosis of breast cancer

The data showed that 72 cases were malignant, while 48 were benign. The sensitivity of mammography for early breast cancer diagnosis was 66.67% (68/102), specificity was 77.78% (14/18), accuracy was 68.33% (82/120; Table 1). The mammography showed that the benign breast tumor was mostly round or oval soft tissue masses with a clear boundary and soft texture, popcorn-like or shell-like shaped with a ring calcification and clinical palpation. Hu YS [2] showed that the imaging features of the breast tumor on mammography were divided into eight characteristics: round tumors, petal-shaped masses, leaf-shaped masses, burr-like masses, translucent round masses, calcified lumps, fuzzy masses, and cystic wall masses, as well as seven indirect characteristics, such as malignant calcification, big ducts, tunnel symptoms, thick signs, abnormal blood vessels, horned masses, and spire signs. The diagnosis symptoms in malignant tumors were as follows: one burr-like mass, translucent ring masses, calcified lumps, or spire signs; one or more petal-shaped masses, leaf-shaped masses, fuzzy masses with indirect symptoms; two more indirect symptoms with round tumors; and calcified lumps with malignant calcification or with two more indirect symptoms.

Table 1 The result of mammography compared with pathological results (*n*)

Mammography	Pathological results		Total
	Malignant tumors	Benign tumors	
Positive	68	4	72
Negative	34	14	48
Total	102	18	120

Table 2 The results of breast DCE-MRI compared with pathological results (*n*)

DCE-MRI	Pathological results		Total
	Malignant tumors	Benign tumors	
Positive	96	2	98
Negative	6	16	22
Total	102	18	120

The difference between mammography and DCE-MRI was statistically significant ($\chi^2 = 43.230$, $P < 0.0005$)

DCE-MRI for early diagnoses of breast cancer

The data showed that 98 tumors were malignant and 22 were benign. The sensitivity of mammography for diagnosis was 94.12% (96/102), specificity was 88.89% (16/18), and the accuracy was 93.33% (112/120; Table 2). DCE-MRI VIEWS scans had higher spatial and temporal resolution, which could further improve the clarity of the lesion and also show tumor blood vessels, chest wall invasion, and lymph node metastasis of the breastbone hind, mediastinum, axilla, and around the breast. The time-signal curve should reflect hemodynamic changes in the disease status. Enhancement of benign breast tumors showed sharp edges, shape, and uniform or diffuse regions with patchy strengthening, and the DCE-enhanced time-signal intensity curve showed a continued rising type (type I) or fast-rise platform type (type II). The morphological features of malignant tumors were mostly blurred or thin spiculate outlines, irregularly shaped or with lobular symptoms, signal heterogeneity, or periph-

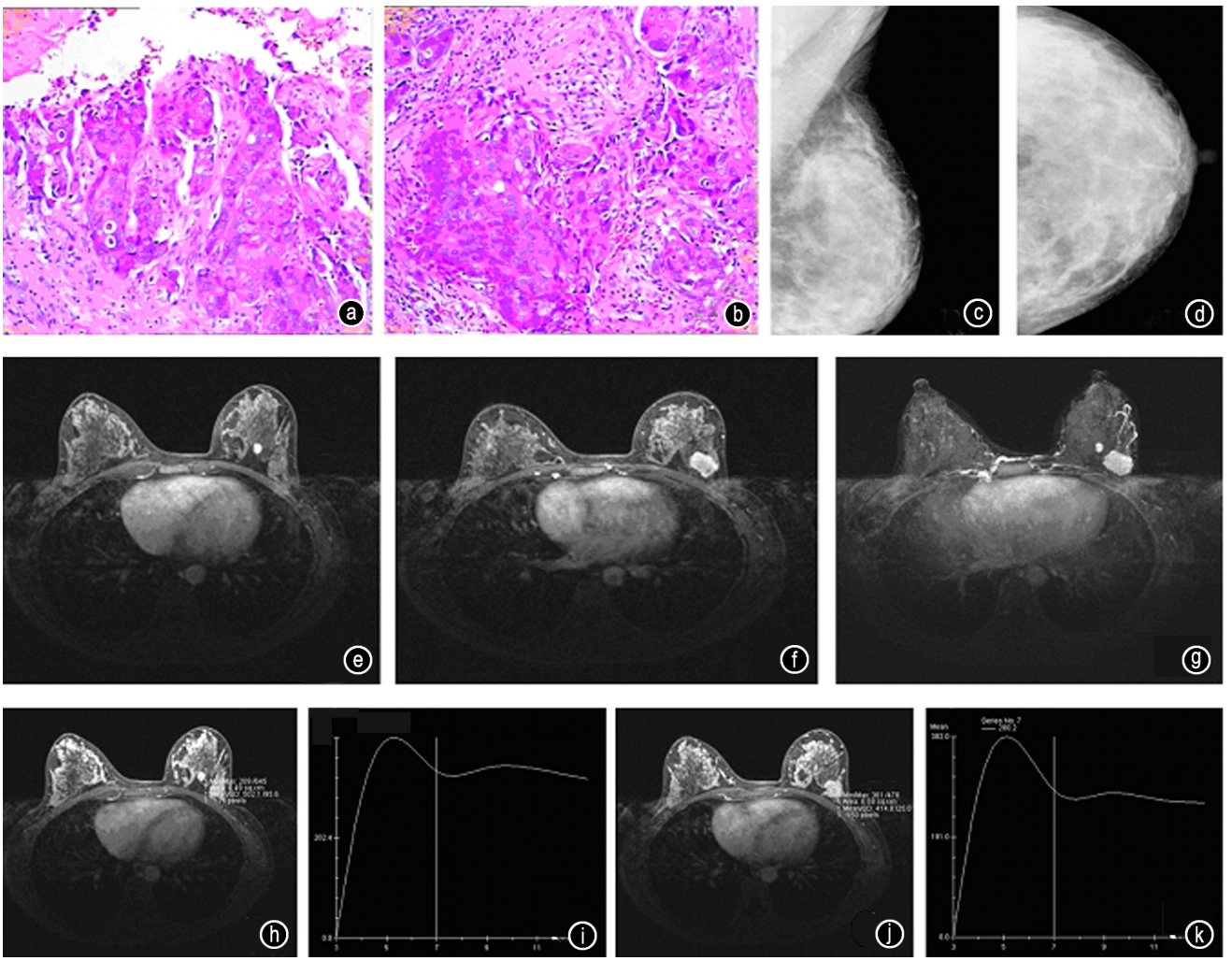

Fig. 1 (a and b) left internal mammary invasive ductal carcinoma as confirmed by biopsy; (c) mammography with standard craniocaudal and (d) mammography with mediolateral oblique showed high-density breast glands and suspicious nodules in left internal mammary, (e and f) DCE-MRI showed it was multicentric breast cancer; (g) tumor adjacent vessels thickening and increased in subtracted images; (h–k) the time-signal intensity curve showed fast rise downhill type (type III)

Table 3 Mammography combined with breast DCE-MRI compared with pathological results (*n*)

Mammography combined with breast DCE-MRI	Pathological results		Total
	Malignant tumors	Benign tumors	
Positive	99	1	100
Negative	3	17	20
Total	102	18	120

eral enhancement on DCE-MRI. Since the pathological features of breast cancer were similar to those of abnormal new rich blood vessels, the DCE time-signal curve showed a fast-rise downhill type (type III) or fast-rise platform type (type II) [3–4].

Mammography combined with breast DCE-MRI for the early diagnosis of breast cancer

Our data showed that the sensitivity, specificity, and accuracy of only mammography were 66.67% (68/102), 77.78% (14/18), and 68.33% (82/120), respectively. However, when using DCE-MRI combined with mammography, the sensitivity, specificity, and accuracy of the differential diagnosis of benign and malignant lesions were found to be improved [97.06% (99/102)， 94.44% (17/18), 96.67% (116/120), respectively; Table 3]. All 28 patients for whom the mammography image of the mammary glands were unclear were examined by DCE-MRI, which clearly showed small lesions within the glands, and malignancy of these lesions can be diagnosed through analysis of the image and the time-signal intensity curve. As shown in the Fig. 1 case of left internal mammary invasive ductal

carcinoma, as confirmed by biopsy, showed high-density breast glands and suspicious nodules in the left internal mammary gland on mammography. Further examination by DCE-MRI showed multiple enhancement sites, abundant blood supply, and the fast-rise downhill type (type III), which indicate multicentric breast cancer. Six cases of intraductal cancer in this set of data showed clustered calcification on molybdenum photography, which is a manifestation of early-stage cancer, while contract-enhanced MRI only showed patchy enhancement; based on these results breast cancer was diagnosed.

Discussion

Mammography is an accurate technique, relatively inexpensive, and convenient, and therefore, is an important method used for diagnosis of breast cancer. When aided by a computer, its resolution and calcification detection rate can be further improved. Calcification within the breast and simple clustered calcification are important early signs of breast cancer and may sometimes be the sole sign of malignancy [5]. Liang HM *et al* [6] reported that molybdenum photography is unparalleled by any other imaging method for the detection of calcification, but it also has limitations. For example, lesions may be overlapped by breast glands when the latter are abundant, in which case the entire lesion may be partially concealed or false-negative are also possible; deep- and high-position lesions as well as small lesions within high-density breast glands may be overlooked [7–8]. For patients with prosthesis implants, misdiagnosis can be a problem since only limited pressure can be applied to the breast. In such cases, MRI can be used for accurate diagnosis. DCE-MRI can effectively reveal the detailed structure of the lesions, and show high sensitivity and accuracy for early diagnosis of breast cancer [94.12% (96/102) and 93.33% (112/120), respectively, for this set of data]. These features are especially useful for detection of lesions in cases with multicentric breast cancer, which helps in the designing of operations [9]. In addition, it also reveals the hemodynamic features of the lesions noninvasively, which greatly aids in the diagnosis of malignancy. However, MRI is not very effective in detecting lesion calcification, takes a long time, generates noise, requires complete cooperation of the patients, and is an expensive technique. Therefore, currently, MRI cannot completely replace mammography as a common method for breast cancer screening. These data indicate that combined use of mammography and contrast-enhanced MRI can effectively improve the sensitivity, specificity, and accuracy of early diagnosis of breast cancer. Therefore, for cases with an indefinite diagnosis after mammography and when a detailed structure of the lesion needs to be clarified, DCE-MRI can be performed to aid diagnosis and development of a more a detailed treatment plan. Yang L *et al* [10] reported that mammography is more effective for the detection of calcified ductal carcinomas, thereby suggesting that despite the advantages of enhanced MRI, mammography features should also be considered to improve the accuracy of the diagnosis of ductal breast cancer. These results suggest that mammography and DCE-MRI should be used in combination for the early diagnosis of breast cancer.

Conflicts of interest

The authors indicated no potential conflicts of interest.

References

1. Ministry of Health of the People's Republic of China. Major Results from the Third National Retrospective Sampling Survey of Death Causes. China Cancer (Chinese), 2008, 17: 344–345.
2. Hu YS. The Modern Breast Image Diagnosis. Beijing: Science Press, 2001. 46–49.
3. Liu PF, Bao RX, Niu Y, *et al*. Angiogenesis and dynamic contrast enhanced MRI of benign and malignant breast lesions: preliminary results. Chinese Journal of Radiology (Chinese), 2002, 36: 967–973.
4. He YK, Xu GH, Ren J, *et al*. The application of breast DCE-MRI combined with time signal curve in diagnosing early breast cancer. Chinese-German J Clin Oncol, 2013, 2: 72–75.
5. He ZY, Huo SY, Xu KY. Mammographic manifestations of early breast cancer——a report of 40 cases. J Clinl Radio (Chinese), 2001, 20: 11–13.
6. Liang HM, Cai SY, Xiao WY, *et al*. Correlative analysis of molybdenum radiological and MRI finding of mammary cancer. J Rare Uncommon Dis (Chinese), 2008, 15: 12–15.
7. Liu JY, Zhao ST, Zhang SW, *et al.* Comparision of MRI with X-ray in the diagnosis of breast cancer. Chin J Breast Dis (Chinese), 2009, 3: 53–54.
8. Yoshikawa MI, Ohsumi S, Sugata S, *et al.* Comparison of breast cancer detection by diffusion-weighted magnetic resonance imaging and mammography. Radiat Med, 2007, 25: 218–223.
9. Wang MQ, Dong M, Xu XY. Relation of MRI features and the expression of immunohistochemistry in breast cancer. J Med Imaging (Chinese), 2010, 20: 1130–1133.
10. Yang L, Wang HY, Zhao YN. Comparative study of mammography and contrast-enhanced magnetic resonance imaging on diagnosis of ductal carcinoma. J Med Imaging (Chinese), 2012, 22: 1465–1469.

DOI 10.1007/s10330-016-0155-7
Cite this article as: He YK, Xu GH, Ren J, *et al*. Mammography combined with breast dynamic contrast-enhanced-magnetic resonance imaging for the diagnosis of early breast cancer. Oncol Transl Med, 2016, 2: 165–168.

Oncology and Translational Medicine
DOI 10.1007/s10330-016-0133-0

August 2016, Vol. 2, No. 4, P169–P173

ORIGINAL ARTICLE

The accuracy of magnetic resonance imaging and ultrasound in evaluating the size of early-stage breast neoplasms

Zheng Wang[1], Hongzhi Chen[1], Xiaobin Ma[2], Zhijun Dai[2], Shuai Lin[2], Huafeng Kang[2] (✉)

[1] Department of Oncology, The Central Hospital of Xi'an City, Xi'an 710004, China
[2] Department of Oncology, The Second Affiliated Hospital of Xi'an Jiaotong University, Xi'an 710004, China

Abstract

Objective Breast cancer is the most frequently diagnosed cancer in women. Accurate evaluation of the size and extent of the tumor is crucial in selecting a suitable surgical method for patients with breast cancer. Both overestimation and underestimation have important adverse effects on patient care. This study aimed to evaluate the accuracy of breast magnetic resonance imaging (MRI) and ultrasound (US) examination for measuring the size and extent of early-stage breast neoplasms.

Methods The longest diameter of breast tumors in patients with $T_{1–2}N_{0–1}M_0$ invasive breast cancer preparing for breast-conserving surgery (BCS) was measured preoperatively by using both MRI and US and their accuracy was compared with that of postoperative pathologic examination. If the diameter difference was within 2 mm, it was considered to be consistent with pathologic examination.

Results A total of 36 patients were imaged using both MRI and US. The mean longest diameter of the tumors on MRI, US, and postoperative pathologic examination was 20.86 mm ± 4.09 mm (range: 11–27 mm), 16.14 mm ± 4.91 mm (range: 6–26 mm), and 18.36 mm ± 3.88 mm (range: 9–24 mm). US examination underestimated the size of the tumor compared to that determined using pathologic examination (t = 3.49, P < 0.01), while MRI overestimated it (t = −6.35, P < 0.01). The linear correlation coefficients between the image measurements and pathologic tumor size were r = 0.826 (P < 0.01) for MRI and r = 0.645 (P < 0.01) for US. The rate of consistency of MRI and US compared to that with pathologic examination was 88.89% and 80.65%, respectively, and there was no statistically significant difference between them (χ^2 = 0.80, P > 0.05).

Conclusion MRI and US are both effective methods to assess the size of breast tumors, and they maintain good consistency with pathologic examination. MRI has a better correlation with pathology. However, we should be careful about the risk of inaccurate size estimation.

Received: 20 January 2016
Revised: 24 March 2016
Accepted: 25 May 2016

Key words: breast neoplasm; magnetic resonance imaging (MRI); ultrasound; pathology

Breast cancer is the most frequently diagnosed cancer in women and also the leading cause of cancer-related death worldwide. It accounted for 23% of the total new cancer cases and 14% of the total cancer-related deaths in 2008 [1]. With increasing attention, improvements in diagnosis methods, and widespread adaption of screening programs, an increasing number of patients with early-stage breast cancer are being diagnosed.

Large-scale randomized trials have shown that breast-conserving surgery (BCS) is a safe surgical procedure for early-stage breast cancer patients and it results in locoregional control similar to that of radical mastectomy [2]. Usually, BCS requires the complete removal of the tumor with a negative margin. The tumor extent is limited to less than 3 cm in order to acquire a negative margin and achieve an acceptable cosmetic result. Therefore, an accurate evaluation of the size and extent of the tumor is crucial in selecting the most appropriate surgical method for patients with breast cancer.

Both overestimation and underestimation have important adverse effects on patient care. Overestimation can result in unnecessary over-resection of normal breast tissues and thus undermine the subsequent cosmetic results of BCS and might even result in the selection of a mastec-

✉ Correspondence to: Huafeng Kang. Email: kanguafeng1973@126.com

tomy when BCS might still have been possible. Underestimation may result in inadequate surgery and thus increase the risk of a positive margin and local failure even after postoperative radiation.

The preoperative assessment of tumor extent in clinical practice is generally performed by physical examination, mammography, ultrasound (US), or magnetic resonance imaging (MRI). Compared to traditional imaging methods such as mammography and US, breast MRI is more sophisticated and more expensive, but its proper indications are yet to be well understood. The primary goal of this study was to evaluate the accuracy and consistency rate of breast MRI and US in measuring the extent of early-stage infiltrating breast cancer with postoperative pathologic examination used as the gold standard.

Materials and methods

Patient selection and ethics statement

Patients admitted to the Second Affiliated Hospital, Xi'an Jiaotong University (China) from January 2010 to December 2011 with $T_{1-2}N_{0-1}M_0$ invasive breast cancer that had been proved histologically by core needle biopsy and who wished to receive BCS and were assessed by breast MRI and US concomitantly before surgery were included. All of the patients underwent BCS successfully. Their clinical and pathological characteristics are listed in Table 1. This study was approved by the Institutional Review Board of the Second Affiliated Hospital of Xi'an Jiaotong University. Written informed consent was obtained at the time of recruitment from all patients involved in the study.

Table 1 The clinicopathological features of the patients with breast cancer

Clinicopathological features	Patients	
	n	%
Age (years)		
≤ 35	9	25.00
> 35	27	75.00
T stage		
T1	25	69.44
T2	11	30.56
ALN status		
Negative	31	86.11
Positive	5	13.89
Histology type		
Infiltrating ductal cancer	27	75.00
Infiltrating lobular cancer	4	11.11
Others	5	13.89
Histology grade		
Grade 1	10	27.78
Grade 2	19	52.78
Grade 3	7	19.44
ER		
Negative	15	41.67
Positive	21	58.33
PR		
Negative	17	47.22
Positive	19	52.78
HER2		
Negative	6	16.67
Positive	30	83.33

Images and pathologic assessment

All of the assessments were performed by two physicians in our hospital who both have more than 10 years' experience in performing US and MRI. They had no access to the clinical data of the patients.

Breast US examinations were performed by using high-frequency transducers (12–15 MHz) and a breast-dedicated imaging preset that was routinely extended to the axillary nodes. The findings were depicted and classified using the Breast Imaging Reporting and Data System (BI-RADS) for US. The longest diameter of the tumors was measured and depicted.

Breast MRI examinations were performed with a 3.0 T high-field MRI device, using a breast-dedicated bilateral surface coil, with the patient in the prone position. The longest diameter of the tumor was calculated in the post-contrast images generated by dynamic evaluation according to the BI-RADS system for MRI.

Breast cancer diagnosis was made pathologically by preoperative core needle biopsy guided by US. The following parameters were evaluated on specimens from the core needle biopsy. The pathologic tumor diameter examinations from the resected tissue were assessed after surgery before paraffin fixation and the final pathologic tumor diameter was obtained from the pathology report provided by the Pathology Department.

Statistical analysis

The differences of means of the longest diameter measured by MRI, US, and the pathology of the tumor were calculated. Differences between the three techniques were tested by the paired-*T* test. If the diameter difference between the imaging method and the pathological method was less than 2 mm, the two methods were deemed consistent. The difference between the consistency rate of MRI and US and that of pathological examination was assessed by using the McNemar test. Correlations between the longest diameters as measured by MRI and pathology and between US and pathology were measured using a linear correlation coefficient. *P* values < 0.05 were considered statistically significant.

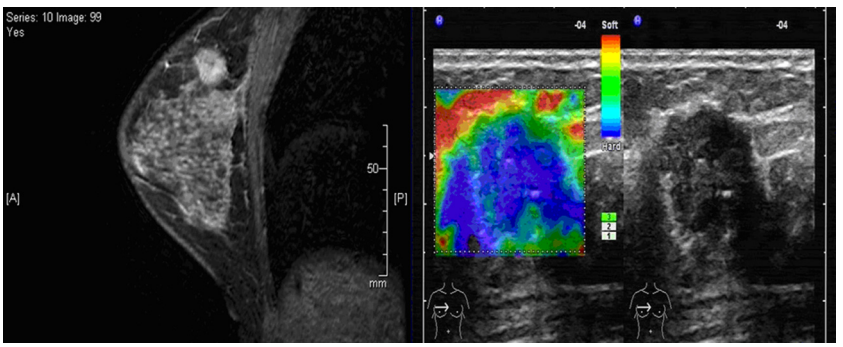

Fig. 1 T size measured by MRI and US was consistent

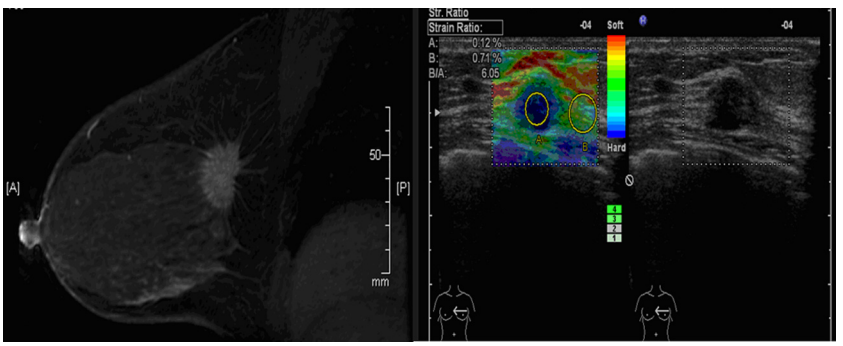

Fig. 2 T size measured by MRI and US was inconsistent

Table 2 The differences between MRI and US and pathology in measuring the breast neoplasms

Examination	Mean (mm)	Standard deviation (mm)	*t*	*P* value
Pair 1				
MRI	20.86	4.09	3.49	0.001
Pathology	18.36	3.88		
Pair 2				
US	16.14	4.91	−6.355	0.000
Pathology	18.36	3.88		

Table 3 The consistency rate of breast MRI and US with pathology in measuring the breast neoplasms

MRI	US		Total	χ^2	*P* value
	Consistent	Inconsistent			
Consistent	28	4	32		
Inconsistent	1	3	4	0.8	0.375
Total	29	7	36		

Results

Results of MRI, US, and pathology for measuring the breast neoplasms

The mean tumor diameters assessed by MRI, US, and pathologic examination were 20.86 mm ± 4.09 mm (range: 11–27 mm), 16.14 mm ± 4.91 mm (range: 6–26 mm), and 18.36 mm ± 3.88 mm (range: 9–24 mm), respectively. The US examination underestimated the size of the tumor compared with pathologic examination ($t = 3.49$, $P < 0.01$), while MRI overestimated it ($t = –6.35$, $P < 0.01$) (Table 2).

Comparison of the consistency rate of breast MRI and US with pathology in measuring the breast neoplasms

The size measured by pathology was considered to be the gold standard. If the difference of diameter between the imaging method and the pathologic method was within 2 mm, it was considered to be consistent with pathology. The size of tumors measured by MRI and US preoperatively was categorized as consistent or inconsistent (Fig. 1 and 2).

The consistency rate of MRI and US with pathology was 88.89% and 80.65%, respectively, and the difference of consistency between MRI and US had no statistical significance ($P > 0.05$) (Table 3).

The correlation between the imaging and pathologic methods of measuring the size of breast neoplasms

The correlation coefficient between MRI and pathology in measuring the size of breast tumors was 0.826 ($P < 0.01$) and for US and pathology it was 0.645 ($P < 0.01$). The correlation of MRI to pathology was better than that of US (Fig. 3 and 4).

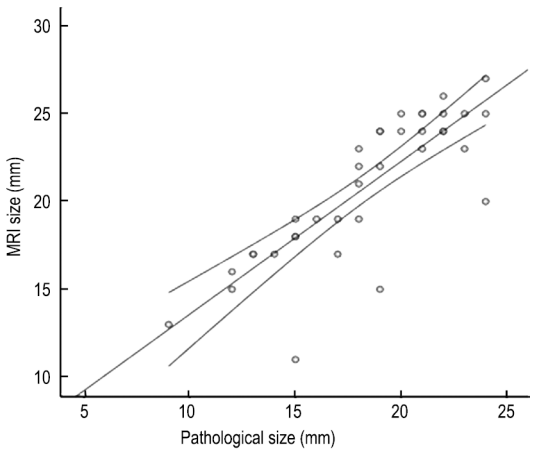

Fig. 3 The correlation between MRI and pathological size

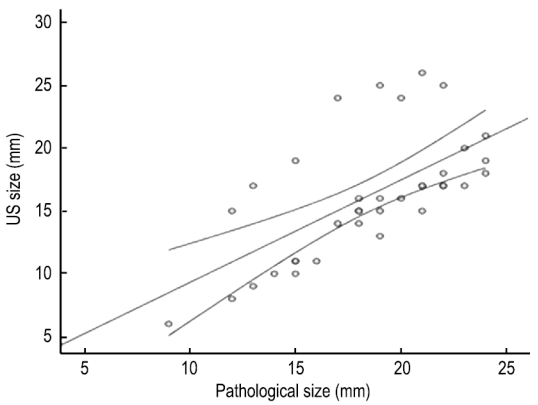

Fig. 4 The correlation between US and pathological size

Discussion

An accurate measurement of tumor size and extent is of key importance to evaluate the possibility of breast conservation and to optimize cosmetic results. In fact, a precise evaluation of a tumor allows correct preoperative planning, with appropriate selection of patient candidates for conservative surgery and a reduced chance of a positive margin, thereby improving local control and the cosmetic effect to the greatest extent.

Imaging techniques, such as mammography, US, and MRI, are widely used in the diagnosis and evaluation for treatment of breast cancer and have their own specific characteristics. In 2002, Kolb *et al* [3] showed breast US improved the sensitivity (97% versus 74%) when used adjunctively with mammography compared to physical examination and mammography. Breast MRI is frequently used as a complementary method to mammography for screening high-risk patients.

In addition to its superiority for the accurate evaluation of the extent of breast tumors, because it is widely available, noninvasive, and relatively inexpensive, US has been shown to produce relatively satisfactory results in clinical practice [4]. However, US is easily affected by breast density and subjective factors. Van *et al* [5] reported that 2-dimensional US usually underestimated the size of breast tumors because breast cancer often presents with an infiltrating growth pattern, and when the acoustic impedance between these two kinds of tissues is similar or the difference is not large enough to discriminate using US, 2-dimensional US may suggest a smaller size compared to the size measured by pathologic examination.

In the present study, the mean tumor diameter assessed by US and pathologic examination was 16.14 mm ± 4.91 mm (range: 6–26 mm) and 18.36 mm ± 3.88 mm (range: 9–24 mm), respectively, and the linear correlation between the US measurement and pathologic size was $r = 0.645$ ($P < 0.01$). If the difference between these two methods was less than 2 mm, it was regarded as consistent. The consistency rate of US compared to that of pathologic measurements was 80.65%, and US showed a tendency to underestimate the true size compared to that determined using pathologic measurements ($t = 3.49$, $P < 0.01$), suggesting that US is an effective method to evaluate the extent of a breast tumor, consistent with other reports [4–6]. Some authors have suggested that contrast-enhanced US may be more accurate in identifying the true size because breast cancer is neoangiogenesis-dependent and has more vessels than do benign tumors and normal breast tissue [5–6]. However, owing to limited evidence, this technique needs large-scale randomized experiments to confirm its superiority.

MRI has advantages of being multi-parameter, multi-sequenced, and multi-dimensional, and it has a higher sensitivity. It is not limited by the location, size, or the breast density. Therefore, MRI has advantages over mammography and US in determining the invasive tumor size, identifying multifocality, and evaluating intraductal components. Because of these advantages, this technique has been claimed to be the ideal tool to diagnose breast cancer and assess tumor extent in recent years, and it is believed that MRI may be able to more exactly identify margins to improve local control.

In this study, a cohort preparing for BCS was examined by MRI and US concomitantly and standardized by pathologic findings. The mean tumor diameters assessed by MRI, US, and pathologic examination were 20.86 mm ± 4.09 mm (range: 11–27 mm), 16.14 mm ± 4.91 mm (range: 6–26 mm), and 18.36 mm ± 3.88 mm (range: 9–24 mm), respectively, and the linear correlation between the image measurement and pathologic size was $r = 0.826$ ($P < 0.01$) for MRI and $r = 0.645$ ($P < 0.01$) for breast US. Although both MRI and US had a good accuracy and the difference in the consistency rate compared with pathology had no statistical significance (88.89% versus 80.65%,

$P > 0.05$), MRI seemed to be slightly superior ($r = 0.826$ versus $r = 0.645$). We also found that MRI displayed a tendency to overestimate the size of the tumor ($t = –6.35$, $P < 0.01$), while US showed a tendency to underestimate the true size compared with pathologic measurements ($t = 3.49$, $P < 0.01$).

However, because it is more sophisticated and expensive, the wide-spread use of MRI in the evaluation of breast masses before BCS remains controversial [7]. Turnbull *et al* [8] reported the addition of MRI to conventional assessment such as clinical palpation, mammography, and US was not associated with a significant reduction in the re-excision rate. Onesti *et al* [9] reported that the MRI-assessed size showed a good correlation coefficient ($r = 0.65$) compared with pathological size, while US measurements showed a worse correlation ($r = 0.47$) compared with pathologic size.

If we define a difference < 5 mm as concordance, MRI overestimates 35% of breast lesions, especially tumors with a diameter > 20 mm, regardless of the histological type of breast cancer. However, some studies have proposed that some patients (not all of them) may benefit from the addition of MRI before BCS [10], especially for those with invasive lobular carcinoma.

Multiplicity is the predisposing factor in local recurrence after BCS. MRI has been thought to be the most sensitive method of detecting multiplicity, but in the study by Choi *et al* [11], US was the most sensitive method in comparison with MRI and 18-fluorodeoxyglucose positron emission tomography/computed tomography in detecting primary lesions and evaluating multiplicity. Some authors have suggested that MRI can more clearly show the tumor boundary, especially the boundary of the tumor and the surrounding breast tissue after neoadjuvant chemotherapy, in invasive lobular carcinoma and ductal carcinoma in situ, and thus, MRI is superior to US.

In the present study, compared with the size on pathologic examination, although MRI showed a better correlation than that of US ($r = 0.826$ versus $r = 0.645$) the difference in the consistency rate between MRI and US compared with pathologic examination showed no statistical difference. Perhaps due to the few cases of invasive lobular carcinoma and ductal carcinoma in situ in this cohort, MRI did not display its superiority. Some authors have suggested MRI shows an extreme advantage over US in assessing the residual tumor extent after neoadjuvant chemotherapy. Perhaps in more sophisticated circumstances, MRI can display its advantages more thoroughly. However, in assessing normal palpable breast cancer, its advantages over US are limited.

Conclusion

In summary, these data suggest that MRI and US correlate well with pathology in assessing the extent of breast cancer, and no statistical difference was found in the consistency rate between MRI and US. Furthermore, US showed a tendency of underestimation while MRI showed a tendency of overestimation compared with pathologic examination.

Conflicts of interest

The authors indicated no potential conflicts of interest.

References

1. Jemal A, Bray F, Center MM, *et al*. Global cancer statistics. CA Cancer J Clin, 2011, 61: 69–90.
2. Veronesi U, Cascinelli N, Mariani L, *et al*. Twenty-year follow-up of a randomized study comparing breast-conserving surgery with radical mastectomy for early breast cancer. N Engl J Med, 2002, 347: 1227–1232.
3. Kolb TM, Lichy J, Newhouse JH. Comparison of the performance of screening mammography, physical examination, and breast US and evaluation of factors that influence them: an analysis of 27,825 patient evaluations. Radiology, 2002, 225: 165–175.
4. Dummin U, Cox M, Plant L. Prediction of breast tumor size by mammography and sonography-A breast scrEen experience. Breast, 2007,16: 38–46.
5. van Esser S, Veldhuis WB, van Hillegersberg R, *et al*. Accuracy of contrast-enhanced breast ultrasound for pre-operative tumor size assessment in patients diagnosed with invasive ductal carcinoma of the breast. Cancer Imaging, 2007, 7: 63–68.
6. Caproni N, Marchisio F, Pecchi A, *et al*. Contrast-enhanced ultrasound in the characterisation of breast masses: utility of quantitative analysis in comparison with MRI. Eur Radiol, 2010, 20: 1384–1395.
7. Grimsby GM, Gray R, Dueck A, *et al*. Is there concordance of invasive breast cancer pathologic tumor size with magnetic resonance imaging? Am J Surg, 2009, 198: 500–504.
8. Turnbull L, Brown S, Harvey I, *et al*. Comparative effectiveness of MRI in breast cancer (COMICE) trial: a randomized controlled trial. Lancet, 2010, 375: 563–571.
9. Onesti JK, Mangus BE, Helmer SD, *et al*. Breast cancer tumor size: correlation between magnetic resonance imaging and pathology measurements. Am J Surg, 2008, 196: 844–850.
10. Sardanelli F, Boetes C, Borisch B, *et al*. Magnetic resonance imaging of the breast: recommendations from the EUSOMA working group. Eur J Cancer, 2010, 46: 1296–1316.
11. Choi YJ, Shin YD, Kang YH, *et al*. The Effects of Preoperative 18F-FDG PET/CT in Breast Cancer Patients in Comparison to the Conventional Imaging Study. J Breast Cancer, 2012, 15: 441–448.

DOI 10.1007/s10330-016-0133-0
Cite this article as: Wang Z, Chen HZ, Ma XB, *et al*. The accuracy of magnetic resonance imaging and ultrasound in evaluating the size of early-stage breast neoplasms. Oncol Transl Med, 2016, 2: 169–173.

Oncology and Translational Medicine
DOI 10.1007/s10330-016-0145-9

August 2016, Vol. 2, No. 4, P174–P178

ORIGINAL ARTICLE

Clinical significance of HBME-1, Galectin-3, and CK19 expression and the status of BRAF mutation in papillary thyroid carcinoma

Li Zheng[1] (✉), Min Zhao[1] (✉), Xiangyang Hu[2], Jin Huang[1], Ling Ang[1], Hongguang Hu[1], Qiang Zou[1], Jin Wang[1], Mingqiang Liu[1], Yang Zhao[1]

[1] Department of Pathology, The Second People's Hospital of Hefei, Hefei 230011, China
[2] Department of Pathology, Anhui Medical University, Hefei 230032, China

Abstract

Objective The aim of this study was to explore the clinical significance of the expression of proteins human bone marrow endothelial cell markers (HBME-1), Galectin-3, and cytokeratin19 (CK19), as well as the status of v-raf murine sarcoma viral oncogene homolog B1 (*BRAF*) mutation in papillary thyroid carcinoma (PTC).

Methods Immunohistochemical staining was performed in 82 specimens each of PTC and papillary benign lesions to detect the expression of HBME-1, Galectin-3, and CK19. Polymerase chain reaction (PCR) and gene sequencing were performed on 60 specimens each of PTC and papillary benign lesions to detect the status of *BRAF* mutation.

Results The positive expression ratios of HBME-1, Galectin-3, and CK19 in PTC were 98.8%, 97.6% and 100% respectively, which were significantly higher than the expressions in papillary benign lesions ($P < 0.05$). No significant relationship was observed between the expression of these makers and the clinicopathological features of PTC. The sensitivity of co-expression of HBME-1 and CK19 or HBME-1 and Galectin-3 as diagnostic criteria of PTC was 99.9%, with a specificity of 95.4%. *BRAF* mutation was detected in 40 of 60 PTC (66.7%) specimens. There was a statistical difference in *BRAF* mutations between PTC and papillary benign lesions ($P < 0.05$); there were no associations between *BRAF* mutation and the clinicopathological features of PTC.

Conclusion Combined immunohistochemical staining of HBME-1, Galectin-3, and CK19 can further improve the sensitivity and specificity of differential diagnosis of PTC. *BRAF* mutation is a significant genetic event, which may have diagnostic value for PTC.

Received: 13 February 2016
Revised: 13 April 2016
Accepted: 25 May 2016

Key words papillary thyroid carcinoma (PTC); human bone marrow endothelial cell markers (HBME-1); Galectin-3; cytokeratin19 (CK19); v-raf murine sarcoma viral oncogene homolog B1 (*BRAF*)

The pathological diagnosis of papillary carcinoma thyroid (PTC) relies mostly on its complex papillary structure and typical nuclear features. Some benign thyroid lesions may also be accompanied by "real papillary structure," which is similar to PTC and hence difficult to distinguish from it. Nuclear features of follicular type of papillary carcinoma are unconspicuous and easily confused with follicular adenoma. In the last few years, the molecular markers Galectin-3, cytokeratin19 (CK19), and human bone marrow endothelial cell markers (HBME-1), or their combinations, have been suggested for differential diagnosis of PTC, but there remain larger controversies regarding the reliability of these markers. In addition, the relationship between the gene v-raf murine sarcoma viral oncogene homolog B1 (*BRAF*) and PTC has been increasingly implicated. Thus, our study attempts to explore the practical value of detecting and analyzing the proteins Galectin-3, CK19, and HBME-1, as well as the status of *BRAF* mutation in the diagnosis of PTC and their correlations with clinicopathological features.

✉ Correspondence to: Min Zhao, Email: Zhao.Min.hi@163.com; Li Zheng, Email: Zhengli352@163.com

Materials and methods

Patients and specimens

The collected cases of thyroid surgical specimens and thyroid fresh resection specimens were archived within two phases in the Department of Pathology at the First Affiliated Hospital of Anhui Medical University, China.

The cases of thyroid surgical specimens included 82 cases each of PTC and thyroid benign lesions, which were collected from January 2009 to December 2010. The cases of PTC included 20 males and 62 females, with ages ranging from 13 to 78 years and a median age of 46 years, of which 10 were that of lymph node metastasis. The cases of thyroid benign lesions were distributed as follows: 20 follicular adenoma, 47 nodular goiter, and 15 Hashimoto's Thyroiditis, including 20 male and 62 females at the ages of 15 to 75 years, with the median age of 46 years.

The cases of thyroid fresh resection specimens included 60 cases each of PTC and thyroid benign lesions, which were collected from January 2011 to October 2012. The cases of PTC included 10 males and 50 females at ages of 16–79 years, with a median age of 49 years, of which 10 were that of lymph node metastasis. The cases of thyroid benign lesions also included 10 males and 50 females, at ages of 15–78 years, and a median age of 48 years.

Main reagents

Anti-human Galectin-3 McAb (ready-to-use), anti-human CK19 McAb (ready-to-use), anti-human HBME-1 McAb (ready-to-use), and the reagent kits for detection, named Envision, were purchased from Fuzhou New Biotechnology Corporation. Ltd. (China). The reagent kits for DNA extraction and PCR reagents were purchased from Shanghai Biological Engineering Corporation. Ltd. (China).

Immunohistochemical staining for Galectin-3, CK19, and HBME-1

Following the two-step method of Envision, the positively stained specimens were compared with a known positive biopsy specimen, and the negatively stained specimens compared with specimens treated with phosphate-buffered saline instead of the antibody. We scored the percentage of positively-stained cells and intensity of the staining per biopsy in five fields, at 400 × magnification, by manual counting. The percentage of positive cells in the area of the field was scored on a 5-point scale as follows: 0, no staining; 1, less than 25% positive; 2, between 26% to 50% positive; 3, between 51% to 75% positive; and 4, more than 75% positive.

The intensity of the positive staining in the area of the field was scored as follows: Score 0: without staining, Score 1: with pale yellow staining, Score 2: with brown-yellow staining, and Score 3: with sepia-yellow staining.

The results were evaluated by combining two different scores as follows: -, negative-score 0; 1+, weakly positive-scores 2 and 3; 2+, moderately positive-scores 4 and 5; and 3+, strongly positive-scores 6 and 7.

PCR and DNA sequencing for *BRAF* gene mutation

After DNA was extracted from tissue specimens according to the directions of the DNA extraction kits, the designed primers (upstream, 5′-TCATAATGCTTGCTCTGATAGGA-3′; downstream, 5′-GGCCAAAAATT—TAATCAGTGGA-3′) were used to amplify the DNA sequence containing *BRAF* gene mutation hot spot (exon 15, T1799A) by PCR. The amplified products (224 bp) were verified by agarose gel electrophoresis, after which they were sent to Sangon Biotech (China) Co. Ltd. For sequencing. The mutation was verified by sequence alignment between the *BRAF* gene and products of DNA sequencing.

Statistical analysis

Statistical evaluations were performed by χ^2-test and Fisher's exact test, using the SPSS 13.0 software. A $P < 0.05$ was considered statistically significant. Specificities of independent and joint detection of different protein markers were also calculated and compared for differential diagnosis of thyroid papillary carcinoma.

Results

Expression of Galectin-3, CK19 and HBME-1 and the mutation of *BRAF* gene in benign lesions and PTC

Galectin-3 protein was mainly located in the cytoplasm with nuclear occurrences observed occassionally. The positive ratio of Galectin-3 in PTC was 97.6%, with the main expression of medium seen to be above intensity. The positive ratio of Galectin-3 in thyroid benign lesions was 25.6%, with its main expression being weakly positive. The expression of Galectin-3 revealed a statistically significant difference between PTC and thyroid benign lesions ($P < 0.05$; Fig. 1a and Table 1).

The positive signal of CK19 was located in the cytoplasm and occassionally at the cellular membrane. The positive expression ratio of CK19 was 100%, and 81 cases showed expression with above medium intensity, and the positive expression ratio in benign lesions was 50%, with weakly positive expression. The expression of CK19 revealed a statistically significant difference between PTC and thyroid benign lesions ($P < 0.05$; Fig. 1b and Table 1).

The positive signal of HBME-1 was mainly located at the cellular membrane, with occassional staining at the edge of glandular lumens. The positive expression ratio in

Table 1 Expression of Galectin-3, CK19, HBME-1 in PTC and thyroid benign lesions (*n*)

	n	Galectin-3				%	CK19				%	HBME-1				%
		–	+	++	+++		–	+	++	+++		–	+	++	+++	
PTC	82	2	4	11	65	97.6	0	1	11	70	100.0	1	4	26	51	98.8
TBL	82	61	18	3	0	25.6#	41	39	2	0	50.0*	77	4	1	0	6.1△
FA	20	15	4	1	0	25.0	11	8	1	0	45.0	18	1	1	0	10.0
NG	47	31	14	2	0	34.0	22	24	1	0	53.2	45	2	0	0	4.3
HT	15	15	15	0	0	0	8	7	0	0	46.7	14	1	0	0	6.7

Compared with markers of corresponding to PTC: # $P = 0.000$, * $P = 0.000$, △ $P = 0.000$, PTC = Papillary thyroid carcinoma; TBL = Thyroid benign lesions; FA = Follicular adenoma; NG = Nodular goiter; HT = Hashimoto's thyroiditis

Table 2 The relationships between the clinicopathological features and the expressions of Galectin-3, CK19, HBME-1

Items	*n*	Galectin-3		*P*	CK19		*P*▲	HBME-1		*P*
		n	%		*n*	%		*n*	%	
Sex										
Male	20	20	100.0	1.000	20	100.0	–	20	100.0	1.000
Female	62	60	96.8		62	100.0		61	98.4	
AGE (years)										
< 45	46	46	100.0	0.190	46	100.0	–	46	100.0	0.439
≥ 45	36	34	94.4		36	100.0		35	97.2	
Diameter (cm)										
< 2	23	23	100.0	0.169	23	100.0	–	23	100.0	0.397
2–4	30	28	93.3		30	100.0		30	100.0	
> 4	29	29	100.0		29	100.0		28	96.5	
LNM										
Positive	10	10	100.0	1.000	10	100.0	–	10	100.0	1.000
Negative	72	70	97.2		72	100.0		71	98.6	

▲ The positive expression ratio of CK19 was 100% in all PTC which showed no statistically comparability in the different clinicopathological features. LNM = Lymph node metastasis

PTC was of 98.8%, mostly expressed with above-medium intensity, and the positive expression ratio in benign lesions was 6.7%, all of which expressed weakly, except for one case that was moderately positive. The expression of HBME-1 revealed a statistically significant difference between PTC and thyroid benign lesions ($P < 0.05$; Fig. 1c, and Table 1).

Relationships between the clinicopathological features and expression of Galectin-3, CK19, and HBME-1 in PTC

As depicted in Table 2, the expression of the three protein markers showed no statistically significant differences in different sexes, ages, tumor sizes, and with or without lymph node metastasis.

Comparisons of sensitivity and specificity of protein markers in diagnosis of PTC

Comparisons of the sensitivity and specificity of Galectin-3, CK19 and HBME-1 in differential diagnosis as well as combining HBME-1 (the highest specificity) with other expressions revealed that the results of combined Galectin-3, CK19, and HBME-1, and co-expression of HBME-1 and CK19 or HBME-1 and Galectin-3 had the best specificity and sensitivity in PTC diagnosis (Table 3).

BRAF gene mutation status in PTC and papillary benign lesions

The *BRAF* gene T1799A mutation in exon 15 was studied in 60 cases with PTC by sequencing, and heterozygous mutation was detected in 40 out of 60 cases, yielding a mutation ratio of 66.7% (Fig. 2), whereas in the benign lesions, the ratio was 0% (Fig. 3; $\chi^2 = 24.000$, $P < 0.05$). In addition, according to the Table 4， the *BRAF* gene mutation in PTC showed no statistically significant differences

Table 3 The sensitivity and specificity of Galectin-3, CK19, HBME-1 and combinations in PTC diagnosis

Expressions of markers	Sensitivity (%)	Specificity (%)
Galectin-3 (+)	97.6	74.4
CK19 (+)	100.0	50.0
HBME-1 (+)	98.8	93.9
HBME-1 (+), Galectin-3 (+)	96.4	98.4
HBME-1 (+), CK19 (+)	98.8	97.0
HBME-1 (+), Galectin-3 (+), CK19 (+)	96.4	99.2
HBME-1 (+), CK19 (+) or HBME-1 (+), Galectin-3 (+)	99.9	95.4

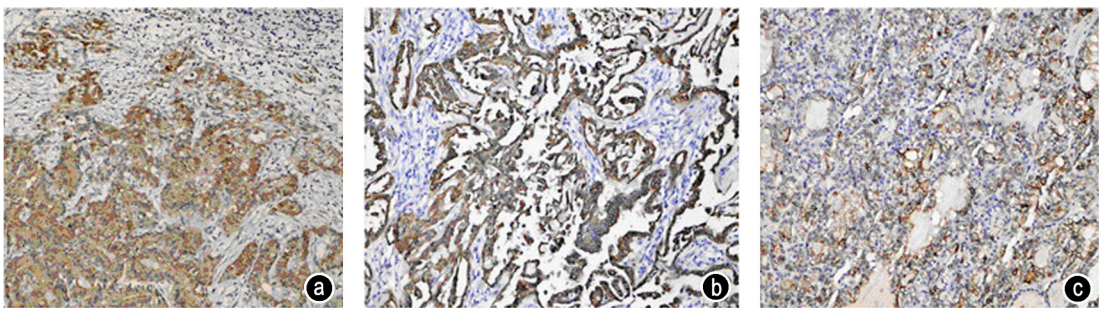

Fig. 1 Expression of Galectin-3, CK19、HBME-1 in PTC (Envision × 100). (a) Galectin-3; (b) CK19; (c) HBME-1

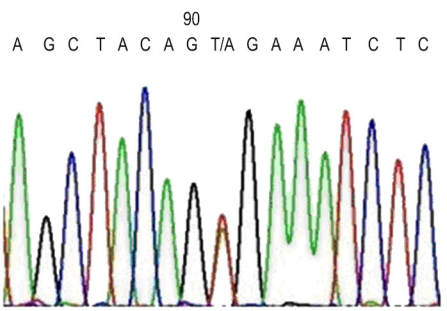

Fig. 2 Heterozygous mutation of *BRAF* gene in PTC

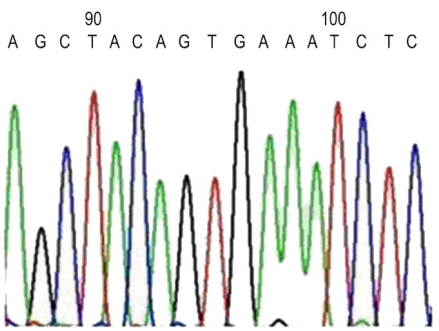

Fig. 3 Nodular goiter without *BRAF* gene mutation

in different sexes, ages, tumor sizes, and with or without lymph node metastasis.

Discussion

Galectin-3 is a β-galactoside-binding protein, which may be involved in cell growth, cell adhesion, inflammation, immune regulation, and cell apoptosis [1], and some studies had shown that Galectin-3 is also involved in processing of many neoplastic formations and transformation, such as colon cancer [2] and PTC [3–5]. In this study, the positive expression ratio of Galectin-3 in PTC was significantly higher than in thyroid benign lesions, which was consistent with previous reports [6–7]. However, Galectin-3 had low specificity in distinguishing PTC and thyroid benign lesions, making it difficult to diagnose PTC independently, while the intensity of positive expression in thyroid benign lesions is very weak, so the observed above-medium intensity of the positive expression has important significance. Other studies [4, 8] have shown that Galectin-3 negatively regulates metastasis and invasion of PTC cases, and lymph node metastasis was the primary means for metastasis of thyroid carcinoma. In our study of 10 cases of lymph node metastasis in PTC, we observed that there was no distinct difference with the group without lymph node metastasis, and majority of Galectin-3 still expressed positively.

Table 4 The relationships between *BRAF* mutation and the clinicopathological features

Items	*n*	Positive expression	%	*P*
Sex				
Male	10	6	60.0	0.903
Female	50	34	68.0	
Ages (years)				
< 45	24	7	58.3	0.264
≥ 45	36	33	72.2	
Diameter (cm)				
< 2	35	27	77.1	
2–4	20	10	50.0	0.114
> 4	5	3	60.0	
LNM				
Positive	10	7	70.0	1.000
Negative	50	33	66.0	

CK19 is a low-molecular-weight keratin that is expressed in many epithelial tissues. Some studies [6–7, 9] have reported stronger CK19 expression in PTC, with positive ratios from 70% to 100% compared to the inconformity reports in thyroid benign lesions. Our study revealed stronger CK19 expression in PTC than in thyroid benign lesions, with a sensitivity for diagnosing PTC of 100%, but much lower specificity. This low specificity imposes limits on its diagnostic use for PTC. The independent positive expression cannot diagnose PTC, however, the above-medium intensity of positive expression has a good

vigilance for PTC, whereas strong sensitivity of CK19 imparts a unique value to differential diagnoses for PTC, implying that negative CK19 expression can be used as an exclusive index for PTC diagnosis.

HBME-1 was widely reported [10–11] to be expressed in thyroid tumors, especially in PTC. Its use has been suggested for differential diagnosis between benign thyroid lesions and malignant thyroid tumors, but there were few domestic reports with different opinions. In our study, HBME-1 shows statistically significant differences between thyroid benign lesions and PTC with higher sensitivity and specificity. It was thus concluded that HBME-1 is a better marker for differential diagnosis of PTC.

Besides, we found that the results of pathological diagnosis can be more reliable if we combined the highest specificity of HBME-1 with Galectin-3 and CK19, and compared the co-expression of HBME-1 and CK19 or HBME-1 and Galectin-3 as a diagnostic criteria of PTC.

BRAF is a member of the *RAF* gene family location at 7q34, and plays an important role in the MAPK signaling pathway. Several studies [12–13] have reported that the *BRAF* T1799A mutation may be involved in thyroid carcinoma, and that the most mutated locus for this gene lies in exon 15 T1799A. This mutation causes the 600th valine of the protein to be replaced by glutamic acid, leading to abnormality in mediating the downstream signaling pathway. Studies have also implicated the mutation in PTC alone and in some undifferentiated carcinomas that may originate from PTC, with the mutation ratio of PTC ranging from 30% to 45%. However, such mutations have been rarely documented in domestic reports of China. Our study was similar to other studies [13–15] that revealed many cases of *BRAF* T1799A in PTC compared to no case in thyroid benign lesions. *BRAF* mutation is a significant event in PTC, which may be useful for early diagnosis of the disease; however, the *BRAF* mutation ratio in our study was slightly higher than that reported previously. This discrepancy can be attributed to the different backgrounds in the studies. There remain some controversies [14] to the relationship between *BRAF* gene mutation and the clinicopathological features of PTC, however, our study did not find any significant relationship between *BRAF* gene mutation and patients' sexes, ages, tumor sizes as well as presence or absence of lymph node metastasis.

Overall, our study suggests that combined immunohistochemical staining of HBME-1, Galectin-3, and CK19 can further improve the sensitivity and specificity of PTC diagnosis, with co-expression of HBME-1 and CK19 or HBME-1 and Galectin-3 proving to be a more potent diagnostic criteria. *BRAF* mutation is a significant genetic event, which may have diagnostic importance in PTC.

Conflicts of interest

The authors indicated no potential conflicts of interest.

References

1. Krześlak A, Lipińska A. Galectin-3 as a multifunctional protein. Cell Mol Biol Lett, 2004, 9: 305–328.
2. Zaia Povegliano L, Oshima CT, de Oliveira Lima F, *et al*. Immunoexpression of galectin-3 in colorectal cancer and its relationship with survival. J Gastrointest Cancer, 2011, 42: 21–21.
3. Song Q, Wang D, Lou Y, *et al*. Diagnostic significance of CK19, TG, Ki67 and galectin-3 expression for papillary thyroid carcinoma in the northeastern region of China. Diagn Pathol, 2011, 21: 126–132.
4. Htwe TT, Karim N, Wong J, *et al*. Differential expression of galectin-3 in advancing thyroid cancer cells: a clue toward understanding tumor progression and metastasis. Singapore Med J, 2010, 51: 856–859.
5. Türkoz H K, Oksüz H, Yurdakul Z, *et al*. Galectin-3 expression in tumor and progression metastasis of papillary thyroid carcinoma. Endocr Pathol, 2008, 19: 92–96.
6. Laco J, Ryska A, Cáp J, *et al*. Expression of galectin-3, cytokeratin 19, neural cell adhesion molecule and E-cadhedrin in certain variants of papillary thyroid carcinoma. Cesk Patol, 2008, 44: 103–107.
7. Zhu X, Sun T, Lu H, *et al*. Diagnostic significance of CK19, RET, Galectin-3 and HBME-1 expression for papillary thyroid carcinoma. J Clin Pathol, 2010, 63: 786–789.
8. Salajegheh A, Dolan-Evans E, Sullivan E, *et al*. The expression profiles of the galectin gene family in primary and metastatic papillary thyroid carcinoma with particular emphasis on galectin-1 and galectin-3 expression. Exp Mol Pathol, 2014, 96: 212–218.
9. Liu Z, Yu P, Xiong Y, *et al*. Significance of CK19, TPO, and HBME-1 expression for diagnosis of papillary thyroid carcinoma. Int J Clin Exp Med, 2015, 8: 4369–4374.
10. Schmitt AC, Cohen C, Siddiqui MT. Paired box gene 8, HBME-1 and cytokeratin 19 expression in preoperative fine-nee dle aspiration of papillary thyroid carcinoma: diagnostic utility. Cancer Cytopathol, 2010, 118: 196–202.
11. Cheung CC, Ezzat S, Freeman JL, *et al*. Immunohistochemical diagnosis of papillary thyroid carcinoma. Mod Pathol, 2001, 14: 338–342.
12. Nikiforov YE, Nikiforova MN. Molecular genetics and diagnosis of thyroid cancer. Nat Rev Endocrinol, 2011, 7: 569–580.
13. Frasca F, Nucera C, Pellegriti G, *et al*. BRAF (V600E) mutation and the biology of papillary thyroid cancer. Endocr Relat Cancer, 2008, 15: 191–205.
14. Li C, Lee K C, Schneider EB, *et al*. BRAF V600E mutation and its association with clinicopathological features of papillary thyroid cancer: a Meta-analysis. J Clin Endocrinol Metab, 2012, 97: 4559–4570.
15. Park KS, Oh YL, Ki CS, *et al*. Evaluation of the Real-Q BRAF V600E detection assay in fine-needle aspiration samples of thyroid nodules. J Mol Diagn, 2015, 17: 431–437.

DOI 10.1007/s10330-016-0145-9
Cite this article as: Zheng L, Zhao M, Hu XY, *et al*. Clinical significance of HBME-1, Galectin-3, and CK19 expression and the status of BRAF mutation in papillary thyroid carcinoma. Oncol Transl Med, 2016, 2: 174–178.

Oncology and Translational Medicine
DOI 10.1007/s10330-016-0154-8

August 2016, Vol. 2, No. 4, P179–P184

ORIGINAL ARTICLE

A dosimetric evaluation of flattening filter-free volumetric modulated arc therapy for postoperative treatment of cervical cancer*

Fuli Zhang, Huayong Jiang, Weidong Xu, Yadi Wang (✉), Junmao Gao, Qingzhi Liu, Ping Wang, Na Lu, Diandian Chen, Bo Yao, Jun Hou, Heliang He, Jianping Chen

Radiation Oncology Department, The PLA Army General Hospital of China, Beijing 100700, China

Abstract

Objective The aim of the study was to compare flattening filter-free (FFF) beams and conventional flattening filter (FF) beams in volumetric modulated arc therapy (VMAT) for cervical cancer after surgery, through a retrospective planning study.

Methods VMAT plans of FFF beams and normal FF beams were designed for a cohort of 15 patients. The prescribed dose was 45 Gy to 1.8 Gy per fraction, and at least 95% of the planning target volume received this dose. Doses were computed with a commercially available treatment planning system using a Monte Carlo (MC) algorithm. Plans were compared according to dose-volume histogram analysis in terms of planning target volume homogeneity and conformity indices (HI and CI), as well as organs at risk (OAR) dose and volume parameters.

Results FFF-VMAT was similar to FF-VMAT in terms of CI, but inferior to FF-VMAT considering HI. No statistically differences were observed between FFF-VMAT and FF-VMAT in following organ at risks including pelvic bone marrow, small bowel, bladder, rectum, and normal tissue (NT). .

Conclusion For patients with cervical cancer after hysterectomy, the FFF beam achieved target and OAR dose distribution similar to that of the FF beam. Reduction of beam-on time in cervical cancer is beneficial.

Received: 26 March 2016
Revised: 25 June 2016
Accepted: 25 July 2016

Key words: flattening filter-free (FFF); cervical cancer; dosimetry; volumetric modulated arc therapy (VMAT)

In recent years, volumetric modulated arc therapy (VMAT) has been introduced in clinical practice to overcome some of the limitations associated with fixed field intensity modulated radiation therapy (IMRT) and three-dimensional conformal radiation therapy (3DCRT). VMAT allows the continuous delivery of radiation by simultaneously varying the dose rate, the positions of the multileaf collimator (MLC), and the gantry rotation speed. Some studies demonstrated that VMAT could achieve highly conformal dose distributions, with improved target volume coverage and sparing of normal tissues, compared with conventional IMRT [1–10]. In addition, VMAT has the potential to offer additional advantages over conventional static gantry IMRT in treatment delivery efficiency, because of the reduction in both treatment delivery time and monitor units (MU) usage. More recently, linear accelerators with flattening filter-free (FFF) beams such as Varian's TrueBeam™ (Varian Medical System, Palo Alto, CA) and Elekta's Versa HD™ (Elekta Versa HD, Elekta Oncology systems, Stockholm, Sweden) were introduced into clinical operation [11–17]. FFF beams are characterized by high-dose rates, which combined with VMAT result in greater treatment efficiency compared to traditional fixed field techniques. According to these published results, a further reduced treatment delivery time and comparable plan quality seem to have been verified for VMAT plans with FFF beams.

Many studies on the application of VMAT in various tumor locations including cervical cancer usually choose 6-MV beam energy, although some researchers suggest that there is still a value to higher energies (≥ 10 MV) for deep-seated pelvic/abdominal targets, as the volume

✉ Correspondence to: Yadi Wang. Email: wangyadi@hotmail.com
* Supported by a grant of the Military Medical Metrology Project (No. 2011-JL2-005).

of the target increases [18]. In addition, some studies published on FFF beams are limited to cases with relatively small planning target volume (PTV), including the prostate, lungs, larynx, chest wall, and esophagus [11, 14, 19–30]. Few studies on the dosimetric effects of the FFF beam on VMAT planning for cervical cancer after surgery have been conducted, while faster treatments could have a clinical impact on cervical cancer patients in terms of comfort on the treatment table, immobility, and minimization of internal organ status changes, such as bladder or rectum filling changes over time, as well as the reduction of intra-fractional patient motion. Therefore, we present a planning comparison of VMAT of flattening filter (FF) beams with 6-MV and 10-MV energy (6FF-VMAT and 10FF-VMAT) versus VMAT of FFF beams with 6-MV and 10-MV (6FFF-VMAT and 10FFF-VMAT) for treatment of cervical cancer after hysterectomy. The study was also motivated by the expectation that changes in nominal energy and penumbra of FFF beams may influence the dosimetric outcome for this specific deep-seated treatment location, as changes in secondary build-up may have an impact on target coverage and sparing of organs at risk (OAR).

Patients and methods

Patient selection, positioning, and computed tomography

Fifteen cervical cancer patients who had been treated with postoperative radiotherapy after hysterectomy from May 2012 to November 2013 were chosen for retrospective analysis. The mean and median ages were 53.9 and 55.5 years, respectively. Computed tomography (CT) scans of all patients in the treatment position were obtained on our departmental CT scanner (Brilliance Bigbore CT, Philips Medical systems, Cleveland, OH, USA) using 5-mm slice interval and thickness. The CT scans were extended from the T11 vertebral body to mid-thigh and were imported to the Monaco planning system (version 5.0, Elekta AB, Stockholm, Sweden). Before implementing CT, a contrast agent was administered orally or intravenously. In addition, to minimize intra-fractional setup variability and maintain inter-fractional repeatability as much as possible, a custom immobilization device (Thermoplastic mold, MedTec Inc, USA) was fabricated with each patient in the treatment position. The study was approved by the ethics committee of the PLA Army General Hospital of China. All patients provided written consent for storage of their medical information in the hospital database and for research use.

Target volumes

The clinical target volume (CTV) and OAR for all patients were delineated by a single radiation oncologist with extensive experience in the treatment of cervical cancer on individual CT slices. Based on the ICRU 62 report [31] and some published guidelines [32, 33], the CTV included the upper one-half of the vagina and the stump, parametrial tissue, and pelvic lymph nodes. Because nonenlarged lymph nodes are poorly visualized on CT, contrast-enhanced vessels plus a 2-cm margin were used to define the common, external, and internal iliac nodal regions to the level of the L4–5 interspace. The presacral region was included to the bottom of the S3 vertebral body to ensure coverage of the presacral lymph nodes and attachment of the uterosacral ligament. The PTV was generated using a 1.0-cm uniform expansion of the CTV. The PTV mean volume in this study was (1368.90 ± 644.12) cm^3. All plans were normalized to deliver 45 Gy to 95% of PTV in 25 fractions.

Critical structures

OAR included the rectum, bladder, bowel, pelvic bone marrow (PBM) and normal tissue (NT). The rectum was defined from the level of the sacral promontory to the ischial tuberosities. The contour of the bladder in full-filling condition was delineated. The peritoneal cavity (excluding the rectum and bladder) from the level of L4–5 was used to define the small bowel region and the individual loops of small bowel were not separately contoured. The PBM comprised the lumbosacral bone marrow, iliac bone marrow, and ischium, pubis, and proximal femoral bone marrow and femoral heads. The NT was defined as the whole body volume covered by the CT scan minus the PTV.

Treatment planning

For each patient, four VMAT plans were designed using FFF and FF beams of nominal energy 6-MV (6FF-VMAT, 6FFF-VMAT) and 10-MV (10FF-VMAT, 10FFF-VMAT) photons of Elekta Versa HD™ accelerator on the Monaco planning system (version 5.1, Elekta AB, Stockholm, Sweden), respectively. VMAT plans were generated using 2 full arcs of clockwise rotation from the initial angle of 180 degrees to the end angle of 180 degrees. All plans were normalized to cover 95% of the PTV with the prescription dose using an identical set of PTV and OAR dose-volume constraints. The dose-volume constraints used for the targets and critical structures are listed in Table 1, which summarized our clinical experience while combining the guidelines of Radiation Therapy Oncology Group (RTOG) 0418, and were kept the same for all plans.

Dosimetric comparisons

The dose-volume histograms (DVH) of four types of VMAT plans were compared in terms of homogeneity index (HI), conformity index (CI), Dmax, Dmin, and Dmean

of PTV, V10, V20, V30, and V40 of the rectum (fraction of rectum volume receiving > 10 Gy, 20 Gy, 30 Gy, 40 Gy); V20, V30, and V40 of the bladder; V10, V20, V30, and V40 of the bowel; V5, V10, V20, V30, and V40 of PBM; and V10, V20, V30, and V40 of NT. The HI was defined as minimum dose in 5% of the PTV (D5) / minimum dose in 95% of the PTV (D95). Smaller values of HI correspond to more homogenous irradiation of the target volume. A value of 1 corresponds to absolute homogeneity of dose within the target. The CI reflected the degree of conformity and was defined as follows [22]: CI = the percentage of the PTV volume receiving at least prescription dose × the ratio of the volume of the PTV receiving at least prescription dose to the total volume covered by prescription dose. The perfect conformity is 1 and the higher (closer to 1) the CI, the better the dose conformity. Dmax represents the minimum absorbed dose received by 2% of the PTV while Dmin represents the minimum absorbed dose received by 98% of the PTV [34].

Statistical analysis

Statistical analysis was performed using SPSS software (version 18.0, SPSS Inc., Chicago, IL, USA). Quantitative data were expressed in the form of mean ± standard deviation ($\overline{\chi} \pm s$). The statistical significance was tested using factorial design analysis of variance (ANOVA). A *P*-value ≤ 0.05 was considered statistically significant, and the 95% confidence intervals (CI) were calculated.

Results

PTV coverage

Table 2 summarizes the PTV coverage for four types of VMAT plans. Significant differences for HI were found ($P = 0.039$), with FF-VMAT showing better heterogeneity while CI was similar ($P = 0.288$, $P = 0.294$, and $P = 0.499$, respectively). In addition, Dmax also demonstrated significant differences between FFF-VMAT and FF-VMAT ($P = 0.039$).

Comparison of dosimetric parameters of OAR for four modalities

Dosimetric parameters of OAR including the PBM, small bowel, bladder, rectum, and NT are listed in Table 3. No significant difference was observed for V5, V10, V20, V30, and V40 of the PBM ($P > 0.05$); V10, V20, and V30 of the small bowel ($P > 0.05$); V20, V30, and V40 of the bladder ($P > 0.05$); V10, V20, V30, and V40 of the rectum ($P > 0.05$); and V10, V30, V40, and Dmean of NT ($P > 0.05$). Only V10 of NT showed significant difference ($P = 0.039$).

Table 1 Dose-volume constraints for targets and critical structures

Structures	Volume (%)	Dose (Gy)
PTV	95	45
Pelvic bone marrow	≤ 90	10
	≤ 80	20
Small bowel	≤ 30	25
Bladder	≤ 25	30
Rectum	≤ 60	40

Comparison of monitor units (MU) and beam-on time (BOT) for two modalities

The data of monitor units (MU) and beam-on time (BOT) are listed in Table 4. The BOT of FFF-VMAT reduced delivery time compared with FF-VMAT.

Discussion

It was demonstrated that for medium- and small-size targets, FFF beams might be suitable for IMRT planning and that the out-of-field dose could be significantly reduced owing to the lower contamination from head scatter, resulting in better OAR risk protection [35]. It would be important to demonstrate whether the two effects could also be confirmed for larger targets in complex anatomic situation.

Spruijt *et al* [15] compared FF and FFF beams for breast cancer using four IMRT techniques and pointed out that all four IMRT techniques allowed FFF beams to generate acceptable plans for breast cancer. Nicolini *et al* [16] carried out a feasibility study by using 6FFF-VMAT on advanced esophageal cancer and concluded that 6FFF-VMAT plans acquired minor improvements in plan quality, but with the potential for additional useful reduction in the treatment time. A study by Kretschmer *et al* [17]

Table 2 Comparison of HI, CI, Dmax, Dmin, and Dmean for 6FF-VMAT, 10FF-VMAT, 6FFF-VMAT, and 10FFF-VMAT

	6FF-VMAT (%)	10FF-VMAT (%)	6FFF-VMAT (%)	10FFF-VMAT (%)	*P* value
Dmax	50.45 ± 1.61	50.56 ± 1.86	51.01 ± 1.73	52.16 ± 2.56	0.220*, 0.039**, 0.310***
Dmin	43.59 ± 0.57	43.61 ± 0.50	43.65 ± 0.50	43.52 ± 0.50	0.667*, 0.917**, 0.607***
Dmean	47.95 ± 0.90	48.04 ± 1.07	48.12 ± 0.85	48.66 ± 1.16	0.233*, 0.130**, 0.394***
HI	1.11 ± 0.03	1.11 ± 0.04	1.12 ± 0.03	1.14 ± 0.05	0.194*, 0.039**, 0.294***
CI	0.78 ± 0.06	0.78 ± 0.07	0.78 ± 0.06	0.75 ± 0.06	0.288*, 0.294**, 0.499***

*, represents the effect of energy; **, represents the effect of flattening filter; and ***, represents the interactive effect of energy and flattening filter

Table 3 Comparison of dosimetric parameters of OARs for four modalities

OARs parameters	6FF-VMAT(%)	10FF-VMAT(%)	6FFF-VMAT(%)	10FFF-VMAT(%)	*P* value
PBM					
V5	98.20 ± 3.22	98.78 ± 2.39	98.73 ± 2.59	98.46 ± 2.99	0.831*, 0.885**, 0.565***
V10	87.32 ± 6.07	89.69 ± 4.87	89.96 ± 4.76	89.70 ± 5.40	0.444*, 0.337**, 0.342***
V20	72.25 ± 7.50	73.59 ± 6.62	73.12 ± 6.50	73.20 ± 6.98	0.692*, 0.894**, 0.725***
V30	54.86 ± 9.67	55.73 ± 9.55	55.07 ± 9.44	56.43 ± 8.03	0.640*, 0.848**, 0.920***
V40	28.85 ± 10.40	30.03 ± 11.67	29.25 ± 10.57	30.68 ± 11.04	0.646*, 0.853**, 0.964***
Small bowel					
V10	74.66 ± 24.42	75.65 ± 24.58	76.25 ± 24.93	75.78 ± 24.67	0.967*, 0.893**, 0.909***
V20	46.51 ± 18.79	46.61 ± 17.94	46.91 ± 17.84	46.46 ± 18.53	0.970*, 0.979**, 0.954***
V30	25.44 ± 12.90	25.43 ± 12.96	25.66 ± 12.29	26.13 ± 13.16	0.945*, 0.888**, 0.943***
Bladder					
V20	86.42 ± 11.51	87.67 ± 12.14	86.67 ± 11.00	89.68 ± 10.54	0.468*, 0.700**, 0.766***
V30	59.09 ± 18.14	60.57 ± 17.90	60.37 ± 17.84	61.96 ± 17.52	0.740*, 0.773**, 0.991***
V40	39.74 ± 22.38	40.90 ± 23.87	40.26 ± 22.06	41.03 ± 23.34	0.872*, 0.957**, 0.974***
Rectum					
V10	97.71 ± 4.53	97.71 ± 4.50	97.68 ± 4.61	97.81 ± 4.42	0.955*, 0.971**, 0.957***
V20	93.61 ± 5.83	93.43 ± 6.26	93.44 ± 5.86	92.79 ± 5.88	0.788*, 0.792**, 0.880***
V30	70.65 ± 18.09	72.38 ± 17.61	71.47 ± 17.16	71.19 ± 18.26	0.875*, 0.967**, 0.827***
V40	46.13 ± 27.32	45.96 ± 27.06	46.74 ± 26.50	46.95 ± 28.69	0.998*, 0.910**, 0.978***
NT					
V10	43.93 ± 9.09	44.21 ± 8.71	44.40 ± 8.62	44.74 ± 8.74	0.220*, 0.039**, 0.310***
V20	24.52 ± 7.17	24.69 ± 6.91	24.43 ± 6.73	24.95 ± 7.01	0.864*, 0.887**, 0.889***
V30	11.71 ± 4.80	11.73 ± 4.79	11.61 ± 4.56	12.64 ± 5.15	0.706*, 0.697**, 0.638***
V40	4.55 ± 2.81	4.74 ± 3.05	4.55 ± 2.79	5.16 ± 3.25	0.642*, 0.751**, 0.755***
Dmean	11.42 ± 2.36	11.46 ± 2.37	11.48 ± 2.28	11.68 ± 2.46	0.842*, 0.813**, 0.898***

*, represents the influence of energy on parameters; **, represents the influence of flattering filter on parameters; and ***, represents the influence of interaction between energy and flattening filter on parameters

Table 4 Comparison of monitor units (MU) and beam-on time (BOT) for two techniques

	MU	BOT (sec)
6FF-VMAT	1275.9 ± 227.4	243 ± 28
10FF-VMAT	1138.1 ± 209.1	246 ± 36
6FFF-VMAT	1724.7 ± 255.1	216 ± 26
10FFF-VMAT	1746.7 ± 272.2	206 ± 31
P value	0.358*, 0.000**, 0.207***	0.642*, 0.000**, 0.376***

*, represents the effect of energy, **, represents the effect of flattening filter, and ***, represents the interactive effect of energy and flattening filter

compared FF and FFF beam field-in-field plans in several tumor locations, including breast, neurocranium, lung, and bone metastases, and demonstrated that the exclusive use of a linear accelerator in FFF mode is feasible in 3DCRT. Bell *et al* [35] probed the used of modulated arc (mARC) technique using FFF and FF beams for prostate treatment, respectively. The conclusion was that the combination of the high dose rate with mARC appears to be the preferable option as it benefits from a marked decrease in treatment time and out-of-field dose. Bahrainy *et al* [36] investigated the influence of FFF beam on breast cancer with simultaneous integrated boost in the hybrid plan technique and concluded that in comparison to the FF-based plan, the FFF mode allowed further reduction of the average left anterior descending artery (LAD) dose for comparable target volume coverage without adverse low-dose exposure of contralateral structures.

The purpose of our study was to compare FFF beams and conventional FF beams in VMAT of cervical cancer after surgery through a retrospective planning study, focusing on the extent of BOT reduction and feasibility of clinical use of FFF beams. Considering that the FFF-VMAT plans are not intended for clinical use, dosimetric verification was thus not presented in this work.

In our study, FFF-VMAT achieved inferior heterogeneity compared to FF-VMAT while the conformity of the modalities was similar. In terms of dosimetric parameters of OAR, no significant difference was observed for dose-volume parameters for the PBM, small bowel, bladder, rectum, and NT, excluding V10 of NT.

The increase in dose rate is one of the most obvious and attractive effects when removing the FF. The increased dose rate can translate into shorter treatment times for the same technique. The BOT in our study was approximately 11% less for 6FFF-VMAT plans and approximately 16% less for 10FFF-VMAT plans. Obviously, in terms

of treatment time, patients could benefit more from the increased dose rate of the FFF beam for cervical cancer to improve comfort on the treatment table, immobility, minimize internal organ movement such as bladder or rectum filling changes over delivery, and reduce intrafractional patient motion.

Conclusion

For patients with cervical cancer after hysterectomy, the FFF beam achieved similar target and OAR dose distribution as the FF beam. Reduction of BOT in cervical cancer is beneficial.

Conflicts of interest

The authors indicated no potential conflicts of interest.

References

1. Scorsetti M, Navarria P, Mancosu P, *et al.* Large volume unresectable locally advanced non-small cell lung cancer: acute toxicity and initial outcome results with rapid arc. Radiat Oncol, 2010, 5: 94.
2. Scorsetti M, Bignardi M, Clivio A, *et al.* Volumetric modulation arc radiotherapy compared with static gantry intensity-modulated radiotherapy for malignant pleural mesothelioma tumor: a feasibility study. Int J Radiat Oncol Biol Phys, 2010, 77: 942–949.
3. Fogliata A, Bergström S, Cafaro I, *et al.* Cranio-spinal irradiation with volumetric modulated arc therapy: a multi-institutional treatment experience. Radiother Oncol, 2011, 99: 79–85.
4. Mancosu P, Cozzi L, Fogliata A, *et al*. Collimator angle influence on dose distribution optimization for vertebral metastases using volumetric modulated arc therapy. Med Phys, 2010, 37: 4133–4137.
5. Mancosu P, Navarria P, Bignardi M, *et al.* Re-irradiation of metastatic spinal cord compression: a feasibility study by volumetric-modulated arc radiotherapy for in-field recurrence creating a dosimetric hole on the central canal. Radiother Oncol, 2010, 94: 67–70.
6. Fogliata A, Cozzi L, Clivio A, *et al.* Preclinical assessment of volumetric modulated arc therapy for total marrow irradiation. Int J Radiat Oncol Biol Phys, 2011, 80: 628–636.
7. Mancosu P, Navarria P, Castagna L, *et al.* Anatomy driven optimization strategy for total marrow irradiation with a volumetric modulated arc therapy technique. J Appl Clin Med Phys, 2012, 13: 3653.
8. Scorsetti M, Mancosu P, Navarria P, *et al.* Stereotactic body radiation therapy (SBRT) for adrenal metastases: a feasibility study of advanced techniques with modulated photons and protons. Strahlenther Onkol, 2011, 187: 238–244.
9. Fogliata A, Clivio A, Nicolini G, *et al.* Intensity modulation with photons for benign intracranial tumours: a planning comparison of volumetric single arc, helical arc and fixed gantry techniques. Radiother Oncol, 2008, 89: 254–262.
10. Palma D, Vollans E, James K, *et al*. Volumetric modulated arc therapy for delivery of prostate radiotherapy: comparison with intensity-modulated radiotherapy and three-dimensional conformal radiotherapy. Int J Radiat Oncol Biol Phys, 2008, 72: 996–1001.
11. Vassiliev ON, Kry SF, Kuban DA, *et al.* Treatment-planning study of prostate cancer intensity-modulated radiotherapy with a Varian Clinac operated without a flattening filter. Int J Radiat Oncol Biol Phys, 2007, 68: 1567–1571.
12. Zhang GG, Ku L, Dilling TJ, *et al.* Volumetric modulated arc planning for lung stereotactic body radiotherapy using conventional and unflattened photon beams: a dosimetric comparison with 3D technique. Radiat Oncol, 2011, 6: 152.
13. Stevens SW, Rosser KE, Bedford JL. A 4 MV flattening filter-free beam: commissioning and application to conformal therapy and volumetric modulated arc therapy. Phys Med Biol, 2011, 56: 3809–3824.
14. Mancosu P, Castiglioni S, Reggiori G, *et al*. Stereotactic body radiation therapy for liver tumours using flattening filter free beam: dosimetric and technical considerations. Radiat Oncol, 2012, 7: 16.
15. Spruijt KH, Dahele M, Cuijpers JP, *et al*. Flattening filter free vs flattened beams for breast irradiation. Int J Radiat Oncol Biol Phys, 2013, 85: 506–513.
16. Nicolini G, Ghosh-Laskar S, Shrivastava SK, *et al*. Volumetric modulation arc radiotherapy with flattening filter-free beams compared with static gantry IMRT and 3D conformal radiotherapy for advanced esophageal cancer: a feasibility study. Int J Radiat Oncol Biol Phys, 2012, 84: 553–560.
17. Kretschmer M, Sabatino M, Blechschmidt A, *et al*. The impact of flattening-filter-free beam technology on 3D conformal RT. Radiat Oncol, 2013, 8: 133.
18. Söderström S, Eklöf A, Brahme A. Aspects on the optimal photon beam energy for radiation therapy. Acta Oncol, 1999, 38: 179–187.
19. Vassiliev ON, Kry SF, Chang JY, *et al*. Stereotactic radiotherapy for lung cancer using a flattening filter free Clinac. J Appl Clin Med Phys, 2009, 10: 2880.
20. Navarria P, Ascolese AM, Mancosu P, *et al*. Volumetric modulated arc therapy with flattening filter free (FFF) beams for stereotactic body radiation therapy (SBRT) in patients with medically inoperable early stage non small cell lung cancer (NSCLC). Radiother Oncol, 2013, 107: 414–418.
21. Lang S, Shrestha B, Graydon S, *et al.* Clinical application of flattening filter free beams for extracranial stereotactic radiotherapy. Radiother Oncol, 2013, 106: 255–259.
22. Prendergast BM, Fiveash JB, Popple RA, *et al*. Flattening filter-free linac improves treatment delivery efficiency in stereotactic body radiation therapy. J Appl Clin Med Phys, 2013, 14: 4126.
23. Scorsetti M, Alongi F, Castiglioni S, *et al.* Feasibility and early clinical assessment of flattening filter free (FFF) based stereotactic body radiotherapy (SBRT) treatments. Radiat Oncol, 2011, 6: 113.
24. Prendergast BM, Dobelbower MC, Bonner JA, *et al*. Stereotactic body radiation therapy (SBRT) for lung malignancies: preliminary toxicity results using a flattening filter-free linear accelerator operating at 2400 monitor units per minute. Radiat Oncol, 2013, 8: 273.
25. Stathakis S, Esquivel C, Gutierrez A, *et al.* Treatment planning and delivery of IMRT using 6 and 18 MV photon beams without flattening filter. Appl Radiat Isot, 2009, 67: 1629–1637.
26. Huang BT, Lu JY, Lin PX, *et al.* Comparison of two RapidArc delivery strategies in stereotactic body radiotherapy of peripheral lung cancer with flattening filter free beams. PloS one, 2015, 10: e0127501.
27. Lang S, Reggiori G, Puxeu Vaquee J, *et al.* Pretreatment quality assurance of flattening filter free beams on 224 patients for intensity modulated plans: a multicentric study. Med Phys, 2012, 39: 1351–1356.
28. Kragl G, Baier F, Lutz S, *et al*. Flattening filter free beams in SBRT and IMRT: dosimetric assessment of peripheral doses. Z Med Phys, 2011, 21: 91–101.
29. Ong CL, Dahele M, Slotman BJ, *et al*. Dosimetric impact of the interplay effect during stereotactic lung radiation therapy delivery using flattening filter-free beams and volumetric modulated arc therapy. Int J Radiat Oncol Biol Phys, 2013, 86: 743–748.

30. Ong CL, Dahele M, Cuijpers JP, *et al.* Dosimetric impact of intrafraction motion during RapidArc stereotactic vertebral radiation therapy using flattened and flattening filter-free beams. Int J Radiat Oncol Biol Phys, 2013, 86: 420–425.
31. Prescribing, recording and reporting photon beam therapy. In: Washington DC., 1999.
32. Group RTO. A phase II study of intensity modulated radiation therapy (IMRT) to the pelvis +/–chemotherapy for post-operative patients with either endometrial or cervical carcinoma. 2011.
33. Roeske JC, Lujan A, Rotmensch J, *et al*. Intensity-modulated whole pelvic radiation therapy in patients with gynecologic malignancies. Int J Radiat Oncol Biol Phys, 2000, 48: 1613–1621.
34. Hodapp N. The ICRU Report 83: prescribing, recording and reporting photon-beam intensity-modulated radiation therapy (IMRT). Strahlenther Onkol (German), 2012, 188: 97–99.
35. Bell K, Dzierma Y, Palm J, *et al*. mARC prostate treatment planning with Varian Eclipse for flat vs. FFF beams. Phys Med, 2016, 32: 474–478.
36. Bahrainy M, Kretschmer M, Jöst V, *et al.* Treatment of breast cancer with simultaneous integrated boost in hybrid plan technique: Influence of flattening filter-free beams. Strahlenther Onkol, 2016, 192: 333–341.

DOI 10.1007/s10330-016-0154-8
Cite this article as: Zhang FL, Jiang HY, Xu WD, *et al*. A dosimetric evaluation of flattening filter-free volumetric modulated arc therapy for postoperative treatment of cervical cancer. Oncol Transl Med, 2016, 2: 179–184.

Oncology and Translational Medicine
DOI 10.1007/s10330-016-0162-8

August 2016, Vol. 2, No. 4, P185–P188

ORIGINAL ARTICLE

The diagnostic value of tumor abnormal protein and high sensitivity C reactive protein in screening for endometrial cancer with endometrial thickness less than 8 mm*

Yi Li[1] (✉), Ruiqin Yue[1], Dongrui Qin[2], Yanqing Wang[2], Xinling Zhou[1], Xinyong Jing[1], Chuanzhong Wu[1]

[1] Department of Gynecology, The Second People's Hospital of Liaocheng City, Shandong 252600, China
[2] Department of Pathology, The Second People's Hospital of Liaocheng City, Shandong 252600, China

Abstract

Objective This study aimed to combine tumor abnormal protein (TAP) and high-sensitivity C-reactive protein (hs-CRP) level detection to diagnose endometrial cancer in patients with endometrial thickness less than 8 mm, and to provide a reference for clinical screening and diagnosis.

Methods Clinical data from 19 cases of endometrial cancer, diagnosed on the basis of pathological findings, were collected from September 2014 to December 2015. The inclusion criteria were as follows: the patients were first diagnosed with endometrial thickness less than 8 mm and were all in menopause. Perimenopausal patients (n = 26) with uterine fibroids seen during the same period were selected as a control group. Serum TAP and hs-CRP levels of the patients in the two groups were simultaneously determined on admission.

Results We found that both TAP and hs-CRP levels in the experimental group were higher than those in the control group [(182.95 ± 72.14) μm^2 vs. (133.19 ± 55.18) μm^2, P = 0.019; (7.52 ± 19.03) mg/L vs. (1.66 ± 2.31) mg/L, P = 0.136]. The sensitivity of TAP for the diagnosis of endometrial cancer was 73.68%, the specificity was 69.23%, and the Youden index was 0.4291. The diagnostic sensitivity and specificity of hs-CRP was 15.79% and 100%, respectively, and the Youden index was 0.1579. After plotting the receiver operating characteristics curves, the optimal cut-off value for TAP in diagnosing endometrial cancer was found to be 160.662 μm^2 and that for hs-CRP was 1.07 mg/L.

Conclusion For patients suspected of having endometrial cancer with endometrial thickness less than 8 mm, combined detection of TAP and hs-CRP levels can be used as a screening tool and can provide new ideas regarding clinical diagnosis and treatment.

Received: 27 May 2016
Revised: 14 July 2016
Accepted: 25 July 2016

Key words: tumor abnormal protein (TAP); high-sensitivity C-reactive protein (hs-CRP); endometrial thickness; endometrial carcinoma

Endometrial cancer is a common gynecologic malignancy. Endometrial thickness is closely related to endometrial cancer. Currently, hysteroscopic biopsy is recommended to confirm the diagnosis for patients with endometrial thickness more than 8 mm on ultrasonography [1]. For patients with endometrial thickness less than 8 mm, follow-up is recommended and unnecessary hysteroscopy should be minimized. However, there are currently no known specific endometrial cancer markers; therefore, when endometrial thicknesses of less than 8 mm is found on ultrasonography, it is difficult to objectively formulate treatment programs [2]. Previous studies have reported that endometrial cancer may express abnormal protein (TAP) [3]. However, TAP has poor diagnostic specificity. This study aimed to combine detection of TAP and high-sensitivity C-reactive protein (hs-CRP) levels to diagnose endometrial cancer in patients with endometrial thickness less than 8 mm and to provide a

Correspondence to: Yi Li. Email: 15965259952@163.com
* Supported by a grant from the Medical and Health Technology Development Program in Shandong Province (No. 2015WS0407).

reference for clinical screening and diagnosis.

Materials and methods

Material source and grouping

Clinical data from 19 cases of endometrial cancer, ultimately diagnosed based on pathologic findings, were collected from September 2014 to December 2015. The inclusion criteria were as follows: the patients were first diagnosed with endometrial thickness less than 8 mm and were all in menopause. In terms of pathological types, 17 cases were of adenocarcinoma, 1 case was of clear cell carcinoma, and 1 case of squamous cell carcinoma. In terms of degrees of differentiation, 4 cases were of high differentiation, 12 cases of moderate differentiation, and 3 cases of low differentiation. Perimenopausal patients (n = 26) with uterine fibroids, diagnosed during the same time period on the basis of pathological findings, were selected as the control group. The serum TAP and hs-CRP levels of patients in the two groups were determined on admission.

Measurement method

Fasting fingertip blood samples collected in the morning from patients of each group were obtained from the pathology department. Two slides of thin blood were prepared by pushing the blood across the slide and were kept still for drying. A special dropper was used to take the TAP detection reagent (Rising Medical Technology) and vertically drop 3 drops on each slide. The blood smear was kept still for 2 hours and re-dried to form "gathering spots". The slide was put under a TAP integrated chip-specific microscope (Rising Medical Technology). The "gathering spots" on the blood slices were sequentially scanned with an achromatic objective (× 4) and measured. At the same time, aggregates with abnormal forms were searched. The gathering spot diameter was used as the basic evaluation criteria: (1) 0–121 μm^2 and no obvious aggregates: normal TAP; (2) 121–225 μm^2 and smaller aggregates: abnormal TAP; (3) ≥ 225 μm^2 and relatively large aggregates: obviously abnormal TAP.

Fasting blood sample of patients in the inspection department was collected. The hs-CRP levels were measured using an immunoturbidimeter (GE automatic biochemical analyzer) according the reagent specification standards: (1) 0–10 mg/L: normal range and (2) > 10 mg/L: abnormal range.

Statistical methods

SPSS 17.0 was used to perform the chi-square test to detect differences between the groups for categorical data and the t test was used for continuous data. $P < 0.05$ was considered statistically significant. The diagnostic sensitivity refers to the correct determination of the proportion of actual patients with positive results and was calculated as: [number of true positive cases/(number of true positive cases + number of false negative cases)] × 100. The diagnostic specificity means the correct determination of the proportion of healthy people and was calculated as: [number of true negative cases/(number of true negative cases + number of false positive cases)] × 100. The Youden index is defined as the sum of sensitivity and specificity subtracted from 1. The Youden index ranges from 0 to 1, and a greater value indicates a higher diagnostic value. A receiver operating characteristic (ROC) curve was plotted to confirm the diagnostic value, which uses 1-specificity as the x-axis, and sensitivity as the y-axis. The cut-off value was obtained when the miter was 45°, and the sensitivity and specificity were good.

Table 1 Comparisons of clinical data between two groups

	Experimental group (n = 19)	Control group (n = 26)	P value
Age (years)	54.03 ± 6.01	52.23 ± 5.03	0.192
Menopausal duration	6.36 ± 3.57	5.94 ± 2.81	0.302
Gravidity	2.95 ± 1.54	2.78 ± 1.48	0.145
Parity	1.62 ± 0.92	1.57 ± 0.87	0.207
Vaginal bleeding or liquid discharge (Yes/No)	18/1	25/1	0.819

Results

No significant differences were found in age, menopausal status, pregnancy status, or clinical symptoms between the experimental and control groups, indicating that the indexes were comparable (Table 1).

The expression levels of TAP in the experimental group and control group were (182.95 ± 72.14) μm^2 and (133.19 ± 55.18) μm^2, respectively (P = 0.019). Fig. 1–3 show the expression levels of TAP in different pathological diagnoses. The expression levels of hs-CRP in both groups were (7.52 ± 19.03) mg/L and (1.66 ± 2.31) mg/L, respectively (P = 0.136).

By using recommended laboratory cutoff values as a standard, the sensitivity and specificity of TAP for the diagnosis of endometrial cancer were 73.68% and 69.23%, respectively, and the Youden index was 0.4291. The diagnostic sensitivity and specificity of hs-CRP were 15.79% and 100%, respectively, and the Youden index was 0.1579. The sensitivity and specificity of the combination of the two indexes were 77.83% and 69.23%, respectively, and the Youden index increased to 0.4706. However, using TAP and hs-CRP in a binary logistic regression analysis, the results showed that a positive result for TAP had a statistically significant predictive value for endometrial cancer (P = 0.014), but a positive result for hs-CRP had no statistical significance (P = 0.167). This illustrates that

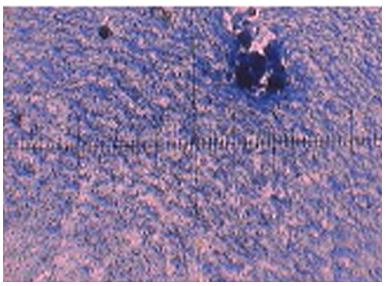

Fig. 1 Qi, uterine fibroids and a TAP level of 92.793 μm^2

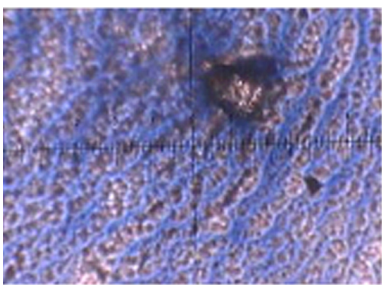

Fig. 2 Wan, moderate differentiated endometrial adenocarcinoma and a TAP level of 197.675 μm^2

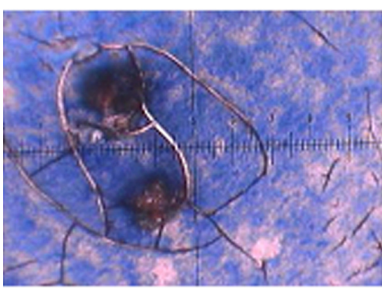

Fig. 3 Wang, poorly differentiated endometrial adenocarcinoma and a TAP level of 256.879 μm^2

a positive TAP result has a high predictive diagnostic value.

The ROC curves were used to analyze the screening and diagnostic value of TAP and hs-CRP for endometrial cancer in patients with endometrial thickness less than 8 mm. The areas under the curve (AUCs) for TAP and hs-CRP were 0.678 and 0.651, respectively. A TAP level > 160.662 μm^2 and hs-CRP level > 1.07 mg/L indicated possible endometrial cancer (Table 2 and Fig. 4).

Table 2 ROC curve analyzing the diagnostic values of TAP and hs-CRP

ROC curve parameters	TAP	hs-CRP
Area under the curve (AUC)	0.678	0.651
Youden index	0.4464	0.3423
Cut-off value	> 162.662	> 1.07
Sensitivity	63.16	65.00
Specificity	81.48	69.23
P value	0.0468	0.0704

Discussion

Endometrial cancer is one of the three gynecological malignancies and is an endometrial carcinogenesis [4]. In recent years, the incidence of endometrial cancer has increased gradually. As a result, early detection of and intervention in endometrial cancer has gained increasing attention from clinicians. At present, hysteroscopic biopsy is recommended to confirm the diagnosis for patients with endometrial thickness more than 8 mm, as measured on ultrasonography. For patients with endometrial thickness less than 8 mm, regular follow-up is recommended and unnecessary hysteroscopy should be minimized if no abnormal endometrial morphological changes are found and no symptoms associated with vaginal bleeding or abdominal [5] discomfort develop over long-term follow-up. However, clinically, there are still endometrial cancer patients with endometrial thickness less than 8 mm, and the consequences of omissions in these patients could be disastrous. For primary level health-care institutions in our country, serum marker levels for endometrial cancer should be particularly evaluated during screening, diagnosis, and timely intervention of endometrial cancer with obscure endometrial thickening.

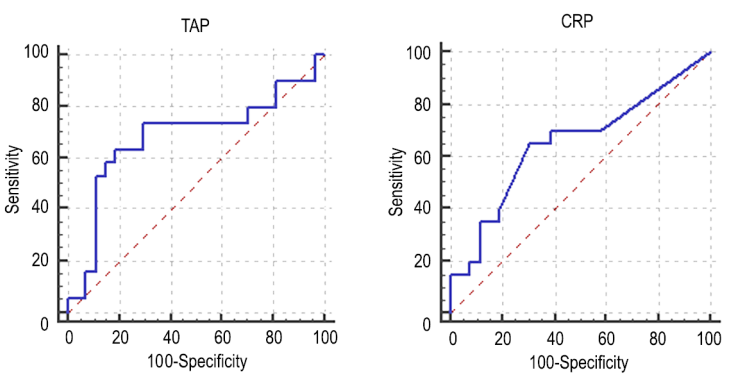

Fig. 4 ROC curve analysis of TAP and hs-CRP in endometrial cancer screening

TAP detection is a one-time combined detection of a variety of abnormal tumor sugar chain glycoproteins and involves aggregations of different glycoproteins to greatly amplify cancer signaling. Studies have reported that TAP has higher diagnostic values for a variety of digestive tract cancers [6–7], ovarian cancer [8], and bladder cancer [9]. TAP has also been reported to be expressed in endometrial cancer [3], with the level of TAP reflecting the endometrial cancer prognosis and recurrence [10], and can be a suitable serum marker for endometrial cancer.

hs-CRP is a clinically commonly used serum marker for the inflammatory response and tumors. hs-CRP can be highly expressed in a variety of diseases, but lacks specificity. One study reported that the hs-CRP level of patients with endometrial cancer after surgery significantly decreased compared with that before surgery [11], suggesting that hs-CRP may also be expressed in patients with endometrial cancer. Prior to this study, no method combined TAP and hs-CRP in screening for and diagnosing endometrial cancer.

In this study, all the included patients were first diagnosed with endometrial thickness less than 8 mm, but the diagnosis was confirmed as endometrial cancer. We found that the TAP and hs-CRP levels in the experimental group were both higher than those in the control group [(182.95 ± 72.14) μm^2 vs. (133.19 ± 55.18) μm^2, P = 0.019; (7.52 ± 19.03) mg/L vs. (1.66 ± 2.31) mg/L, P = 0.136]. The difference between the two groups in TAP level was statistically significant. By using the laboratory recommended cutoff value as a standard, the sensitivity of TAP for the diagnosis of endometrial cancer was 73.68%, specificity was 69.23%, and the Youden index was 0.4291. The diagnostic sensitivity and specificity of hs-CRP were 15.79% and 100%, respectively, and the Youden index was 0.1579. The sensitivity and specificity of the combined diagnosis of the two indexes were 77.83% and 69.23%, respectively, and the Youden index rose to 0.4706. However, the results of binary logistic regression analysis showed that a positive TAP result had a higher predictive diagnostic value (P = 0.014) than hs-CRP (P = 0.167) did.

After plotting the ROC curves, the optimal cut-off value for TAP to diagnose endometrial cancer was found to be 160.662 μm^2 and that for hs-CRP was 1.07 mg/L. The AUC of TAP was slightly higher than that of hs-CRP (0.678 vs. 0.651). Both of the indexes had moderate diagnostic value, and the diagnostic value of TAP was statistically significant. All the data suggest that TAP was more suitable for suspected positive endometrial cancer, while a negative hs-CRP result was more appropriate for excluding the diagnosis of endometrial cancer. However, the sample size of the study was relatively small; no long-term follow-up was conducted, and larger scale clinical trials are needed to confirm the conclusions.

In summary, for patients suspected of having endometrial cancer with endometrial thickness less than 8 mm, combined detection of TAP and hs-CRP levels can be used as a screening tool and can provide new ideas for clinical diagnosis and treatment.

Conflicts of interest

The authors indicated no potential conflicts of interest.

References

1. Li X, Yang X, Yang Y, *et al*. Value of hysteroscopy and dilatation and curettage in diagnosis of endometrial cancer. Chin J Obstet Gynecol, 2015, 50: 120–124.
2. Mingzhu Yang, Yajun Li, Wensu Wang. Clinical characteristics of endometrial cancer among postmenopausal women with endmetrial thickening. J China-Japan Friendship Hospital, 2015, 29: 166–168
3. Zhihui Yang. Expression of abnormal tumor protein in endometrial carcinoma. Hebei Med J (Chinese), 2013, 35: 2030.
4. Zhu J, Wen H, Wu XH. Clinicopathological characteristics and treatment of carcinosarcoma of the female genital tract. Oncol Transl Med, 2015, 1: 233–238.
5. Ling Chen, Qiheng Liang, Pengtao Sun, *et al*. The risk assessment of endometrial cancer in postmenopausal women presenting with aginal bleeding by transvaginal color doppler ultrasound and the malignant risk model. Chin J Pract Gynecol Obstet (Chinese), 2014, 30: 285–288.
6. Yao SY, Wu YM. The singificances tumor abnormal protein detection for diagnosis and prediction of prognosis in gastrointetsinal tumors. J Pract Oncol (Chinese), 2015, 29: 122–126.
7. Wu XY, Huang XE. Clinical application of serum tumor abnormal protein (TAP) in colorectal cancer patients. Asian Pac J Cancer Prev, 2015, 16: 3425–3428.
8. Thakkar V, Patel P, Prajapati N, *et al.* Serum levels of glycoproteins are elevated in patients with ovarian cancer. Indian J Clin Biochem, 2014, 29: 345–350.
9. Zhang L, Guo X, Min Y, *et al*. Tumor abnormal protein (TAP) examination contributes to primary diagnosis of bladder cancer. Int J Clin Exp Med, 2015, 8: 18528–18532.
10. Zhang YR, Fu Y, Yuan F, et al. Tumor abnormal proteins in the prediction of endometrial cancer diagnosis of postoperative recurrence. J Med Pest Control, 2013, 29: 809–810.
11. Zhang JF, Zou WH, Zhang JY. The Correlation study on the diagnostic value and prognosis of high-sensitivity C-reactive protein and carbohydrate antigen 125 for endometrial cancer. Chin J Human Sexuality (Chinese), 2015, 24: 38–40.

DOI 10.1007/s10330-016-0162-8
Cite this article as: Li Y, Yue RQ, Qin DR, *et al*. The diagnostic value of tumor abnormal protein and high sensitivity C reactive protein in screening for endometrial cancer with endometrial thickness less than 8 mm. Oncol Transl Med, 2016, 2: 185–188.

Oncology and Translational Medicine
DOI 10.1007/s10330-016-0157-5

August 2016, Vol. 2, No. 4, P189–P193

CASE REPORT

Extramedullary skeletal muscle metastasis of glioblastoma: A case report and literature review*

Li Wang[1], Rongqing Li[2], Xudong Feng[2], Shuling Song[1], Yong Zhang[2] (✉)

[1] Department of Pathology, Kunming General Hospital, Kunming 650032, China
[2] Department of Radiation Oncology, First Affiliated Hospital of Kunming Medical University, Kunming 650032, China

Abstract

Objective The aim of the study was to explore the clinicopathologic, immunophenotypic, and diagnostic features of extramedullary metastases of glioblastoma.

Methods One case of extramedullary skeletal muscle metastasis of glioblastoma was studied, including the clinical, histological, and immunohistochemical features.

Results A 24-year-old man underwent surgical resection for glioblastoma (WHO grade IV) in the left temporal parietal region followed by radiotherapy and temozolomide therapy. One year and nine months later, he developed an extramedullary skeletal muscle metastasis in L4, and the histology was remarkably different from that of the primary glioblastoma specimen. The immunohistochemical analysis also showed changes. In the metastasis, the small cells were negative for GFAP; weakly positive for S-100; and positive for nestin, NSE, and CD56, with 60% of cells positive for p53 and 40% positive for Ki-67. The giant cells showed strong positivity for GFAP and S-100, and weak expression of p53, Ki-67, nestin, NSE, and CD56. The primary glioblastoma specimen showed strong positivity for GFAP and S-100 and was negative for NSE, nestin, and CD56, with around 25% of the tumor cells positive for p53 and a Ki-67 labeling index of 20%.

Conclusion Extraneural metastasis (ENM) is a rare complication of glial tumors and glioma stem cells may be related to the metastasis. Since extraneural metastasis may occur in patients without central nervous symptoms, any unusual signs during the follow-up of patients diagnosed with glioblastoma should not be underestimated.

Received: 27 April 2016
Revised: 6 June 2016
Accepted: 25 July 2016

Key words: glioblastoma; metastasis; histopathology

Extraneural metastasis (ENM) is a rare complication of tumors of the nervous system [1–3]. ENMs affect only 0.96% of those with tumors of the nervous system [4]. Among these, ENMs of glioblastomas are also a rare finding, and lungs and lymph nodes are particularly susceptible to extraneural spread [5]. Here we report on a patient with an extramedullary skeletal muscle metastasis from a World Health Organization (WHO) grade IV glioblastoma.

Case history

A 24-year-old man presented with headaches and vomiting. A brain magnetic resonance imaging (MRI) scan revealed a left temporal parietal occupied lesion (Fig. 1a–1c). Complete resection of the lesion was performed and pathological examination revealed a WHO grade IV glioblastoma. Subsequently, the patient was treated with TomoTherapy radiotherapy combined with temozolomide. Routine MRI scans of the brain performed every 2 months did not show any local recurrence.

Approximately 1 year and 9 months later, the patient experienced backache. An MRI scan of the lumbar vertebra showed a mass in the canalis vertebralis, spinal marrow, and right rear muscle of L4. The lesion spread backward to the bilateral accessory and spinous process and showed marked homogeneous enhancement (Fig. 1g–1j). An MRI scan of the brain showed a local recurrence (Fig. 1d–1f).

✉ Correspondence to: Yong Zhang. E-mail: newkaryon@163.com
* Supported by grants from the National Nature Science Foundation of China (No. 81560462) and the Applied & Basic Research Funds of Yunnan Province, China.

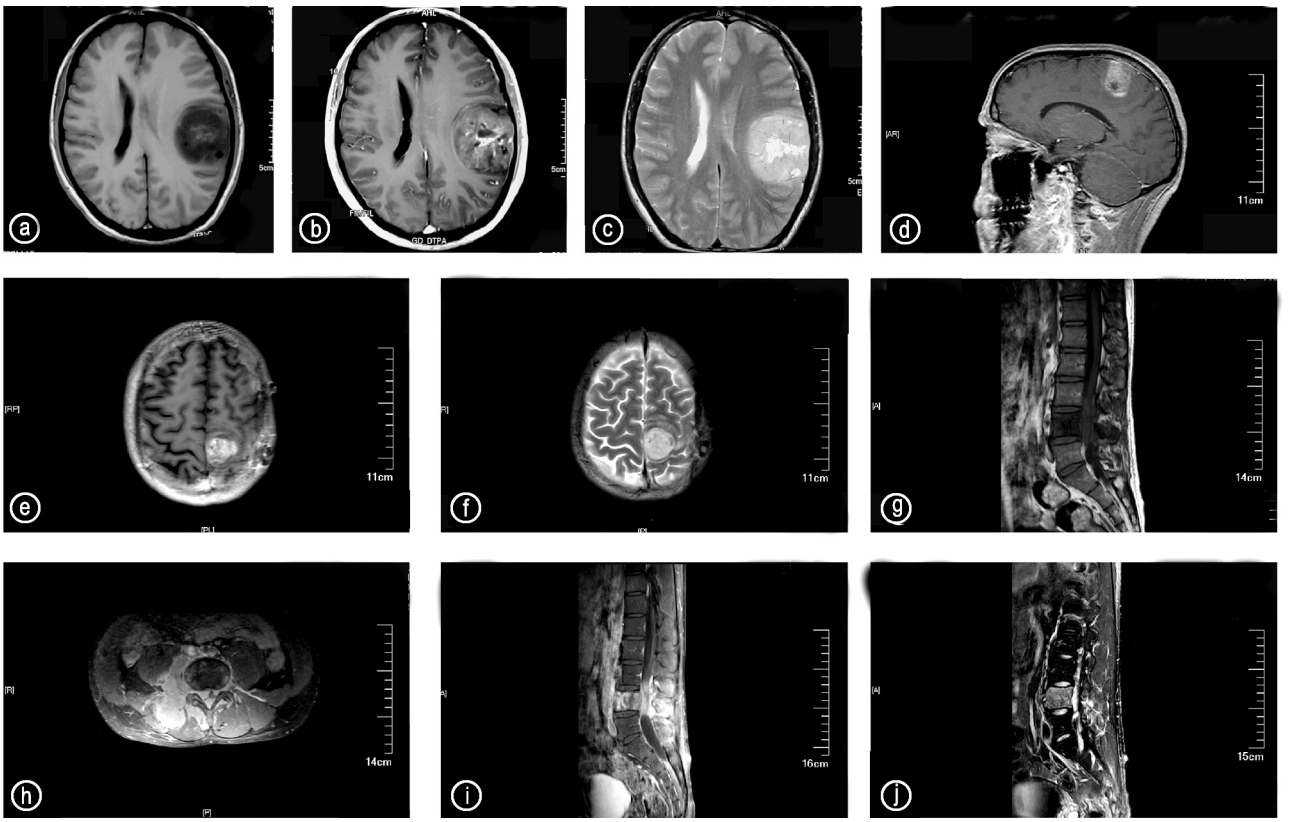

Fig. 1 MRI scans of the different tumor locations. (a–c) The tumor preoperative of brain: T1 axial MRI (a), T1-weighted axial MRI (b) and T2 axial MRI (c); (d–f) A year and nine months later, MRI scan of the brain showed a local recurrence: T1-weighted coronal MRI (d), T1-weighted axial MRI (e) and T2 axial MRI (f); (g–j) MRI scan of the lumbar vertebra showed the metastasis: T1 coronal MRI (g), T1 axial MRI (h), T1-weighted coronal MRI (i) and T2 coronal MRI (j)

Resection of the lesions in L4 was performed and we found the tumor, measuring around 10 cm × 7 cm, had invaded the endorhachis and both sides of the psoas, erector spinae, and quadratus lumborum. The tumor was diagnosed as an extramedullary skeletal muscle metastasis of a WHO grade IV glioblastoma. Subsequently, the patient received radiotherapy combined with temozolomide and irinotecan-cisplatin chemotherapy. The patient died 1 year and 3 months after surgical resection of the metastasis.

Pathological findings

Primary glioblastoma

Histopathologically, the specimen consisted of brain tissue with diffuse infiltration of atypical cells with oval pleomorphic hyperchromatic nuclei in a fibrillary background. The cells were arranged densely and demonstrated increased mitotic activity and necrosis and microvascular proliferation. Immunohistochemically, the tumor cells showed strong positivity for GFAP (almost all of the tumor cells were positive) and S-100. No positivity for mutant IDH1 (R132H), EGFR, AE1/3, CD99, CgA, Syn, NSE, LCA, nestin, CD56, or CD133 was found. About 25% of the tumor cell nuclei showed positive reactions for p53. The Ki-67 labeling index was 20% (Table 1). The pathological diagnosis of the primary tumor was glioblastoma (WHO grade IV; Fig. 2a and 2b).

L4 metastasis

For the submitted surgical specimen taken from L4, the histopathology showed that numerous atypical cells were infiltrated as solid nests among the skeletal muscle tissues. The tumor cells were different from those seen in the primary tumor. On hematoxylin and eosin staining, the tumor was composed of two different cell morphologies: uniform small round cells with oval nuclei and unremarkable nucleoli, and giant cells similar to glioblastoma composed of highly anaplastic giant and syncytial cells. Immunohistochemically, the staining pattern also differed between the two cell types. The small cells were negative for GFAP, weakly positive for S-100, had more cells (around 60%) positive for p53, a Ki-67 positive index of 40%, and some demonstrated positive expression of the neural stem cell (NSC) marker nestin and the neuro-

blast cell markers NSE and CD56. The giant cells showed strong positivity for GFAP and S-100 and lower expression of p53, Ki67, nestin, NSE, and CD56. All of the tumor cells were negative for mutant IDH1 (R132H), EGFR, LCA, and CD133 (Table 1). The tumor was diagnosed as an extramedullary skeletal muscle metastasis of a WHO grade IV glioblastoma (Fig. 2c–2h).

Table 1 Summary of immunohistochemical findings

Antibodies	Primary tumor	Small cells in the metastasis	Giant cells in the metastasis
GFAP	+++	–	+++
S-100	+++	+	+++
p53	25%	60%	10%
Ki67	20%	40%	10%
Nestin	–	++	+
CD56	–	+++	++
NSE	–	++	+
CgA	–	–	–
Syn	–	–	–
CD133	–	–	–
IDH1 (R132H)	–	–	–
LCA	–	–	–
EGFR	–	–	–
AE1/3	–	–	–
CD99	–	–	–

+++, Strong reactivity; ++, Moderate reactivity; +, Week reactivity; –, No reactivity

Discussion

Metastatic spread from a cranial primary tumor is unusual, especially for glial tumors. Possible explanations include [6]: the absence of lymphatic vessels in the brain; presence of the blood-brain barrier; survival duration in cases of malignant gliomas is too short to develop metastases; glial tumor cells may require a special metabolic environment found only in the central nervous system; and the immunological response of the host organ to glial tumor cells may prevent growth outside of the central nervous system. Neurosurgical operations, especially ventriculoperitoneal shunts and multiple craniotomies, have been suggested to increase the risk of ENMs [2, 6, 7].

Extracranial metastases from glioblastoma have been detected for many years, with the first documented case in 1928 [8]. In a meta-analysis by Lun *et al* [9], 83 published cases of extracranial metastases from glioblastoma were found in the period from 1928 to 2009. In a single institution experience of extracranial metastasis in glioma by Amitendu *et al* [10] from the Brain Tumor Database of the National Neuroscience Institute of Singapore, between September 2004 and October 2009, the incidence of metastasis was 2.7% (4 of 148 patients). Extracranial metastases have been observed almost exclusively in cases of high-grade (III and IV) gliomas, but there has been no discrimination between WHO grade III and IV tumors in published cases [2]. Metastases from well-differentiated gliomas are very uncommon [11]. Of those that metastasize extraneurally, metastases to the vertebral bodies repre-

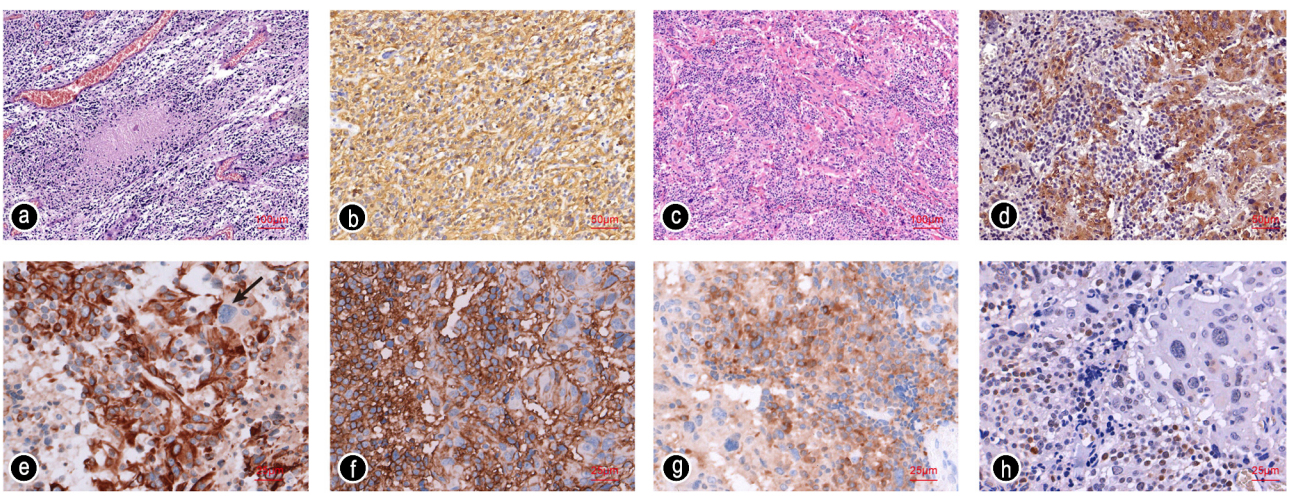

Fig. 2 Histopathological appearance of the different tumor locations. (a and b) Fist surgical brain tumor resection showing diffuse infiltration of atypical cells with oval hyperchromatic nuclei in a fibrillary background with necrosis and pathological microvascular proliferations by H & E staining (a) and strong positivity for GFAP by immunohistochemistry (b); (c–h) The surgical specimen in L4 showing the tumor was composed of two different cell morphologies: one is uniform small round cells with oval nuclei and unremarkable nucleoli; the other is composed of highly anaplastic giant and syncytial cells on H & E stain (c); Immunohistochemically, the component of small cells was negative for GFAP while the part of giant cells showed strong positivity for GFAP (d); There were more strong positive cells for nestin in small cells part than that in giant cells (e), also for CD56 (f), NSE (g) and p53 (h); The arrow showed negative expression for nestin in a giant cell

sent a significant proportion. Goodwin *et al* [12] reviewed 28 cases from the published literature of glioblastoma multiforme metastasis to the vertebra and found the mean age at presentation was 38.4 years with an average overall survival duration of 26 months. Patients were either asymptomatic with metastasis discovered at autopsy or presented with varying degrees of pain, weakness of the extremities, or other neurologic deficits. Hematogenous spreading is equally important as cerebrospinal fluid spread for ENM [13].

In our case, although our patient underwent surgical resection followed by radiotherapy and temozolomide therapy, neither a ventriculoperitoneal shunt nor multiple craniotomies were performed, and the time to recurrence was short (only 1 year and 9 months). The intravasation of tumor cells during the intraoperative injury of blood vessels may be associated with ENM. In addition, many researchers have demonstrated that in tumor tissue the blood brain barrier is not intact, which can promote ENM [5, 7]. Furthermore, based on an admittedly small number of cases, adjuvant radiation therapy may reduce the dura tightness, facilitating transdural tumor cell migration.

Intrinsic molecular properties of tumor cells may be involved in the process of extraneural spread. The increased expression of EGFR and mutations in the p53 and IDH1 genes may play a role in ENM of glioblastomas [5, 14–16]. In our case, we found neither the primary lesion nor the metastatic tumor expressed EGFR or had mutant IDH1 (R132H) expression, but the positive expression rate of p53 and Ki-67 in the metastasis doubled in comparison with the original lesion.

Interestingly, the pathological morphology and immunohistochemical expression of GFAP, p53, and Ki-67 had changed greatly in the metastatic lesion. The primary specimen consisted of similar uniform atypical cells, which almost all showed strong positivity for GFAP. The metastatic tumor was composed of two different cell morphologies, uniform small round cells negative for GFAP expression, higher mutant p53 expression, and a higher Ki-67 labeling index; and anaplastic giant and syncytial cells with GFAP expression, less mutant p53 expression, and a lower Ki-67 labeling index. This interesting phenomenon indicated the possible existence of glioma stem cells [17, 18].

Glioma stem cells account for a fraction of the tumor cell population, with stem cell-like properties including multi-potency, self-renewal, and tumorigenesis [19–21]. We speculated the small, uniform, round, GFAP-negative tumor cells in the metastasis might be related to glioma stem cells, and with the microenvironment and metabolic changes (from the left temporal parietal to extramedullary skeletal muscle), this group of cells differentiated into GFAP-positive giant tumor cells that were different from the primary lesion. Further research including immunohistochemical analysis with the neural stem cells marker nestin [22–24] and neuroblast cell markers NSE and CD56 showed the small cells were positive for nestin, NSE, and CD56, while the giant cells showed weaker expression of these markers.

Conclusion

ENM of glioblastoma is extremely rare. Because patient survival has increased these days, the incidence of this atypical presentation is likely to increase. Because ENM may occur in patients with a short disease history and without any central nervous symptoms, any unusual symptom occurring during the follow-up of these patients should not be underestimated. The best treatment for these tumors is excision of the mass followed by radiotherapy and chemotherapy.

Conflicts of interest

The authors indicated no potential conflicts of interest.

References

1. Ammerman JM, Kerr PB, Roberti F. Acute tetraplegia and cardiac arrest following high cervical leptomeningeal metastasis of giant cell glioblastoma. J Clin Neurosci, 2011,18: 1133–1135.
2. Martens T, Matschke J, Müller C, *et al*. Skeletal spread of an anaplastic astrocytoma (WHO grade III) and preservation of histopathological properties within metastases. Clin Neurol Neurosurg, 2013, 115: 323–328.
3. Song YH. Postoperative glioma extracranial metastasis: A case report. Chinese-German J Clin Oncol, 2014, 13: 444–446.
4. Smoll NR, Villanueva EV. The epidemiology of extraneural metastases from primary brain, spinal cord, and meningeal tumors. Neurosurgery, 2010, 67: E1470–E1471.
5. Subramanian A, Harris A, Piggott K, *et al*. Metastasis to and from the central nervous system – the 'relatively protected site'. Lancet Oncol, 2002, 3: 498–507.
6. Mazza E, Belli C, Terreni M, *et al*. Breast metastases from oligodendroglioma: an unusual extraneural spread in two young women and a review of the literature. Crit Rev Oncol Hematol, 2013, 88: 564–572.
7. Schweitzer T, Vince GH, Herbold C, *et al*. Extraneural metastases of primary brain tumors. J Neurooncol, 2001, 53: 107–114.
8. Davis L. Spongioblastoma multiforme of the brain. Ann Surg, 1928, 87: 8–14.
9. Lun M, Lok E, Gautam S, *et al*. The natural history of extracranial metastasis from glioblastoma multiforme. J Neurooncol, 2011, 105: 261–273.
10. Amitendu S, Mak SK, Ling JM, *et al*. A single institution experience of the incidence of extracranial metastasis in glioma. J Clin Neurosci, 2012, 19: 1511–1515.
11. Longee DC, Friedman HS, Phillips PC, *et al*. Osteoblastic metastases from astrocytomas: a report of two cases. Med Pediatr Oncol, 1991, 19: 318–324.
12. Goodwin CR, Liang L, Abu-Bonsrah N, *et al*. Extraneural glioblastoma multiforme vertebral metastasis. World Neurosurg, 2016, 89: 578–582.
13. Johansen MD, Rochat P, Law I, *et al*. Presentation of two cases with early extracranial metastases from glioblastoma and review of the

literature. Case Rep Oncol Med, 2016: 8190950. Epub 2016 May 9.
14. Takahashi Y, Nakamura H, Makino K, *et al*. Prognostic value of isocitrate dehydrogenase 1, O6-methylguanine-DNA methyltransferase promoter methylation, and 1p19q co-deletion in Japanese malignant glioma patients. World J Surg Oncol, 2013, 11: 284.
15. Balss J, Meyer J, Mueller W, *et al*. Analysis of the IDH1 codon 132 mutation in brain tumors. Acta Neuropathol, 2008, 116: 597–602.
16. Yan H, Parsons DW, Jin G, *et al*. IDH1 and IDH2 mutations in gliomas. N Engl J Med, 2009, 360: 765–773.
17. Germano IM, Binello E. Stem cells and gliomas: past, present, and future. J Neurooncol, 2014, 119: 547–555.
18. Cheng L, Bao S, Rich JN. Potential therapeutic implications of cancer stem cells in glioblastoma. Biochem Pharmacol, 2010, 80: 654–665.
19. Sampetrean O, Saya H. Characteristics of glioma stem cells. Brain Tumor Pathol, 2013, 30: 209–214.
20. Ilkanizadeh S, Lau J, Huang M, *et al*. Glial progenitors as targets for transformation in glioma. Adv Cancer Res, 2014, 121: 1–65.
21. Modrek AS, Bayin NS, Placantonakis DG. Brain stem cells as the cell of origin in glioma. World J Stem Cells, 2014, 6: 43–52.
22. Miconi G, Palumbo P, Dehcordi SR, *et al*. Immunophenotypic characterization of human glioblastoma stem cells: correlation with clinical outcome. J Cell Biochem, 2015, 116: 864–876.
23. Kong BH, Moon JH, Huh YM, *et al*. Prognostic value of glioma cancer stem cell isolation in survival of primary glioblastoma patients. Stem Cells Int, 2014: 838950. Epub 2014 Dec 11.
24. Brehar FM, Arsene D, Brinduse LA, *et al*. Immunohistochemical analysis of GFAP-δ and nestin in cerebral astrocytomas. Brain Tumor Pathol, 2015, 32: 90–98.

DOI 10.1007/s10330-016-0157-5
Cite this article as: Wang L, Li RQ, Feng XD, *et al*. Extramedullary skeletal muscle metastasis of glioblastoma: A case report and literature review. Oncol Transl Med, 2016, 2: 189–193.

Oncology and Translational Medicine

Aims & Scope

Oncology and Translational Medicine is an international professional academic periodical. The Journal is designed to report progress in research and the latest findings in domestic and international oncology and translational medicine, to facilitate international academic exchanges, and to promote research in oncology and translational medicine as well as levels of service in clinical practice. The entire journal is published in English for a domestic and international readership.

Copyright

Supervised by

Ministry of Education of the People's Republic of China.

Administered by

Tongji Medical College, Huazhong University of Science and Technology.

Submission information

Manuscripts should be submitted to:
http://otm.tjh.com.cn
dmedizin@sina.com

Subscription information

ISSN edition: 2095-9621
CN: 42-1865/R

■ Subscription rates
Subscription may begin at any time. Remittances made by check, draft or express money order should be made payable to this journal. The price for 2015 is as follows: US $ 30 per issue; RMB ￥28.00 per issue.

Database

Oncology and Translational Medicine is abstracted and indexed in EMBASE, Index Copernicus, Chinese Science and Technology Paper Citation Database (CSTPCD), Chinese Core Journals Database, Chinese Journal Full-text Database (CJFD), Wanfang Data; Weipu Data; Chinese Academic Journal Comprehensive Evaluation Database.

Business correspondence

All matters relating to orders, subscriptions, back issues, offprints, advertisement booking and general enquiries should be addressed to the editorial office.

Mailing address
Editorial office of
Oncology and Translational Medicine
Tongji Hospital
Tongji Medical College
Huazhong University of Science and Technology
Jie Fang Da Dao 1095
430030 Wuhan, China
Tel.: +86-27-83662630
Fax: +86-27-83662645
Email: dmedizin@tjh.tjmu.edu.cn

Printer
Changjiang Spatial Information Technology Engineering Co., Ltd. (Wuhan)
Hangce Information Cartorgraphy Printing Filial, Wuhan, China
Printed in People's Republic of China

Managing director

Executive editors

Typesetting editor